Parametric Study on Analysis and Design of Permanently Anchored Secant Pile Wall for Earthquake Loading

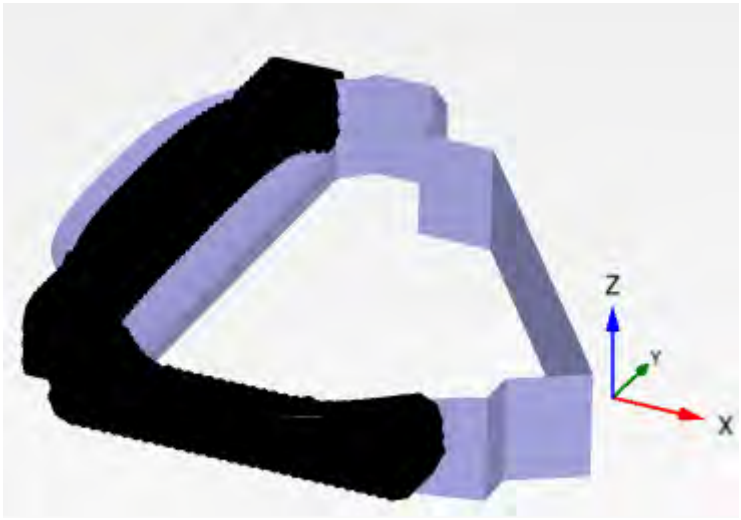

Julius Emmanuel Emuriat

A Thesis Submitted to
The School of Civil and Environmental Engineering

Prepared in Fulfillment of the Requirements for the
Degree of Masters of Science in Civil Engineering (Geotechnical)

Addis Ababa University
Addis Ababa, Ethiopia
March, 2017

Copyright

Addis Ababa University

School of Civil and Environmental Engineering

This is to certify that the thesis prepared by Julius Emmanuel Emuriat, titled: **Parametric Study on Analysis and Design of Permanently Anchored Secant Pile Wall for Earthquake Loading** and submitted in Partial Fulfillment of the Requirements for the Degree of Master of Science (Geotechnical Engineering) complies with the regulations of the University and meets the accepted standards with respect to originality and quality.

Approved by Board of Examiners:

Dr. - Ing. Henok Fikre	…….	……
Research Advisor	Signature	Date
Dr. - Ing. Samuel Tadesse	…….	…….
Internal Examiner	Signature	Date
Prof. Alemayehu Teferra	…….	…….
External Examiner	Signature	Date
Dr. - Ing. Agizew Nigussie	...……	……
Chairman	Signature	Date

List of Abbreviations and Acronyms

General Terms

Z	Depth
σ	Normal stress
φ	Angle of internal friction
γ	Total unit weight
γ_{unsat}	Soil unit weight above phreatic level
γ_{sat}	Soil unit weight below phreatic level
ε	Shear strain
q	Deviatoric Stress
c	Cohesion
K_0	Ratio of initial horizontal stress/ Initial vertical stress
g	Gravitational acceleration
ρ	Soil density
E	Young"s modulus
E_i	Initial modulus
E_{50}	Secant Young"s modulus at 50% of failure stress from triaxial test
v, μ	Poisson"s ratio
N	Standard penetration test blow count

FEA Finite Element Analyses

FEM Finite Element Method

3DAE Three Dimensional Anniversary Edition

AASHTO American Association of State Highway and Transportation Officials

FHWA Federal Highway Administration

CBE Commercial Bank of Ethiopia

USGS United States Geological Survey

Plaxis Constitutive Model Terms

Mohr Coulomb

φ Friction angle

c Cohesion

ψ Dilation angle

E Young‟s modulus

v Poisson‟s ratio

ρ Unit weight

K_0 Ratio of initial horizontal stress/ Initial vertical stress

V_p Longitudinal wave velocity

V_s Transverse wave velocity

Hardening Soil Model

Φ Friction angle

c Cohesion

ψ Dilation angle

E_{50}^{ref} Secant stiffness in standard triaxial test at P_{ref}

E_{ode}^{ref} Secant stiffness for primary oedometer loading at P_{ref}

m Power for stress level dependency of stiffness

E_{ur}^{ref} Unloading/reloading stiffness

V_{ur} Poisson‟s ratio for unloading-reloading

P^{ref} Reference stress for stiffness

R_f Failure ratio

$\sigma_{tension}$ Tension cutoff

$C_{increment}$ Incremental increase of cohesion with depth

K_0^{nc} $\sigma_{xx}'/\sigma_{yy}'$ Stress ratio in a state of normal consolidation

ρ Unit weight

K_0 Ratio of initial horizontal stress/ Initial vertical stress

POP Preconsolidation Pressure

OCR Overconsolidation Ratio

Hardening Small Strain

E_{50}^{ref} Secant stiffness in standard triaxial test at P_{ref}

E_{ode}^{ref} Secant stiffness for primary oedometer loading at P_{ref}

E_{ur}^{ref} Unloading/reloading stiffness

m Power for stress level dependency of stiffness

c	Cohesion
Φ	Friction angle
ψ	Dilation angle
$\gamma_{0.7}$	Shear strain at which $G_s = 0.722G_0$
G_0	Initial shear modulus
G_0^{ref}	Shear modulus at very small strain
V_{ur}	Poisson‟s ratio for unloading-reloading
G_{ur}	Tangent shear modulus
γ_{ref}	Volumetric threshold shear strain
R_{int}	Strength reduction factor for interface

Acknowledgement

First and foremost I would like to thank the entire faculty and staff of Addis Ababa University School of Civil and Environmental Engineering, the dedication and support did not go unnoticed. When the opportunity arose to study and research at Addis Ababa University, it certainly appeared to be a golden opportunity to learn from the experienced, knowledgeable and superb teaching style of the academic staff of Addis Ababa Institute of Technology. These expectations were indeed fulfilled - what i had not anticipated was the loyal and mutually respectful friendship that was evolved throughout the learning process.

I am very grateful to all those who contributed in different ways to the success of this research. Am highly indebted to the European Union Commission that selected and sponsored me to pursue Masters of Geotechnical Engineering exchange programme to Addis Ababa University, Ethiopia.

Special thanks to Dr. Melaku Duguma, The director graduated programmes and the coordinator Arise Sponsorship in Addis Ababa University (Partner University). He bridged the communication gap between me and the Coordinating University (UCT) and made sure all the funds needed for the project were received in time.

Thanks to friends in Ethiopia who listened attentively to me during at very trying moments and made helpful suggestions to make my stay in Ethiopia meaningful.

Last but not least many thanks to my advisor Dr.Ing. Henok Fikre, he has been of seemingly inexhaustible source of patience, support and inspiration. He guided me through and saw the work evolve from the conceptual point to final work worth execution.

Abstract

Due to space limitations in urban areas, deep excavation in to the ground has become a common practice worldwide. Among the conventional retaining support systems, this study is focused on secant pile walls. The secant pile methodology comprised the formation of overlapping concrete piles. The overlap between the piles is achieved to prevent soil and ground water ingress. The analysis of these deep excavations requires considerations of; nonlinear, dynamic and complicated system and involves consideration of soil parameters, deformation, interaction of soil and retaining configuration. It is difficult to precisely describe the nonlinear system using traditional analysis. Thus, in order to accurately describe the behavior of the anchored secant pile for earthquake loading, 3D finite element simulation was applied. The analysis indicated for 20m excavation step in the fourth stage, showed incremental lateral displacement was 0.0552E-3m and total displacement was 0.114E-3m. The analysis indicated that the displacement induced in the ground increased with excavation depth. As the excavation depth increased, the magnitude of unbalanced forces increased resulting to increase in stresses and displacement. Increase in pile diameter increased displacement near the surface of the wall. In addition, the modulus of deformability of the soil has a great importance in the settlement of the soil. It is visible that when the thickness of the wall increased, the horizontal and vertical displacements near the wall increased. Decreasing the horizontal and vertical spacing of anchors increased stiffness of the anchor per unit width. With high anchor stiffness, displacement occurred near the excavation surface thus, reducing the displacement of the wall.

Key words: secant, pile wall, earthquake loading, plaxis.

Table of Content

Contents **Pages**

List of Abbreviations and Acronyms i
Acknowledgement v
Abstract vi
Table of Content vii
List of Figures xi
List of Tables xiv
List of Appendices xv
List of Appendix Figures xvi
List of Appendix Table s xvii
Chapter 1 - Introduction 1
1.1 Background 1
1.2 Problem Statement 3
1.3 Objective 3
1.3.1 General Objectives 3
1.3.2 Specific objectives 3
1.4 Methodology 3
1.5 Limitations 4
1.6 Thesis Structure 5
Chapter 2 Literature Review 6
2.1 Introduction 6
2.2 Previous Literature Reviews 6
2.2.1 Large initial lateral soil stresses can adversely affect deep excavation 8
2.2.2 Moormann‟s Database 9
2.3 Effect of deep excavation 11
2.4 Effect of supporting structure 12

2.5 Secant Pile Walls 12
2.5.1 Methods used in Secant Wall Construction 13
2.5.2 Secant Piles-merits and demerits 13
2.5.3 Case Histories on Secant Pile Walls 14
2.5.3.1 Design and construction of circular scant pile walls in soft clays in Houston Texas. 14
2.5.3.2 Construction of Access shaft for Tunnels and Deep pipelines in Urban New Zealand with Secant piles. 16
2.6 Factors that affect the performance of excavations 17
2.7 The Design of Composite Materials and Structures 19
2.8 Halpin-Tsai Equations 22
2.9 Potential Geotechnical Failures 23
2.9.1 Rotational Failure 23
2.9.2 Translational Failure 23
2.9.3 Global Stability Failure 23
2.10 Constitutive Models 26
2.10.1 Linear Elastic Model (LE) 26
2.10.2 Mohr Coulomb Model (MC) 27
2.10.3 Hardening Soil Model (HS) 27
2.10.4 Hardening Soil Model with small stiffness (HS small) 27
2.10.5 Soft Soil Model (SS) 28
2.10.6 Soft Soil Creep Model (SSC) 28
2.10.7 Modified Cam Clay Model (MCC) 28
2.11 Response Spectrum 29
2.12 Recent Developments in the Definition of Design Earthquake Ground Motion 30
2.12.1 Seismic Hazard Results 33

2.13 Seismic refraction 33
2.14 Seismic hazards in Ethiopia and its historical record 36
2.14.1 Historical records of earthquakes in Ethiopia 36
Chapter 3 Modelling 37
3.1 Introduction 37
3.2 Project description and site condition 37
3.3 Secant Pile Model 37
3.4 Selection of an appropriate constitutive model and input parameters 39
3.4.1 Constitutive Model 39
3.4.2 Soil and material parameters 39
3.4.2.1 Deformability 40
3.5 Model Geometry 46
3.5.1 Static loading 47
3.5.2 Dynamic loading 47
3.5.3 Base case model and mesh set up 49
3.6 Plaxis 2D Model 51
3.7 Comparision of results according to Plaxis 2D and 3D 52
Chapter 4 Parametric studies 57
4.1 Introduction 57
4.2 Parameter analysis 57
4.2.1 Effect of stage excavation 57
4.2.2 Diameter of Pile wall 59
4.2.3 Height of the pile wall 59
4.2.4 Anchor spacing 60
4.3 Seismic Site Response 61
4.3.1 Accelerations 62

4.3.2 Site Response Spectrum 63
4.3.3 Velocities 64
4.3.4 Ground Amplification 65
Chapter 5 – Results and Discussion 66
Chapter 6 – Conclusions and Recommendations 69
6.1 Introduction 69
6.2 Conclusions of Modeling 69
6.3 Recommendations 71
Reference 72
Appendices 74

List of Figures

Figure 1.1: Site location plan 1
Figure 1.2: Work approach for this research study 4
Figure 2.1 Summary of settlements adjacent to open cuts in various soils, as function of distance from edge of excavation 6
Figure 2.2: Dimensionless settlement profile recommended for estimating the distribution of settlement adjacent to excavations in different soil types. 7
Figure 2.3: Chart for estimating maximum lateral wall movements and ground surface settlements for support systems in clays. 8
Figure 2.4: Definition of symbols by Moormann. 9
Figure 2.5: Variation of maximum horizontal displacement with excavation depth following ... 10
Figure 2.6: Variation of normalized maximum horizontal displacement with system stiffness following. 10
Figure 2.7: Typical secant pile wall arrangement with female (primary) and male (secondary) piles forming hard/soft walls (left) and hard/hard walls (right) after Suckling et al. (2005) 13
Figure 2.8: Plaxis Model of the excavation. 15
Figure 2.9: Oberved and FE predicted settlements since start of LNG dike construction 15
Figure 2.10:Hoop stress and vertical bearing zone 17
Factors that affect the performance of excavations 17
Figure 2.11: Typical profiles of wall and ground movement for anchored wall. 18
Figure 2.12: Aligned continuous fibres 20
Figure 2.13: Stiffness perpendicular to the fibres 21
Figure 2.14: Failure modes for tie-back retaining walls [Source: Sabatini et.al, 1999] 25
Figure 2.15: (a) Response of real soil to hydrostatic stress ;(b) Response of idealized soil to hydrostatic Stress 29
Figure 2.16: Acceleration response spectra during the 22 February 2011 Christchurch earthquake (Cubrinovski and McMahon 2011) 30
Figure 2.17: The seismic hazard map of Ethiopia based on the Global Seismic Hazard assessment program data for return period of 475 year (Journal of EEA, Vol.28, 2011) 31

Figure 2.18: Fourier amplitude spectra of microtremor for the city of Addis Ababa..... 32
Figure 2.19: Predominant period Microtremor measurements for the city of Addis Ababa 32
Figure 2.20: Uniform Hazard Spectra at Addis Ababa (blue curves) compared with elastic acceleration spectra from EN 1998 based on the PGA from RP = 475yr.and country seismic code criteria..... 33
Figure 2.21: P-wave refraction result along profile 1 which clearly shows indentation with relatively low velocity in the middle for the CBE New Building Site. 34
Figure 2.22: P-wave refraction result along profile 2. The P-wave velocity values are shown by the colour Coded legend and the lines are the seismic ray paths the traversed or scanned medium for the CBE New Building Site 34
Figure 2.23: Location of the survey site and alignment of the geophysical survey profiles (thin red lines) modified from google earth map..... 35
Figure 3.1: Site layout for the alternative wall scheme for using secant pile wall (All dimensions in cm) 38
Figure 3.2: Cross section of the secant pile wall as the alternative scheme 39
Figure 3.3: Soil profile in plaxis3D Model..... 47
Figure 3.4: Real time accelerogram of Del Valle Dam - Loma Prieta Earthquake 48
Figure 3.5: Static loading..... 49
Figure 3.6: Overview of mesh set up for model in Plaxis 3D model 50
Figure 3.7: Overview of model and ground anchors in Plaxis 3D model..... 50
Figure: 3.8: Distribution of nodes and stress points in interface elements and their connection to soil elements..... 52
Figure 3.9: Static load condition..... 53
Figure 3.10: Total Acceleration 54
Figure 3.11: Examples of plane strain situation..... 55
Figure 3.12: Comparision of 3D results with 2D reference solution..... 56
Figure 4.1: Effect of stage excavation on deformation under static loading 58
Figure 4.2: Effect of stage excavation on deformation under dynamic loading..... 58
Figure 4.3: Maximum displacement U_x versus pile wall diameter under static and dynamic loading..... 59

Figure 4.4: Effect of length of pile on lateral deformation of pile wall under static and dynamic loading 60
Figure 4.5: Anchor spacing 4m for static and dynamic loading 61
Figure 4.6: Magnitude of acceleration 63
Figure 4.7: Site response spectrum 63
Figure 4.8: Velocity in horizontal direction 64
Figure 4.9: Velocity in vertical direction 64
Figure 4.10: Ground amplification 65

List of Tables

Table 3.1: Summary of ground conditions encountered in borehole 41
Table 3.2 : Summary of Seismic properties encountered in borehole 42
Table 3.3: Material properties of rebar anchor 42
Table 3.4: Material properties of Concrete 42
Table 3.5: Material properties of composite secant pile wall 45
Table 3.6: Material properties of various composite secant pile wall 46

List of Appendices

Appendix A- Hardening Soil Model 74
Appendix B - Geotechnical properties of soil 77
Appendix C – Modelling Outputs for 2D Analyses 78
Appendix D – Modelling Outputs for 3D Analyses 82
Appendix E – Site layout plan 86

List of Appendix Figures

Figure C.1 :Total displacement under static load condition

Figure C.2 :Vertical displacement under static load condition

Figure C.3 :Total Acceleration

Figure C.4 : Horrizontal Acceleration

Figure C.5 : Vertical Acceleration

Figure C.6: Peak Axial, Bending and Shear forces under dynamic load condition

Figure C.7: Peak Axial, Bending and Shear forces under static load condition

Figure D.1 Total displacement under static load condition

Figure D.2: Total displacement for stage excavation under dynamic load condition

Figure D.3: Stage excavation 5m – Total displacement

Figure D.4: Stage excavation 5m – horizontal displacement

Figure D.5: Stage excavation 5m –vertical displacement

Figure D.6: Stage excavation 10m – Total displacement

Figure D.7: Stage excavation 10m – horizontal displacement

Figure D.8: Stage excavation 10m –vertical displacement

Figure E.1: Site layout for the Commercial Bank of Ethiopia New Headquarter Building

List of Appendix Tables

Table B.1: Typical values of Young‟s modulus for granular material (MPa)

Table B.2: Typical values of Young‟s modulus for cohesive material (MPa)

Table B.3: Typical values of Poisson‟s ratio for soils and other material

Chapter 1 - Introduction

1.1 Background

The New Headquarter Building of Commercial Bank of Ethiopia high-rise office tower complex consisting of 48 storey tower multi-functional and a 5 level underground basement. The structure is like a cylinder with exterior framework of steel structure and interior space filled with concrete, measuring 186.90m in height above the ground. The basement area is approximately 50500 sq.m with 20m below the ground level. Figure 1.1 shows site location plan for CBE.

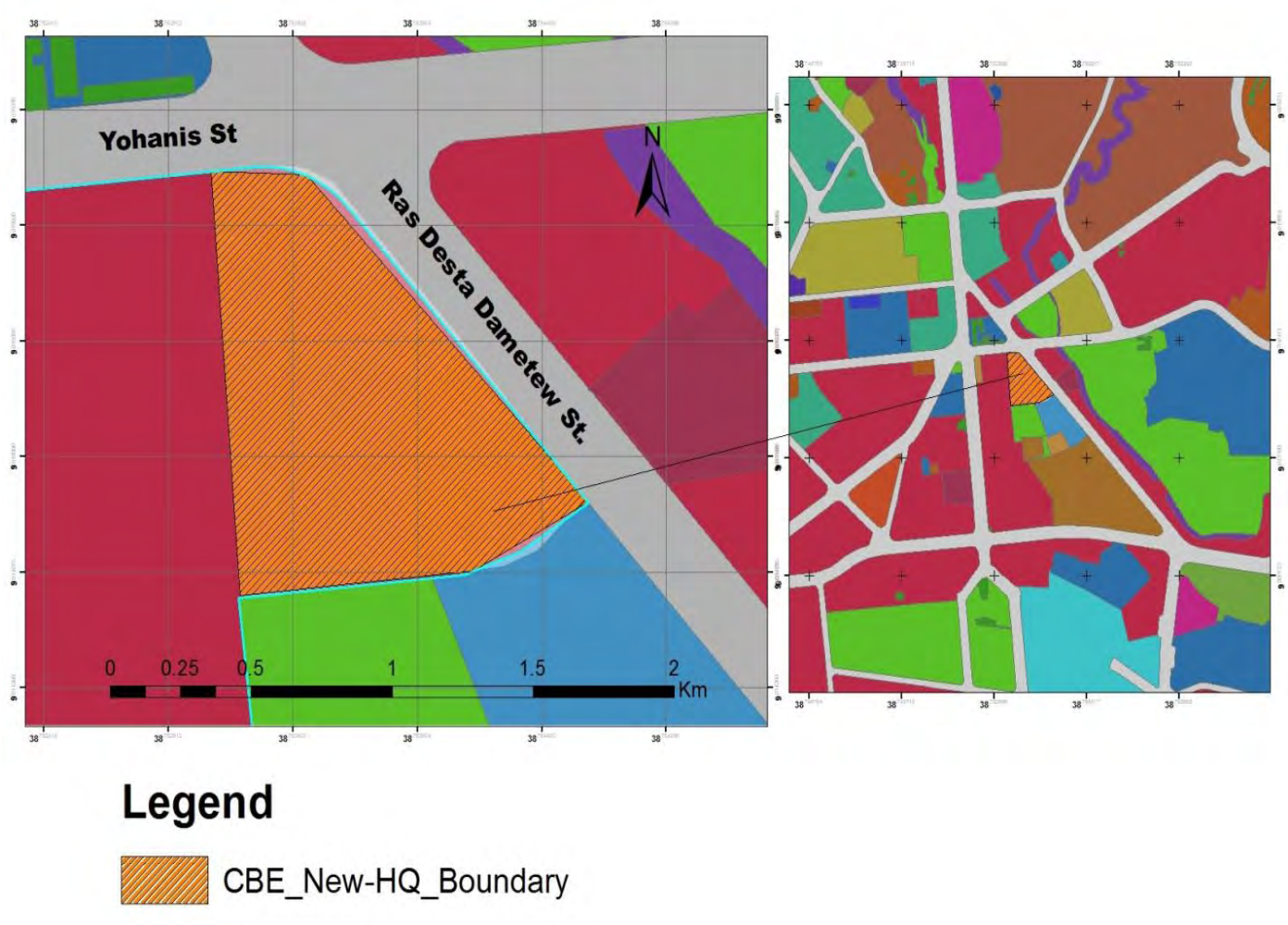

Figure 1.1: Site location plan

Providing space for parking, public amenities, etc in multi-storey buildings at the urban settings has created the need for deep excavations in to the ground to create additional floor space to meet the increasing space requirements. Special features of urban areas are restricted movements, inadequate space for equipment, soil heterogeneity (including fill and remains of old foundations or other unexpected obstructions), effects of changes in the water table, foundation interaction (detrimental effects of construction of new structures on the surrounding buildings).

Structures in the immediate vicinity of excavations, dense traffic scenario, presence of underground obstructions and utilities have made excavations a formidable task to execute. Clearly, deep excavations are posing mounting problems that demand a site specific and tailor made retaining solution.

A deep excavation in to the ground is indispensible to create additional floor space to meet increasing space requirement for parking for multi-storey buildings at the town centers. In this context, analysis and design of proper deep excavations and their supporting systems are essential. Even in a very complicated urban setting, deep retaining systems are being deployed successfully by overcoming construction challenges.

Deep excavations are supported by systems like conventional retaining walls, sheet pile walls, diaphragm walls and secant pile walls. Secant piles are primarily used in unsuitable ground conditions or where there is high water table. Secant piled walls are preferred option near buildings, roads and other sensitive structures. Secant walls can be used to form continuous water tight walls which can be an added benefit to the construction of basement and underground car parks.

Topographically the site is relatively flat with scattered undulating morphologies created by detritus materials from demolished houses. The proposed geology and volcanic stratigraphic sequences of Addis Ababa area from bottom to top are; Alaji basalt, Entoto silicics, Addis Ababa basalts, Nazareth group, and Bofa basalt. The residual soils ranging from red to dark clay are found covering extensive areas in the city. The project site constitutes different weathered rock stratum (basalt) with localized swelling clays within the shattered rock mass.

1.2 Problem Statement

According to the annul “Wealth Report” released by global real estate consultancy Knight Frank on March 5, 2016. Ethiopia Capital; Addis Ababa is among the four cities in the world dubbed as "cities for the future", based on the wealth creation opportunities they will present in the future. Despite the efforts to invest heavily on infrastructure, the multi-storey buildings at the town Centre still lack adequate space for parking due to associated high urbanization cost of land hence necessitating the need for deep excavation.

1.3 Objective

1.3.1 General Objectives

The research attempts to design a permanent anchored secant pile wall using the available soil data for the new Commercial Bank Headquarter Site for Ethiopia. The general objectives are:

- To design the anchored pile retaining wall based on excavation height, soil conditions and loading conditions
- To carry out parametric studies on the anchored secant pile wall by varying different parameter when modelling for static and dynamic loading condition.

1.3.2 Specific objectives

The specific objectives of the study were set out as follows:

- To carry out parametric studies on permanent anchored secant pile wall by varying pile length, pile diameter and spacing between anchors under static and dynamic load condition.
- To determine the seismic response of the anchored secant pile to strong earthquake ground motions.

1.4 Methodology

Firstly, the fundamental theory and literature which will be used in the report are described. The data for the case of the New Commercial Bank Headquarter for Ethiopia was collected. This data included the geotechnical investigation and geophysical investigation report. After the available literature and data has been collected respectively, soil characterization was done in order to determine the model parameters. The secant pile wall was used in the parametric study by varying specific parameters; length of the pile, diameter of pile, and spacing between anchors for both static and dynamic load conditions.

For seismic response analysis, an appropriate dynamic modulus of soil was determined to prescribe the relationship between the stresses and shear strain of the soil. The real accelerogram for strong ground motion of various earthquake histories was used to simulate the earthquake to the secant pile.

The data resulting from parametric studies and the earthquake loading was analyzed and discussed. The whole process was documented in the final report together with the important conclusions and recommendations. Figure 1.2 shows the methodology for the research.

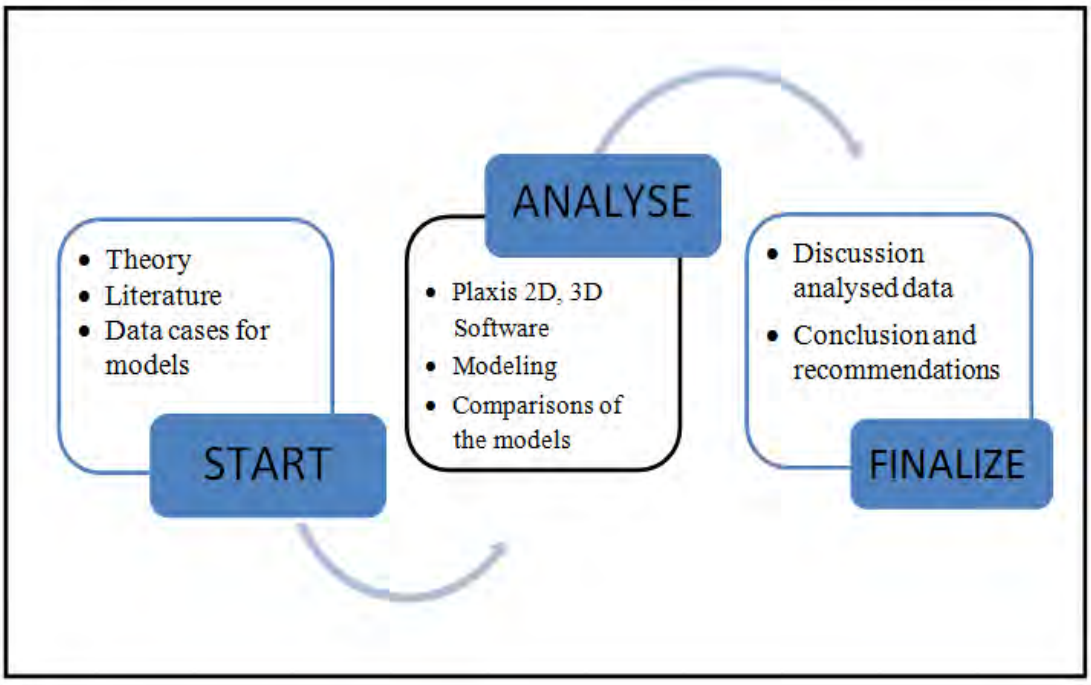

Figure 1.2: Work approach for this research study

1.5 Limitations

There were various influences in the research that are unavoidable and to deal with the interaction between the structure and the soil was difficult to model. Among the soil parameters, the task of incorporating the soil stiffness was very difficult. The soil stiffness used for modelling had to be accurately determined this is because low stiffness values would lead to excessive displacements and vice versa which does not represent reality.

1.6 Thesis Structure

The thesis is structured in to six Chapters. The first Chapter addresses the introduction including the background, problem statement, research objectives, methodology and limitations of the research. Chapter 2 gives the review of previous works, deep excavation systems, review of seismicity to which objective 2 refers. Chapter 3 describes the modelling process and parameters used. Chapter 4 presents parametric studies on secant pile walls for various secant pile wall diameter, pile length and pile spacing under dynamic and static loading and addresses the set specific objectives. Chapter 5 gives discussion of results and Chapter 6 presents the conclusion and recommendations for the future works.

Chapter 2 Literature Review

2.1 Introduction

This chapter serves as a review of the previous studies of secant pile wall design, excavation, and seismicity in Ethiopia.

2.2 Previous Literature Reviews

Perk, summarized information from case histories on ground settlements adjacent to excavations the results indicated that settlements next to deep excavations are correlated to soil types. As shown in Figure 2.1 the settlement is classified in to three zones of settlement profiles based on soil condition and workmanship.

The results further, indicated that wall movement for excavation in sand and gravel or very stiff to hard clay are usually less than 0.4 percent of the excavation depth. The result also indicated that wall movement for excavation in soft soil averaged about 1 percent of excavation depth [20].

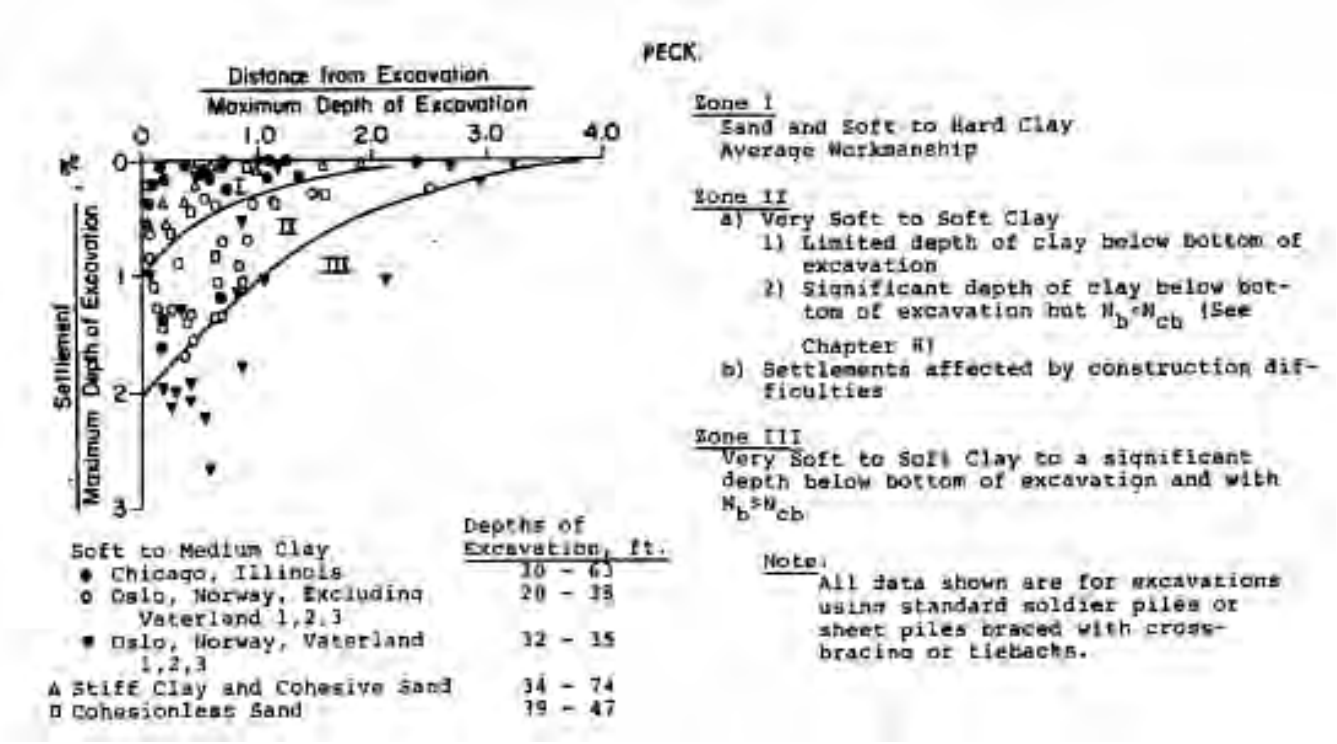

Figure 2.1 Summary of settlements adjacent to open cuts in various soils, as function of distance from edge of excavation [20].

Clough and O'Rourke observed that the pattern of settlements next to excavations is influenced by the soil type. The plot for normalized settlement envelopes proposed for estimating vertical pattern of settlement next to excavation [5].Based on several case histories, Clough and O'Rourke (1990) suggested that the settlement profile is triangular for an excavation in sandy soil or stiff clay. The maximum ground settlement will occur at the wall. The non-dimensional profiles are given in Figure 2.2(a) and 2.2(b),which shows that the corresponding settlement extends to about $2H_e$ and $3H_e$ for sandy soil and stiff to very hard clay respectively. For an excavation in soft to medium clay, the maximum settlement usually occurs at some distance away from the trapezoidal shape of the settlement tough as indicated in Figure 2.2(c).

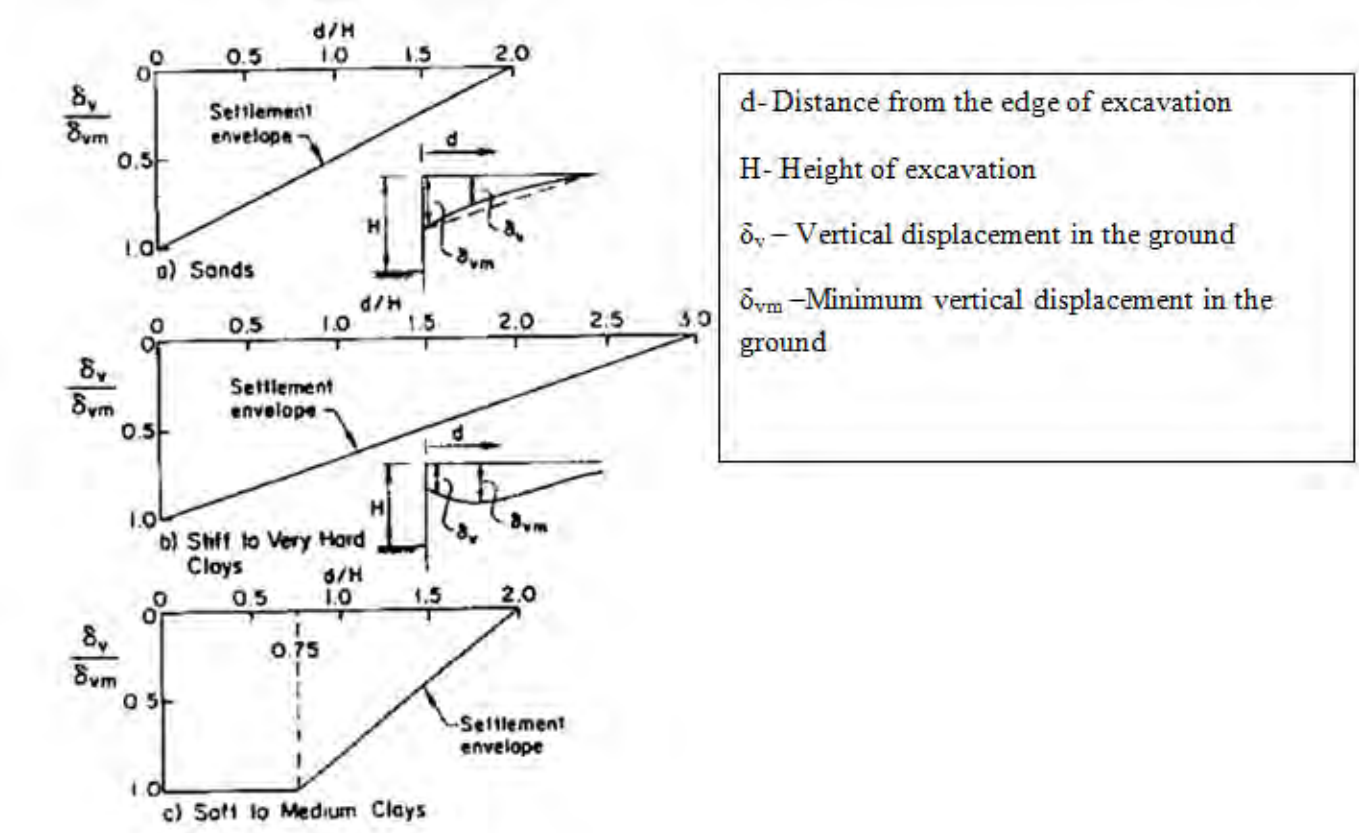

Figure 2.2 Dimensionless settlement profile recommended for estimating the distribution of settlement adjacent to excavations in different soil types [5].

2.2.1 Large initial lateral soil stresses can adversely affect deep excavation

Perk, noted that basal failure could occur in excavation in soils with large initial lateral stresses. Peck also noted that ground next to deep excavations in stiff over consolidated clay might rise instead of settling [20].

Clough and O'Rourke also pointed out that movements in the anchorage zone for tie back walls could occur in over consolidated clays with high lateral stresses [5].

The system stiffness is a function of the wall flexural stiffness, average vertical separation of supports, and unit weight of water which is used as normalizing parameter. Figure 2.3 shows plot of system stiffness and various Factor of safety. The family of curves in the figure is based on average condition, good workmanship, and the assumption that cantilever deformation of the wall contributes only a small fraction of the total movement. A method for estimating cantilever movement is also recommended by Clough et al. to be added directly to those predicted by the

Figure 2.3

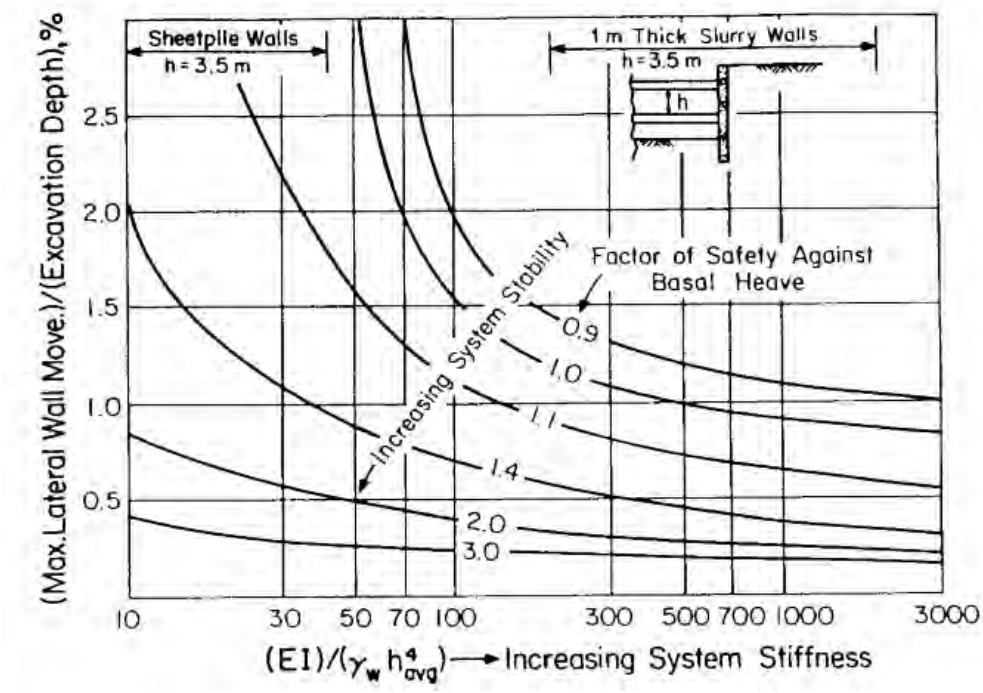

Figure 2.3 Chart for estimating maximum lateral wall movements and ground surface settlements for support systems in clays [5].

2.2.2 Moormann's Database

Moormann, had carried out extensive empirical studies by taking 530case histories of retaining wall and ground movement due to excavation in soft soil (C_u< 75kPa) . It was concluded that the ground conditions and excavation depth H are found to be the most influential parameters for deformation due to excavation [16]. The location of maximum horizontal displacement is at 0.5H to 1.0H below the ground Figure 2.4 and Figure 2.5. The retaining wall and ground movements seem to be largely independent of the system stiffness of the retaining system

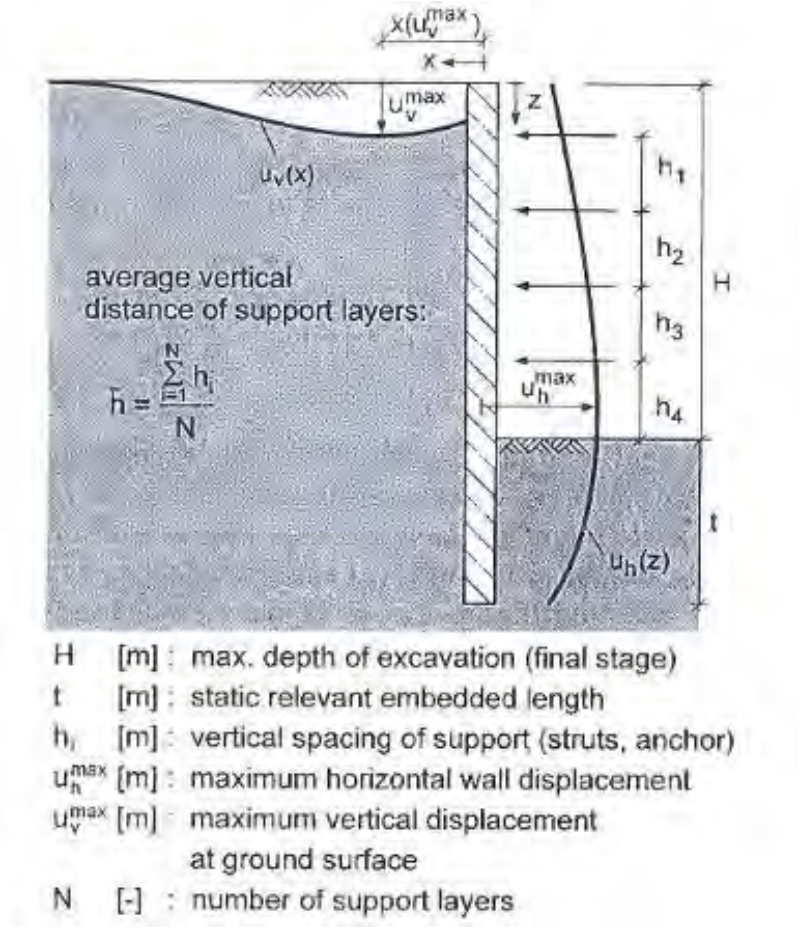

Figure 2.4 Definition of symbols by Moormann [16].

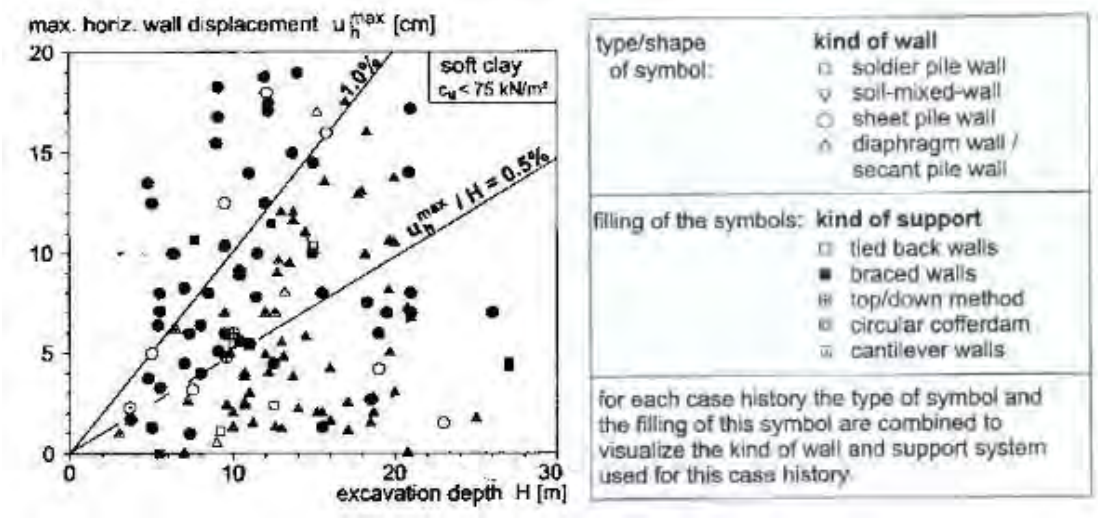

Figure 2.5 Variation of maximum horizontal displacement with excavation depth following [16]

The retaining wall and ground movements seem to be largely independent of the systems stiffness of the retaining system. Figure 2.6 shows variation of normalized horizontal displacement with the system stiffness of the retaining structure.The large scatter was observed and calculated factor of safety of about 1 could lead to observed maximum wall displacement w_{max}/H as low as 0.1% even when the value expected by Clough et al. was about 1% even for the system stiffness support system.

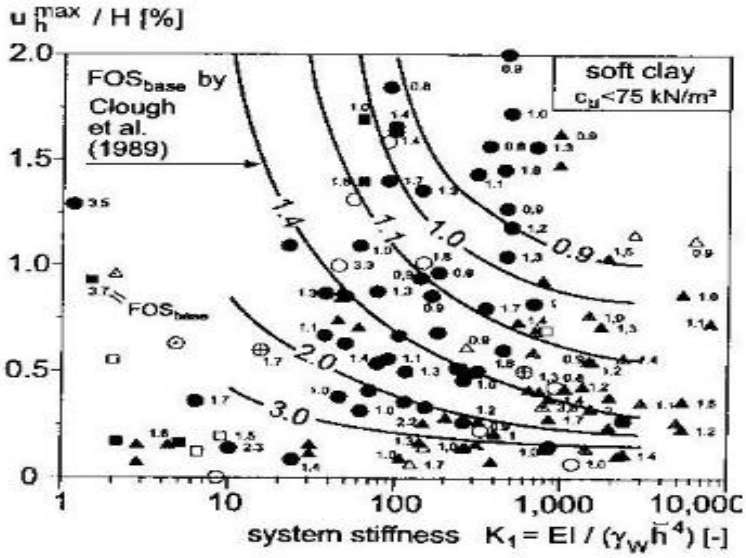

Figure 2.6 Variation of normalized maximum horizontal displacement with system stiffness following [16] .

2.3 Effect of deep excavation

The effect of excavation geometry such as excavation width, depth of the firm stratum, the effect of wall stiffness and the effect of wall embedment depth have been carried out by various researchers:

Ng (1998) reported field measurements of a 10m excavation in over-consolidated stiff-fissured gault clay lion yard, Cambridge. The field monitoring programme included lateral total earth pressure and pore water pressure on both sides of the wall, prop load lateral wall displacement, ground settlement behind the wall and basal heave inside excavation. The field measurements revealed that due to construction of diaphragm wall, a significant reduction of lateral total earth pressure at the soil wall interface is resulted. The piling operation inside the site caused a negligible reduction of lateral earth pressure. Due to low lateral stress in the ground before the main excavation, relatively low prop load and lateral wall displacements are resulted during excavation. The reduction of lateral earth pressure due to excavation was substantially less than that induced by the diaphragm walling [17].

Hashash and Whittle (1996) carried out a series of two dimensional numerical parametric studies to study effects of wall embedment depth and prop spacing on ground deformations due to multi-propped excavations. The research at the Massachusetts Institute of Technology (MIT) has developed a series of generalized rate independent models for clay based on the theory of incremental linear elastro-plasticity. MIT-3 model, describes the rate independent behavior of normally to moderately over consolidated clay (OCR$<$8).Constitutive model (MIT-E3) adopted in the numerical analyses is capable of considering anisotropic stress-strain relationship, stress path dependency and strain dependency of clay. The model has additional features; small strain nonlinear elasticity using a closed hysteric loop and bounding surface plasticity. Computed results indicated that wall length has minimal effect on the pre-failure deformation for excavations in deep layers of clay, but does not have a major effect on the location of failure with in the soil. Use of very deep walls can improve base stability. However; large bending movements can be resulted and may cause flexure failure of the retaining wall. Not only is basal affected by final excavation depth, but also influenced by vertical prop spacing. Larger vertical prop spacing can result in additional basal heave [10].

Jen (1998) carried out numerical parametric studies to study effects of excavation geometry, retaining system and stress history of clay on ground deformations due to excavation. The computed results revealed that distribution of ground deformation is significantly affected by depth and hard stratum below soft clay. While magnitude of ground deformation is governed by excavation width, excavation depth, and stress history of clay. Based on the computed settlement trough behind the wall new design charts are proposed to correlate ground settlement to excavation. Depth of the rock was found to be the key parameter affecting the distribution of ground movements, excavation width, excavation depth and uncertainties in the stress history profile and support stiffness were major factors contributing to the magnitude of the displacement [13].

2.4 Effect of supporting structure

Mana and Clough carried out parametric studies on the effect of wall stiffness and strut spacing, the effect of strut stiffness, and the effect of excavation geometry such as excavation width and depth of the underlying firm layer, the effect of strut preloading and calculation of elastic soil stiffness on the excavation induced deformation. Increasing the wall bending stiffness or decreasing strut spacing decreases movement. This effect is more significant when the factor of safety is low. Increasing the strut stiffness reduces movement, though the effect shows diminishing returns at very high stiffness. Movement increases as excavation width and depth to an underlying firm layer increases. Use of preloads in the struts reduces movement, although there is diminishing return effect at higher preloads. Movement levels are strongly influenced by the modulus. Higher modulus leads to smaller movement [15].

2.5 Secant Pile Walls

Secant piles are innovative way of constructing retaining walls and are formed by a series of interlocking bored concrete piles. The usual practice is to construct alternative piles along the line of the wall leaving a clear space of a little under the diameter of the required intermediate piles. The exact spacing is determined by the construction tolerances which can be achieved. These initially placed piles do not have to be constructed to the same depth as the intermediate piles which follow, depending on the way in which the wall has been designed and reinforced.

Concrete is added and before it has fully set the intermediate holes are drilled along a parallel, but slightly offset, line so that the holes cut into the first piles. The intermediate piles are placed

through a heavy casing whose cutting edge is toothed and enables the casing to cut into the concrete of the initial piles on either side. Subsequent concreting results in a continuous wall [5].

2.5.1 Methods used in Secant Wall Construction

Secant piles can be constructed either with conventional drilling methods or through the use of Continuous Flight Auger (CFA) techniques computer monitoring of the pile installation process is essential for quality assurance. Secant pile walls typically include both reinforced secondary (B) and unreinforced primary piles (A). The secondary piles overlap the primary piles, with the primary piles essentially acting as concrete lagging Figure 2.7. The reinforcement in the secondary piles generally consists of rebar cages or steel beams. Secant pile wall formed by the primary (female) and secondary (male) piles by drilling the piles to the specified diameter and required depth. The secant pile wall is constructed in two stages. The primary piles will be constructed at Stage 1 with the specified strength of mass concrete and the secondary piles will be constructed at stages with the required concrete strength after the reinforcement cage is lowered into the bored holes. The secondary piles are positioned between the primary piles and secant with the primary piles in order to form the interlocking joint [12].

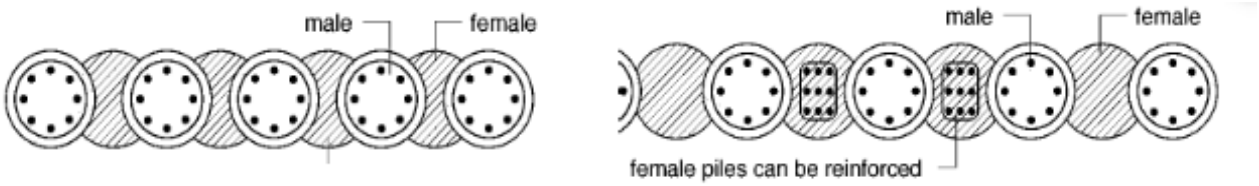

Figure 2.7: Typical secant pile wall arrangement with female (primary) and male (secondary) piles forming hard/soft walls (left) and hard/hard walls (right) after Suckling et al. (2005)

2.5.2 Secant Piles-merits and demerits

The main advantages of secant pile walls are: Increased construction alignment flexibility, increased wall stiffness compared with sheet piles, can be installed in difficult ground (cobbles/boulders), they are primarily used in unsuitable ground conditions or where there is a high water table conditions without excessive dewatering. Properly placed columns can be as close as 3” to 5” from existing buildings, less noisy construction. Secant piled walls are preferred option near buildings, roads and other sensitive structures. Secant walls can also be used to form a continuous water tight wall which can be an added benefit for the construction of basements and underground car parks. Secant pile walls are used as permanent or temporary elements in

foundation, excavations, slope stabilization, retaining walls or hydraulic barriers. However the disadvantages of secant pile walls include: verticality tolerances may be hard to achieve for deep piles, total waterproofing is very difficult to obtain in joints, increased cost compared to sheet pile walls if depth is less than 40‟ feet deep, noise and vibration are generated, if casing is driven in lieu of hydraulically pushed and retrieved casings [4].

2.5.3 Case Histories on Secant Pile Walls

2.5.3.1 Design and construction of circular scant pile walls in soft clays in Houston Texas. The site was underlain by deep deposit of very soft to stiff clay over a layer of dense sand. The soil properties were estimated from the interpreted CPT data, as well as supplemented soil data from extensive geotechnical investigation studies conducted for other terminal facilities which was not limited to in-situ vane shear test and laboratory; triaxial, consolidation and index tests.

The subsurface conditions were explored by two piezocones, CPT-1 and CPT-2 at the center of the basin. Additional geotechnical data were available from comprehensive geotechnical investigations. In general the subsurface conditions at both basins consist of very soft to firm clays to depths about 73ft and 78ft underlain by medium dense to very dense sand followed by stiff to very stiff clays. Ground water is typically encountered at depth of about 6ft below the ground.

The soil properties were estimated from the interpreted CPT data as well supplemented soil data from extensive geotechnical investigation studies conducted for other terminal facilities which included; insitu, vane shear test, laboratory triaxial, consolidation and index test

The FE code PLAXIS V8 was used in the study.Concete secant pile wall was represented by plate elements. Figure 2.8 shows plaxis mode of the excavation. The advanced hardening soil and Mohr coulomb model were used. The reinforced concrete secant pile wall was modeled as linear elastic plate element.

FEM predict ground and support movements and also the effects of construction activities like dewatering, equipment surcharge, and stage construction on deformation and overall stability.

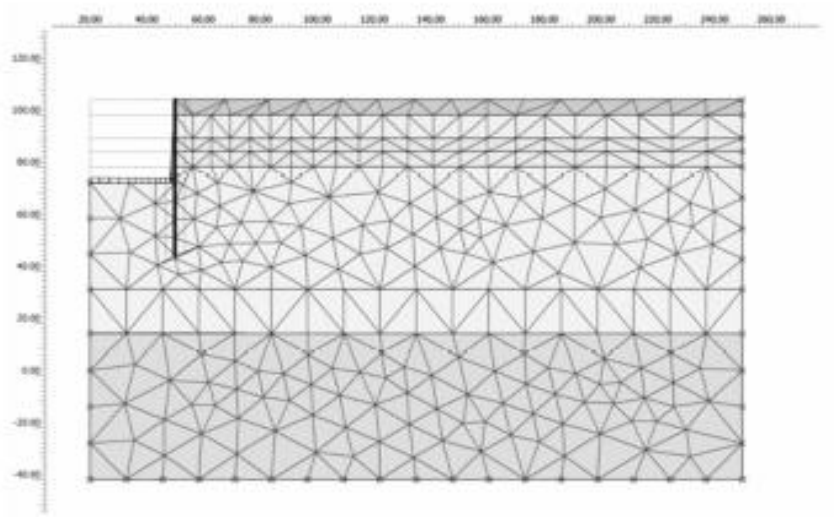

Figure 2.8: Plaxis Model of the excavation [23].

During excavation in to the saturated clays, the weight of the blocks of clay behind the retaining systems tends to displace the underlying clays towards the excavation.

Base stability for excavation in soft clays depends on height of excavation wall embedment depth; undrained shear strength of clays below the base of excavation and the unit weight of the soil. The undrained deformation (plastic) analysis was performed to evaluate base heave and corresponding wall movement during each stage of excavation. The corresponding horizontal movements were negligible as result of rigidity of the circular retention system.

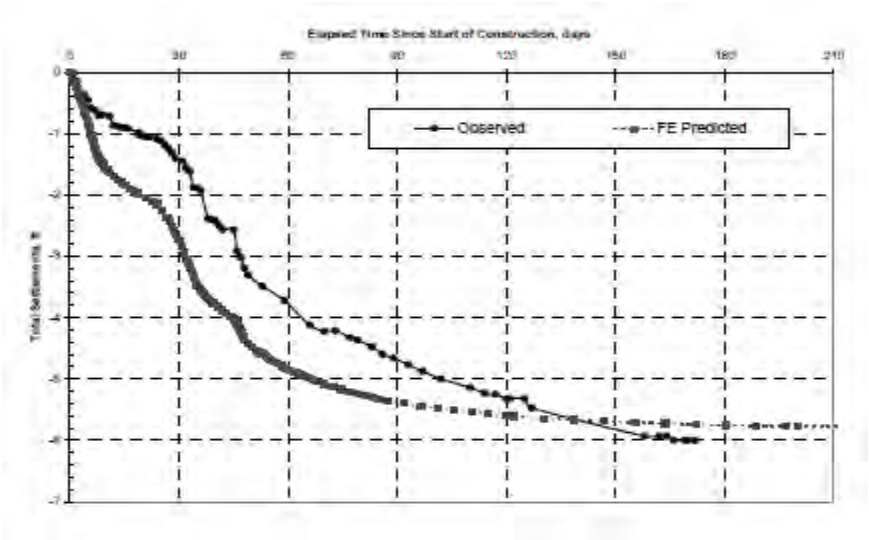

Figure 2.9: Oberved and FE predicted settlements since start of LNG dike construction [23]

Stiffness properties.The construction of impoundment basin involves excavation(unloading condition),as such soil behavior and hence the base heave magnitude will primarily be governed by its unloading modulus.The effective (drained) stiffness properties, modulus and poisson ratio,were used in undrained and drained analysis.Figure 2.9 shows reasonable agreement between the measured settlement of 6.0ft and the estimated end of primary settlement of 5.8ft [23].

2.5.3.2 Construction of Access shaft for Tunnels and Deep pipelines in Urban New Zealand with Secant piles.

The demand for shafts to provide access to pipelines at depth has grown due to the increase in the use of tunneling, pipe jacking and horizontal directional drilling (HDD).These system required effectively as driven reception pits or shafts, which provided the respective starting and finishing point of the drive. Convectional pilling equipment was used to directly bore a shaft to form shaft using secant pilling walling.

For shafts in unstable ground, high ground water level and where the diameter is greater than that achievable using large diameter bored pilling methodologies the use of secant piles can be an effective solution. The secant pile methodology comprises the formation of overlapping concrete piles. Typically alternate unreinforced or female piles are formed using lower strength concrete. The remaining piles are standard reinforced concrete male piles. The strength of the unreinforced low strength is critical to the design as it needs to be sufficient to transmit the hoop compression stresses that enable the structure to be self-supporting without any propping or waler.Based upon the shaft diameter, the hoop compression forces can be assessed from the combined earth and water pressure Figure 2.10., the low radial strain results in little reduction in earth pressure from insitu pressure value. However, from the construction point of view the low strength piles must not be strong as it can result in poor verticality. The strength of the female piles was around 20Mpa at 28days which resulted in reduced drilling rates and localized poor vertical tolerance being achieved, and the supplied slump of the approved structural mix was 140mm [12].

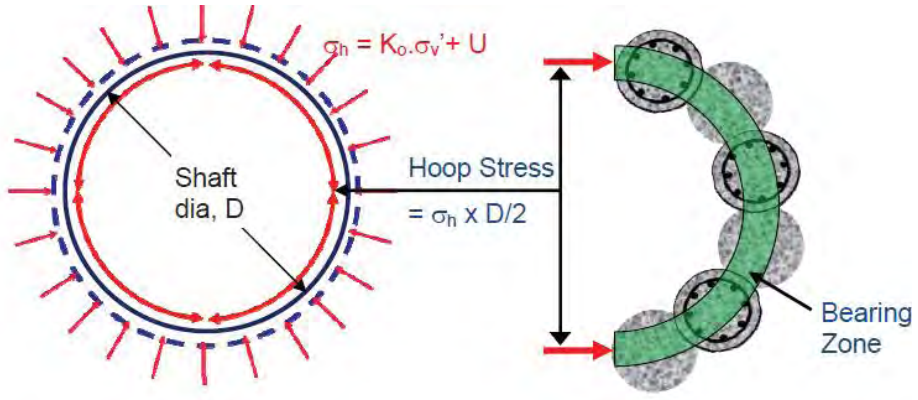

Figure 2.10:Hoop stress and vertical bearing zone [25]

Conventional crane mounted and hydraulic rigs are readily capable of drilling diameters of 2.5m and with modifications over 3.0m due to available torque and drilling tool development. At Waihi gold mine, 2.5m diameter shaft were excavated to 87m depth to provide emergency access and ventilation to the mine workings below [25].

2.6 Factors that affect the performance of excavations

Ground conditions, soil properties and wall stiffness affect the performance of deep excavations. The design includes the type of support and stiffness of the support system. The overall stiffness of the support system is calculated in terms of an effective stiffness of the system. Secant pile walls are considered stiff on the basis of rigidity of the wall element [6].It is difficult to consider all the relevant factors in the detailed analysis of the deformation of deep excavations. The semi empirical study of performance of deep excavation is a viable means to understand the associated deformation. The semi empirical studies of deformation associated with deep excavations worldwide have been conducted by a number of researchers [5 and 16].In these studies, data on wall and ground deformation were categorized based on the ground conditions mainly consisting of sedimentary clayey soil and sand. In each category of ground conditions, the data were analyzed to study the effects of excavation depth, type of support and stiffness of the support system on the magnitude of the wall deformation, and ground settlement of these 14 deep excavations were collected and analyzed. The magnitude of deformation relationship between the lateral wall deflection and the ground surface settlement and effect of the stiffness of the support system on lateral wall deflection were studied and compared with other relevant case histories worldwide. Typical profiles of wall and ground movement have been discussed by [5]

and are shown in Figure 2.11. In excavation with no lateral support or insufficient stiffness in the support at the top during the initial stage of excavation, the wall deforms as a cantilever and the resulting distribution of ground settlement is triangular Figure 2.11b.As excavation proceeds, the upper part of the wall is restrained and the wall deforms inward near the excavation level(deep inward movement).The combination of the cantilever and deep inward movement pattern results in the cumulative movement pattern Figure 2.11(a).The distribution of ground settlement is triangular if cantilever wall movement predominates, while it is trapezoidal if deep inward wall movement predominates.

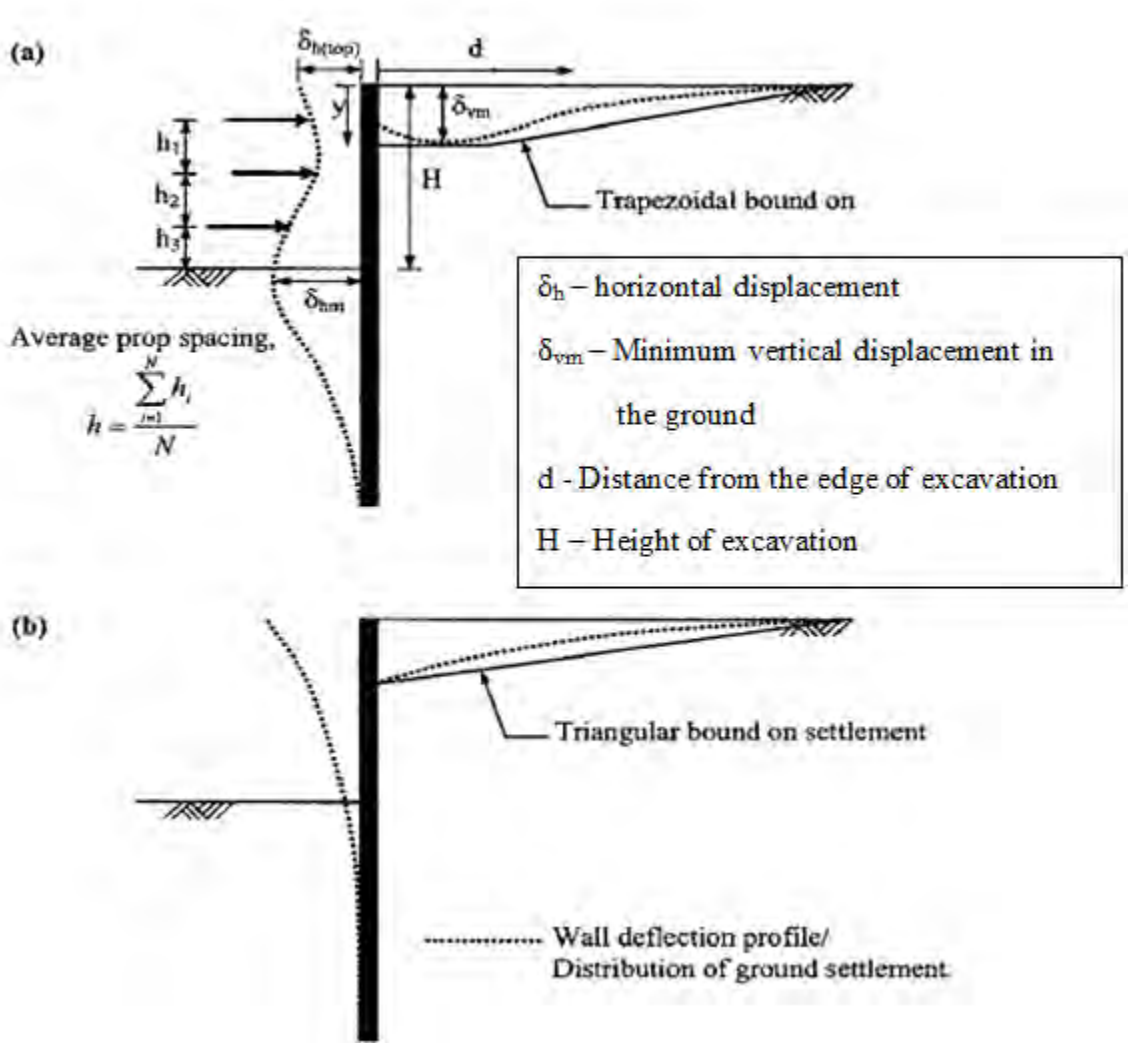

Figure 2.11: Typical profiles of wall and ground movement for anchored wall [6].

2.7 The Design of Composite Materials and Structures

A composite material is a material in which two or more distinct materials are combined together but remain uniquely identifiable in the mixture. Reinforced concrete (a mixture of steel rod and concrete (itself a composite of rock particles and cement).Composite materials are successfully replacing conventional metals in many engineering applications. Light weight, high specific strength and stiffness, affordability and ease of manufacturing are few of the advantages of composite materials. Adoption of composite materials in many engineering applications necessitates a thorough understanding of the strength and mechanics of materials.

First, the numerous materials related variables that contribute to the mechanical and physical properties of the composite material were identified.
Secondly, the appropriate physical and mathematical models that describe how the properties of the individual components of the composite are combined to produce the properties of the required composite material. The composite has tendency to behave elastically almost to the point of failure. If the composite material is to stay in equilibrium then the force is applied to the composite as a whole, F must be balanced by an equal and opposite force in the fibre, F_f and the matrix F_m.

The mechanics of material approach can be considered the simplest and easiest to apply. Several equations have been developed according to this approach. The most widely used are: the rule of mixtures (ROM), and Halpin-Tsai (H-T) equations. The basic assumptions used for the development of (ROM) and (H-T) equations, as well as most micromechanical approaches are: both matrix and fibres are linearly elastic, isotropic, and homogeneous, fibres are perfectly aligned and spaced, matrix is void free, and bonding between matrix and fibre is perfect.
Consider an aligned continuous fibre composite with reinforced metal matrix composite or thermoplastic matrix composite Figure 2.12.At low volume fractions of the fibres, the fibre first fails then breaks and the load transfer to matrix with reduced cross section takes place and there occurs sudden jump in stress depending on the increase in the stress matrix.

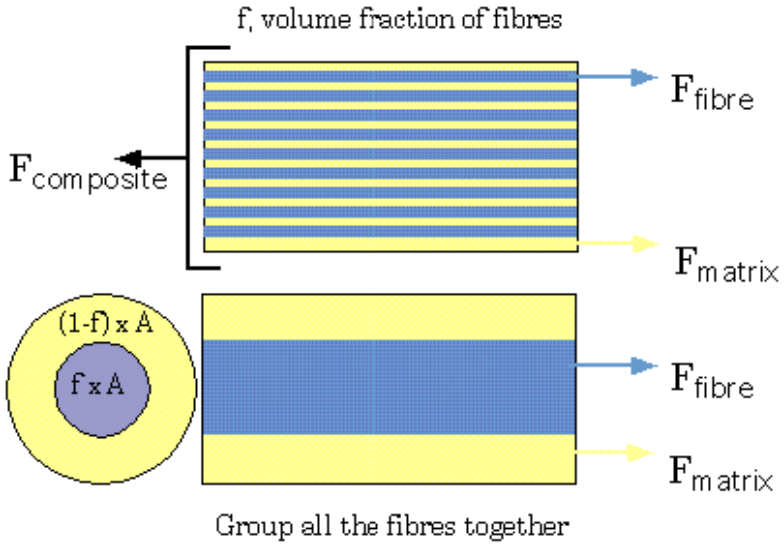

Figure 2.12: Aligned continuous fibres

The cross sectional area of the composite occupied by the fibres is just f, the volume fraction of the fibres multiplied by the cross-sectional area of the composite itself - "A" - i.e. f.A.
Similarly the force on the matrix is just the stress in the matrix multiplied the cross-sectional area of the matrix in the composite, i.e. (1-f).A.
So the stress in the composite is just the sum of the stresses in the fibre and the matrix multiplied by their relative cross-sectional areas.

$$F = F_m + F_f \tag{2.1}$$

The stress in the fibre and the stress in the matrix are not the same. Thus, by applying Hooke‟s Law, which states that the stress (or Force) experienced by a material is proportional to the strain (or deflection).

$$\sigma = E\varepsilon \tag{2.2}$$

For compatibility, the strain, must be the same in both the fibres and the matrix otherwise holes would appear in the ends of the composite as we stretched it. This is known as the **Isostrain rule**.

$$E\varepsilon = (1 - f)E_m\varepsilon + fE_f\varepsilon$$

$$E = (1 - f)E_m + fE_f \tag{2.3}$$

The rule of mixtures has proven adequate for tensile modulus(E) in to the axial direction, isostrain rule of mixtures does not work for Shear modulus (G) and bulk modulus (k). Instead, these moduli depend on the phase morphology of fibres.

$$G = G_m\left(\frac{G_f(1+f)+G_m(1-f)}{G_m(1+f)+G_f(1-f)}\right) \tag{2.4}$$

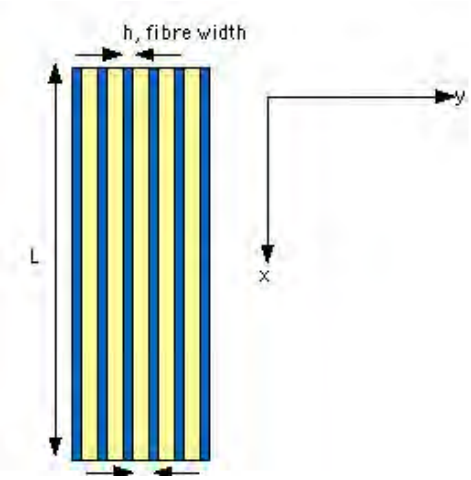

Figure 2.13: Stiffness perpendicular to the fibres

In a fibrous composite with the applied stress aligned perpendicular to the fibres, the stress is transferred to the fibres through the fibre matrix interface and both the fibre and the matrix experience the same stress Figure 2.13. If the matrix and fibre have different elastic properties then each will experience a different strain and the strain in the composite will be the volume average of the strain in each material. Since the stress is the same in each phase this is known as the **Isostress rule** of mixtures.

The material properties of the composite material can be determined accurately by using the halpi-Tsai equations.

2.8 Halpin-Tsai Equations

The Halpin-Tsai equations are a set of empirical relationships that enable the property of a composite material to be expressed in terms of the properties of the matrix and reinforcing phases together with their proportions and geometry. These equations were curve fitted to exact elasticity solutions and confirmed by experimental measurements - they work well but the parameter ξ has no scientific basis nor is it related to any material or geometric property. Halpin and Tsai showed that the property of a composite P_c could be expressed in terms of the corresponding property of the matrix P_m and the reinforcing phase (or fibre) P_f using the following relationships [9]

$$P_c = P_m\left(\frac{1+\xi\eta f}{1-\eta f}\right) \tag{2.5}$$

$$\eta = \frac{\left(\frac{P_f}{P_m}\right)-1}{\left(\frac{P_f}{P_m}\right)+\xi}$$

The factor ξ is used to describe the influence of geometry of the reinforcing phase on a particular property. This factor is different for different properties in the same composite.

The first modulus E_1, is given by [14]:

$$E_1 = fE_f + (1-f)E_m \tag{2.6}$$

The strength of a unidirectional composite σ_c ,can be obtained according to the rule of mixtures from the equation

$$\delta_c = \delta_f V_f + \delta_m(1-V_f) \tag{2.7}$$

These equations are based on the assumption of Isostrain, i.e.

$$\varepsilon_c = \varepsilon_f = \varepsilon_m$$

This assumption is presented by springs in parallel, model.

Equation (2) assumes no interaction between fibres and matrix. Thus, each constituent contributes its full capacity to the strength of the composite.

The second modulus, E_2 according to the rule of mixtures is given by transverse loading; i.e load is applied perpendicular to fibre direction. The stiffness of the composite, measured perpendicular to the fibres increases much more slowly than stiffness measured parallel to the fibres as the volume fraction of fibres is increased. Since the properties of the composite are different in different directions, the composite is anisotropic.

E_2 assumes is stress i.e.

$$\delta_c = \delta_f = \delta_m$$

Modulus E_2 is given by [16]

$$E_2 = \frac{E_f E_m}{fE_m + (1-f)E_f} \tag{2.8}$$

2.9 Potential Geotechnical Failures

2.9.1 Rotational Failure

Lateral earth pressures acting on retaining walls tend to produce lateral forces that can result in toppling of the wall. The wall must balance active and passive earth pressures about the potential rotation point such that resisting moment exceeds driving moment. In a saturated soil, undrained shear strength (rather than effective stress) is used in the calculation of rotational stability [21].

2.9.2 Translational Failure

Similar to the rotational failure of the wall resulting from excess overturning moments, a translational failure can result when lateral driving forces exceed resisting forces. In a saturated soil, undrained shear strength (rather than effective stress) is used in the calculation of translational stability [21].

2.9.3 Global Stability Failure

Circular slump failures are of particular concern to geotechnical engineers. These slides tend to be much larger in scale than translational or rotational wall failures, and are difficult to predict due to variability in the radius of rotation. To calculate for global stability (also known as deep-seated failure), the expected slide area is cut into slices and assessed piecewise. Unlike the rotational and translational failures mentioned above, global stability is not determined by parameters of the retaining wall, but rather by parameters of the soil itself. The primary

parameters are the unit weight and friction angle. Such soil failures are usually observed after periods of extended rainfall. The retained soil becomes saturated, and experiences an increase in pore water pressure which in turn reduces the effective stress in the soil. A left-ward shift in the Mohr-Coulomb failure envelope can result in exceedance of resisting forces, and cause the entire mass of soil to rotate, often without warning and in a catastrophic manner. The soil conditions present at the gardens are some of the stiffest for geotechnical projects [21].

The anchor can provide the required stabilizing forces which are in turn, transmitted back in to the soil at a suitable distance behind the active soil zone loading the wall implying that the anchor bond length must extend in to the ground to intersect any potentially critical failure surface which might pass behind the anchors and below the base of the wall as illustrated in Figure 2.14. The required depth to which anchors must be installed in the soil should be determined based on the location of the deepest potential failure surfaces that have insufficient factor of safety without any anchor force.

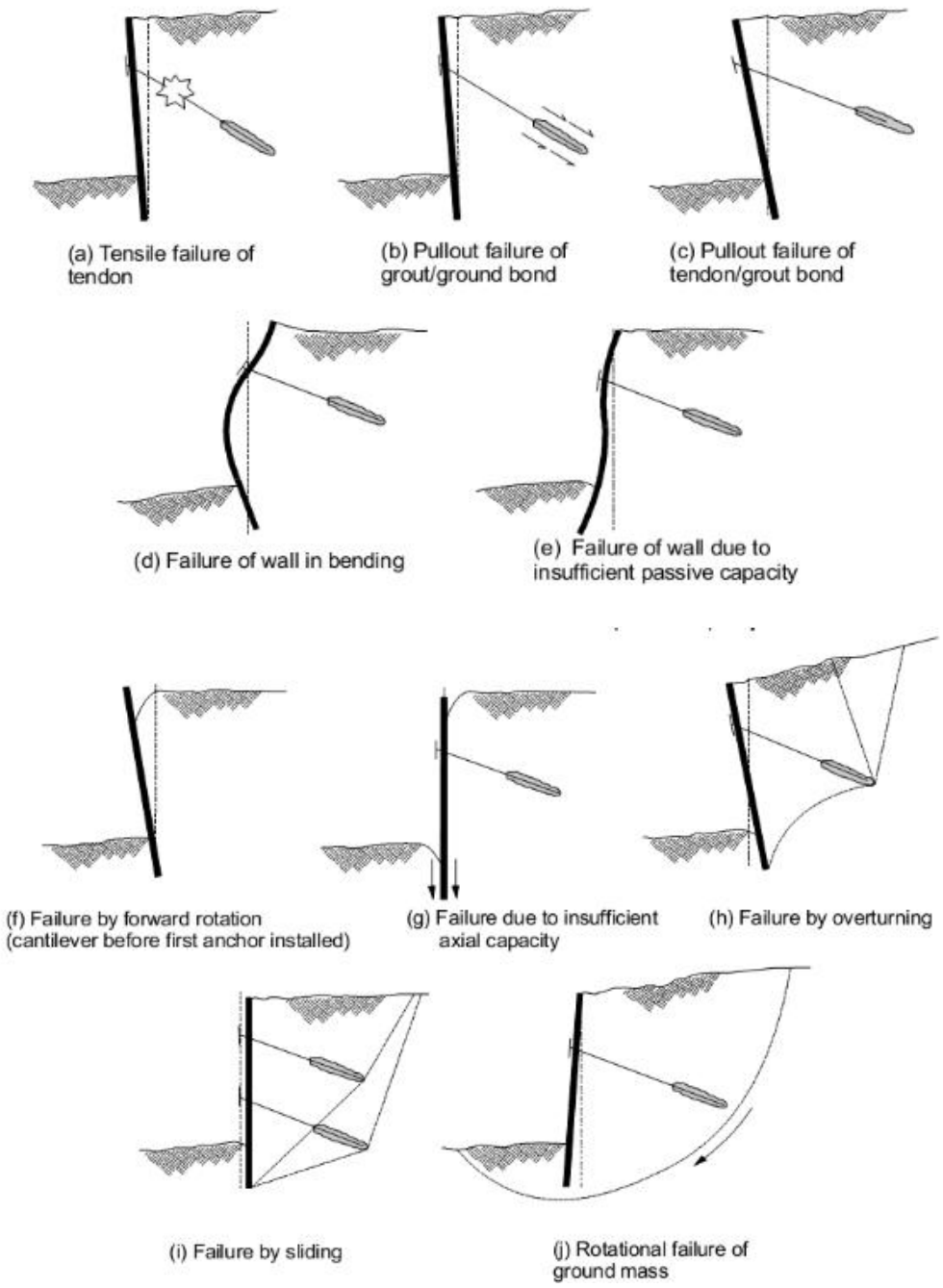

Figure 2.14: Failure modes for tie-back retaining walls [Source: Sabatini et.al, 1999]

2.10 Constitutive Models

Soil is a complicated material that behaves non-linearly and often shows anisotropic and time dependent behavior when subjected to stresses. Generally, soil behaves differently in primary loading, unloading and reloading. It exhibits non-linear behavior well below the failure condition with stress dependent stiffness. Soil undergoes plastic deformation and is inconsistent in dilatancy and also experiences small strain stiffness at very low strains and upon stress reversal. In addition to soil behavior, its failure in three dimensional state of stress is extremely complicated. Numerous criteria have been devised to explain the condition for failure of a material under such loading state.

Currently, various constitutive models for the soil have been developed. These models cover a wide range of soil features such as anisotropy, cyclic loading, creep etc. The selection of a constitutive model for a geotechnical application depends on the mechanical properties of the soil. (i.e permeability, stiffness and strength), previous history on the mechanical properties of the soil and the stress changes that will occur in feature [26].

In the finite element analysis, reliable predictions can be achieved by using an appropriate constitutive model for a particular geotechnical problem. In general, the criterion for the soil model evaluation should always be a balance between the requirements from the continuum mechanics aspect, the requirements of realistic representation of soil behavior from the laboratory testing aspect, convenience of parameter derivation and simplicity in computational application. The application of some constitutive models in Plaxis finite element model and some parameters from correlation and laboratory testing are briefly discussed below:

- Linear Elastic Model(LE)
- Mohr Coulomb Model(MC)
- Hardening Soil Model with small stiffness(HS Small)
- Soft Soil Model(SS)
- Soft Soil Creep Model(SSC)
- Modified Cam Clay Model(MCC)

2.10.1 Linear Elastic Model (LE)

The linear Elastic Model (LE) is based on the Hook‟s law of isotropic elasticity. It only involves two basic parameters Young‟s modulus (E) and poisson ratio ($\mathcal{V}$).The LE Model is not suitable

to model soil because soil behavior is highly nonlinear and irreversible, but it is appropriate to model stiff volumes in soil like concrete walls.

2.10.2 Mohr Coulomb Model (MC)

The Mohr Coulomb Model (MC) is a linear elastic and perfectly plastic model. It involves five parameters, both elastic and plastic behavior parameters i.e Young‟s modulus (E) and Poisson‟s ratio($\mathcal{V}$) for soil elasticity, friction angle($\boldsymbol{\phi}$) and cohesion(c), for soil plasticity and the ditatancy angle($\boldsymbol{\psi}$).

Although the increase of stiffness with depth can be taken in to account. The stiffness behavior below the failure line is assumed to be linear elastic according to Hook‟s law.Hence,the model does not accurately predict deformation behavior before failure, especially in situation where the stress levels are changing or multiple different stresses paths are allowed. For tunnel construction, the MC model predicts too wide settlement trough. As far as its strength behavior is concerned, this model is suitable to analyze the stability of dams, slopes and embankments. However, the model does not show softening behavior after peak strength. Soft soils like normally consolidated clays, generally show a decreasing mean effective stress during undrained shearing, whereas the Mohr-Coulomb model would predict a constant mean effective stress in this case, which results in an over prediction of the shear strength [3].

2.10.3 Hardening Soil Model (HS)

The Hardening Soil (HS) model is a true second order model for soils in general (soft as well as hard soils) for most types of applications. The model, in an undrained loading shows a reduction in mean effective stress for soft soils and an increase in mean effective stress for hard soils, respectively. This model can accurately predict displacements and failure for general types of soils in various geotechnical applications. The model does not include anisotropy and time dependent behavior [3].

2.10.4 Hardening Soil Model with small stiffness (HS small)

The Hardening Soil model with small strain stiffness (HS small) is a modification of the Hardening Soil Model. At low strain levels, most soils show a higher stiffness than at engineering strain level, and the stiffness varies non-linearly with strain. This behavior is captured by HS small model.

2.10.5 Soft Soil Model (SS)

The Soft Soil Moddel is a Cam-Clay type of model for predicting the behavior of normally consolidated soils (clays, clayey silts and peat).The SS model does not over predict the shear strength for over consolidated states of stress. The SS model works well in primary loading conditions, such as embankment or foundation construction. The model has no advantages over the Mohr-Coulomb model in unloading situations, such as excavations or tunnel construction [3].

2.10.6 Soft Soil Creep Model (SSC)

The Soft Soil Creep Model (SSC) is suitable for prediction of creep related settlement of embankments and foundations in soft soils (normally consolidated clays, silt and peat).The SSC model over predicts the range of elastic behavior in unloading situations such as excavations and tunnel construction [3].

2.10.7 Modified Cam Clay Model (MCC)

The Modified Cam Clay Model is an elastic plastic strain hardening model where the non-linear behavior is modeled by means of hardening plasticity. The MCC model uses a logarithmic relationship between the mean effective stress (p′) and the void ratio (e).Virgin compression and recompression lines are linear in the e-inp‟ space, which is most realistic for near-normally consolidated clays Figure 2.15. Hence, the model involves a linear stress-dependency of the stiffness, which is more realistic for normally consolidated clays. For over-consolidated soil, the MCC model predicts an unrealistic elastic range which leads to an unrealistic high peak strength, followed by softening behavior until the critical state is reached. The MCC model is more suitable to describe deformation than failure especially for normally consolidated soft soils. The model also performs best in applications involving loading conditions such as embankment or foundation. However, the MCC model is not suitable for high over-consolidated soils. The model is suitable for soft soils such as normally consolidated clays [3].

However, the short comings of the MCC model are:

- It assumes soil to be isotropic, whereas in natural state soils are anisotropic due to the mode of deposition.

- It over estimates the failure stresses on the dry side (i.e states to the left of the critical state line).It predicts peak strength in undrained heavily over-consolidated clay, which is not usually observed in experiments.
- It can not successfully predict the behavior of sand, because sand does not closely follow the associated flow rule.
- The MCC model, on primary loading produces large plastic strains, but on subsequent unloading-reloading cycles within the yield surface, only produces purely elastic strains (Hau, 2003)[11].

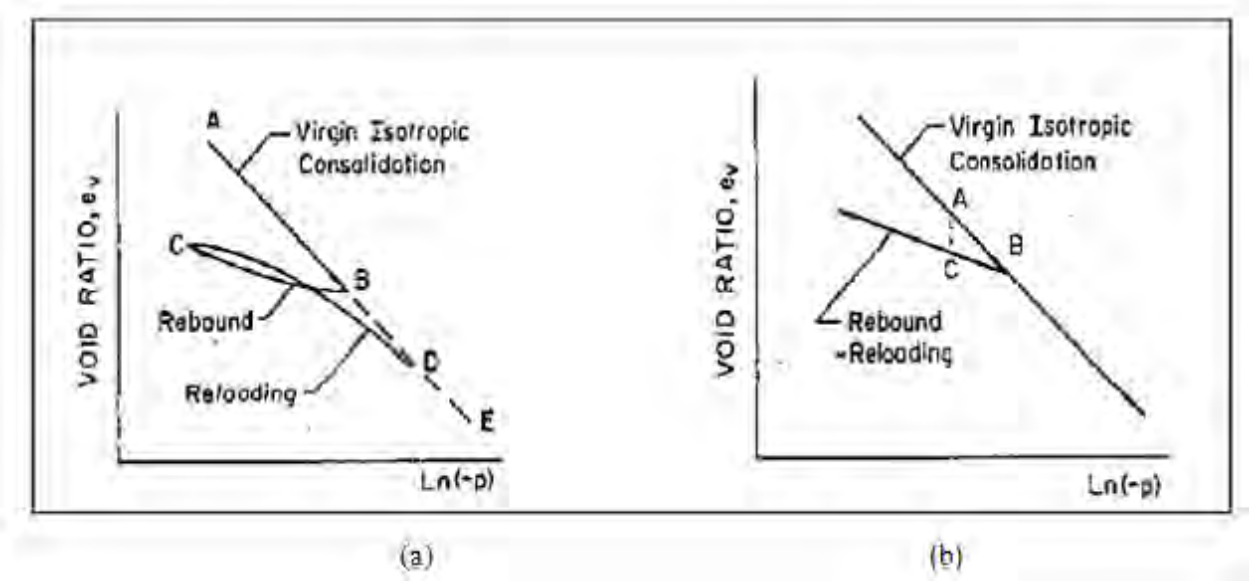

Figure 2.15: (a) Response of real soil to hydrostatic stress ;(b) Response of idealized soil to hydrostatic Stress [Source: Roscoe and Burland, 1968]

2.11 Response Spectrum

Response spectra are curves plotted between maximum response of Single Degree of Freedom (SDOF) system subjected to specified earthquake ground motion and its time period (or frequency). Response spectrum can be interpreted as the locus of maximum response of a SDOF system for a given damping ratio. Response spectra thus helps in obtaining the peak structural response under linear range, which can be used for obtaining lateral forces developed in structure due to earthquake thus, facilitates in earthquake resistant design structure. Usually response of a SDOF system is determined by time domain or frequency domain analysis, and for a given time period of system, maximum response is picked. Final plot with system time period on x-axis and response quantity on y-axis is the required response spectra pertaining to specified damping ratio

and input ground motion Figure 2.16. Same process is carried out with different damping ratios to obtain overall response spectra.

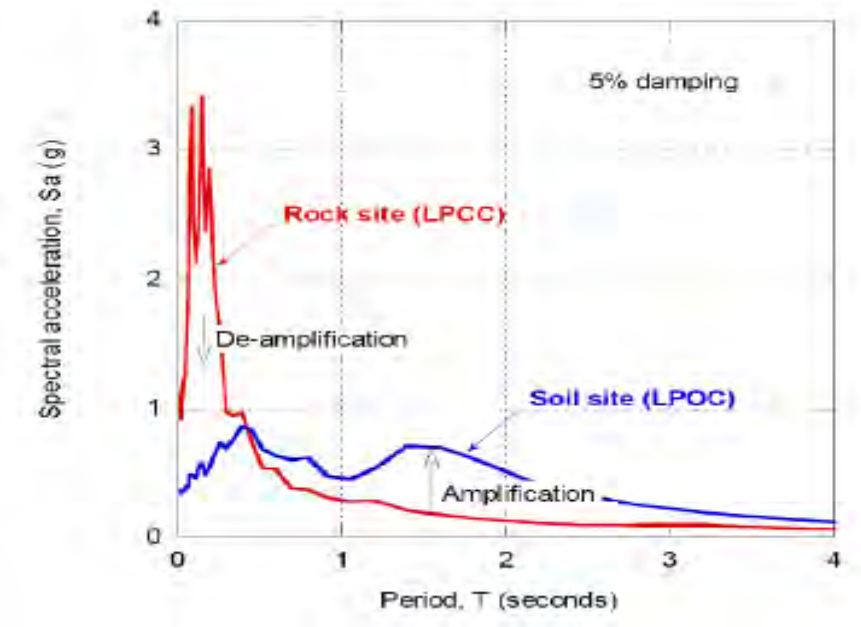

Figure 2.16: Acceleration response spectra during the 22 February 2011 Christchurch earthquake (Cubrinovski and McMahon 2011).

2.12 Recent Developments in the Definition of Design Earthquake Ground Motion

The Global Seismic Hazard Assessment Program (GSHAP) depicts Peak Ground Acceleration (PGA) with 10% chance of exceedance in 50years, corresponding to a return period of 475years.

The PGA values according to the Global Seismic Hazard Assessment Program map (GSHAP) indicates that both seismic regions and the entire size and the extent are assigned much higher PGA .The values of PGA according to GSHAP are shown in Figure 2.17.The new map indicates that the most seismic area of the country is concentrated near the Afar region and characterized by PGA of 0.216g to 0.24g. Addis Ababa city belongs to the second most seismic zone with PGA in the range of 0.1g to 0.16g.

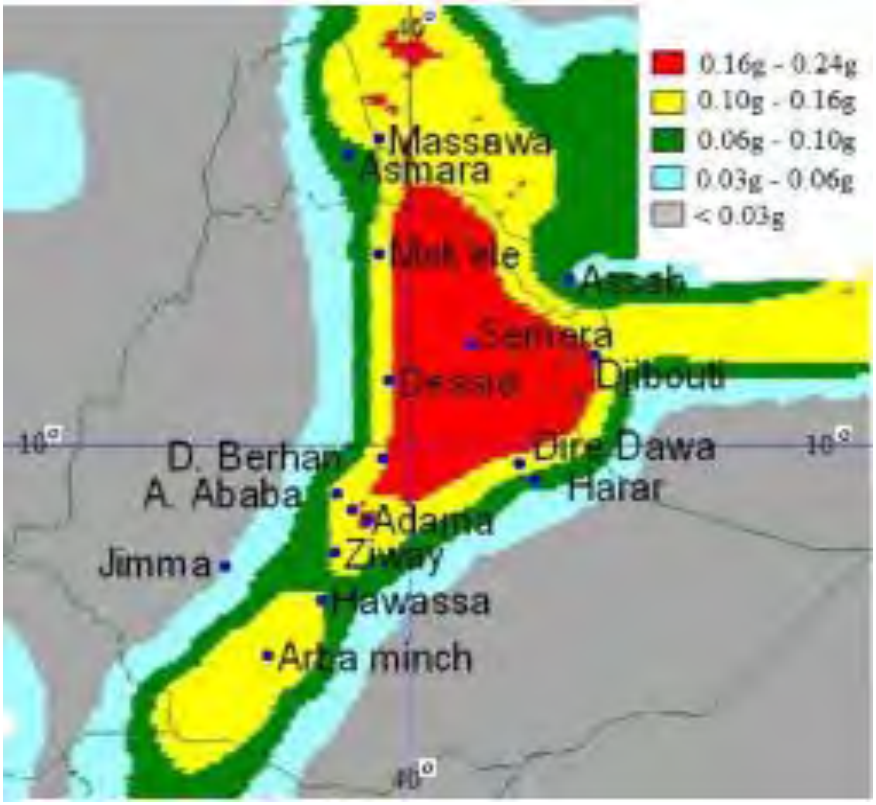

Figure 2.17: The seismic hazard map of Ethiopia based on the Global Seismic Hazard Assessment Program data for return period of 475 year (Journal of EEA, Vol.28, 2011)

Fourier amplitude and predominant periods are determined for each measurement site.The numerical value for locations between measurement sites is obtained by interpolation.Finally the seismic microzonation map of the more developed part of Addis Ababa is prepared by using Fourier amplitude and predominant period.The fourier amplitude spectra of microtremor for Addis Ababa city is shown in Figure 2.18.Similarly,the predominant period for Addis Ababa city is indicated in Figure 2.19.

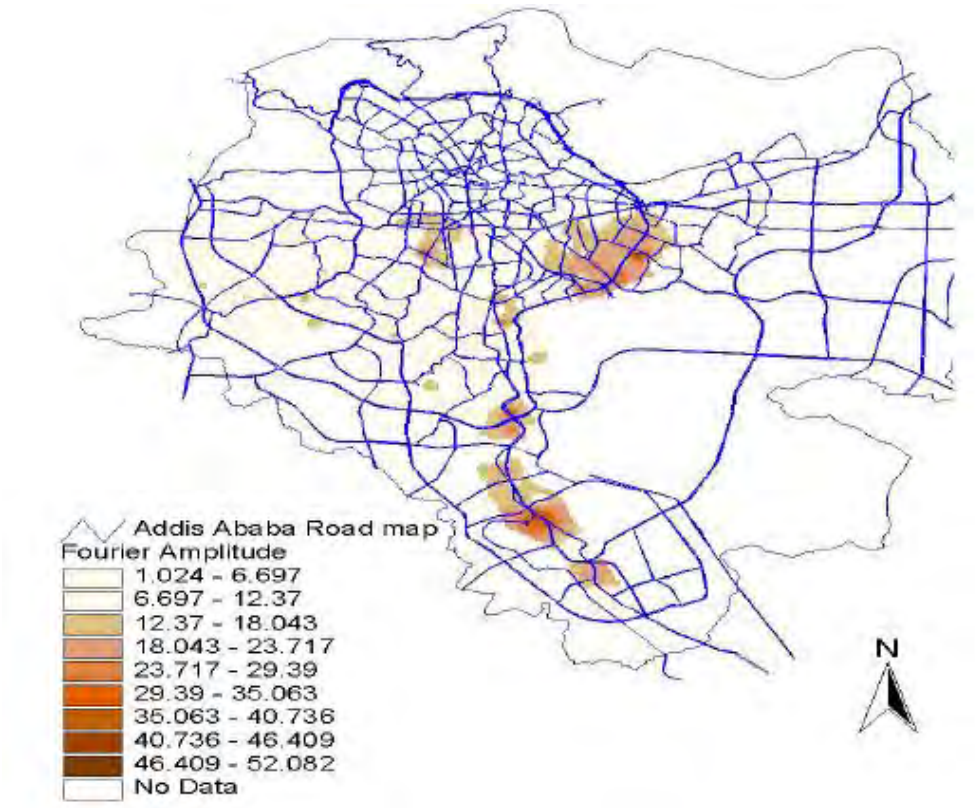

Figure 2.18: Fourier amplitude spectra of microtremor for the city of Addis Ababa
Source: 13th World Conference on Earthquake Engineering Vancouver, B.C., Canada. August 1-6, 2004.

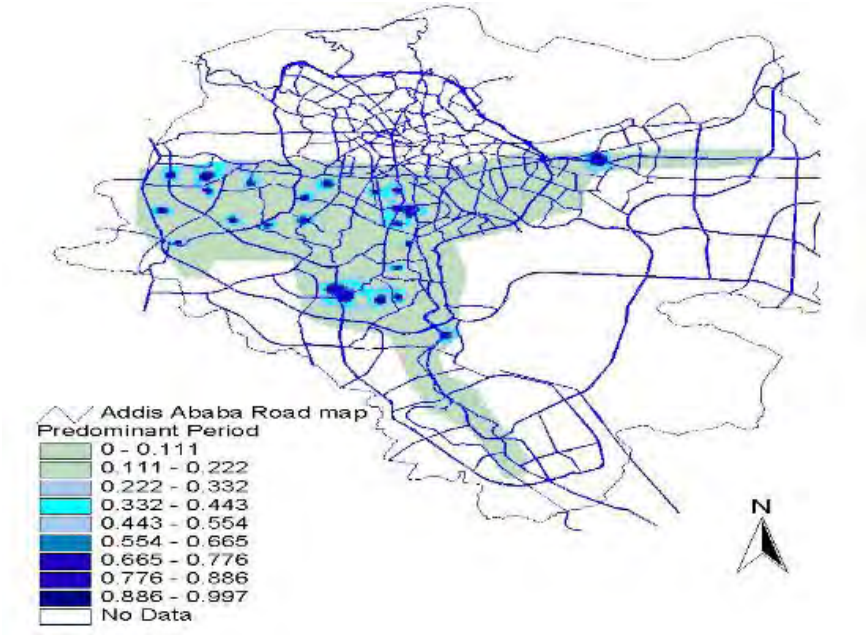

Figure 2.19: Predominant period Microtremor measurements for the city of Addis Ababa
Source: 13th World Conference on Earthquake Engineering Vancouver, B.C., Canada. August 1-6, 2004.

2.12.1 Seismic Hazard Results

The Probabilistic Seismic Hazard Assessment (PSHA) combines seismic source zoning, earthquake recurrence and the ground motion attenuation to produce hazard curves in terms of level ground motion and associated annual frequency of exceedance.The results are expressed in terms of Uniform Hazard Response Spectra (UHRS) which is represented for a fixed probability of exceedance (return period), the value of the ground motion parameters versus the structural period with 5% damped UHRS on rock are computed from return period of 475yr. (probability of 10% in the next 50yr.) and of 2,475yr (probability of 0.02% in the next 50yr). Figure 2.20 shows the UHRS spectra for 475yr-RP at Addis Ababa City.

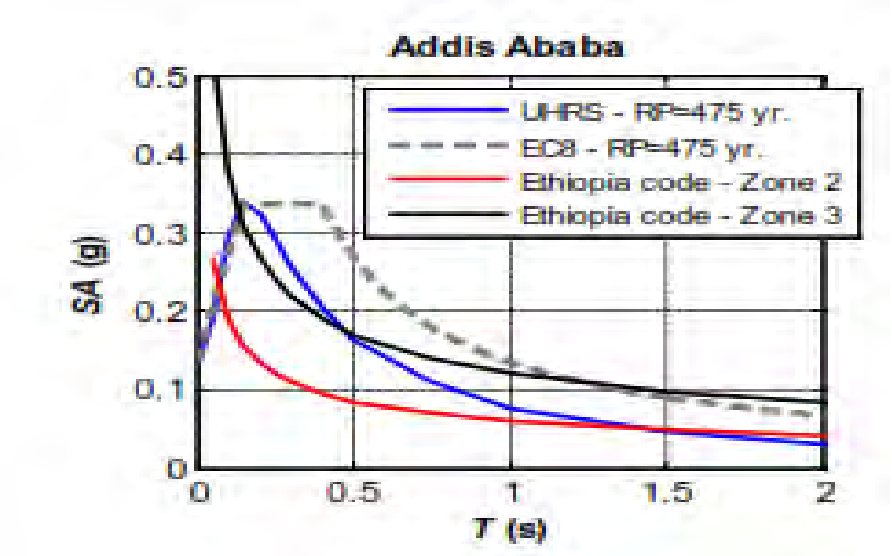

Figure 2.20: Uniform Hazard Spectra at Addis Ababa (blue curves) compared with elastic acceleration spectra from EN 1998 based on the PGA from RP = 475yr.and country seismic code criteria
Source: 2nd European Conference on Earthquake Engineering and Seismology, Istanbul Aug.25-29, 201

2.13 Seismic refraction

The seismic refraction method is non-invasive test method, used for determination of the p-wave velocity of the different subsurface layers and thickness of each layer. The analysis of geotechnical earthquake engineering requires characterization of the dynamic soil properties using geophysical method. Figure 2.21 and Figure 2.22 show P-wave refraction result along profiles [1].Figure 2.23 shows the location of profiles in the site.

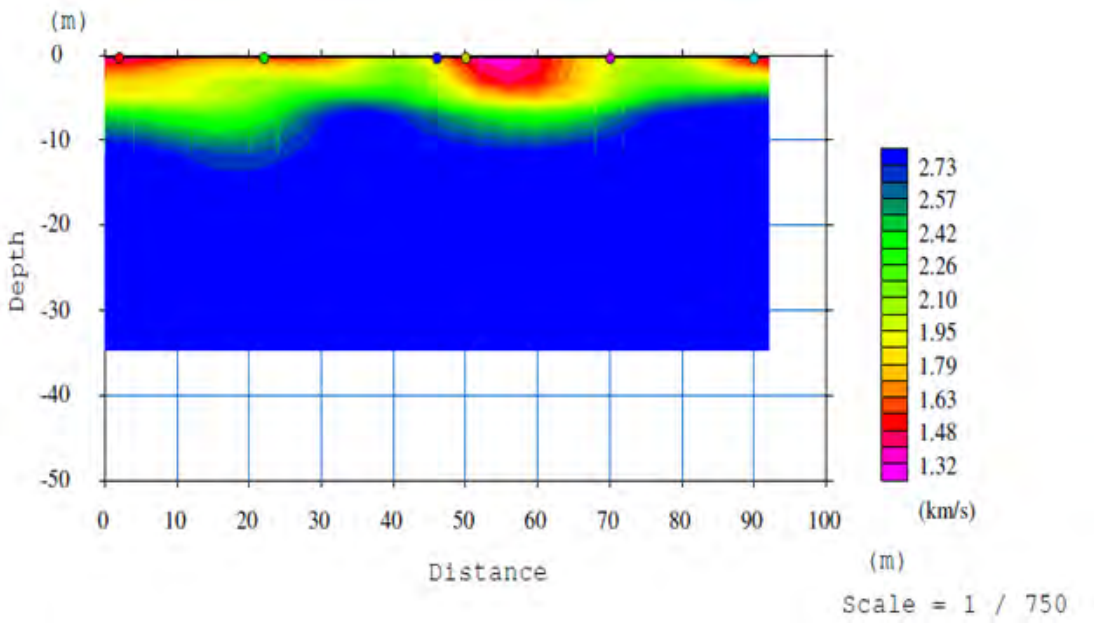

Figure 2.21: P-wave refraction result along profile 1 which clearly shows indentation with relatively low velocity in the middle for the CBE New Building Site [1].

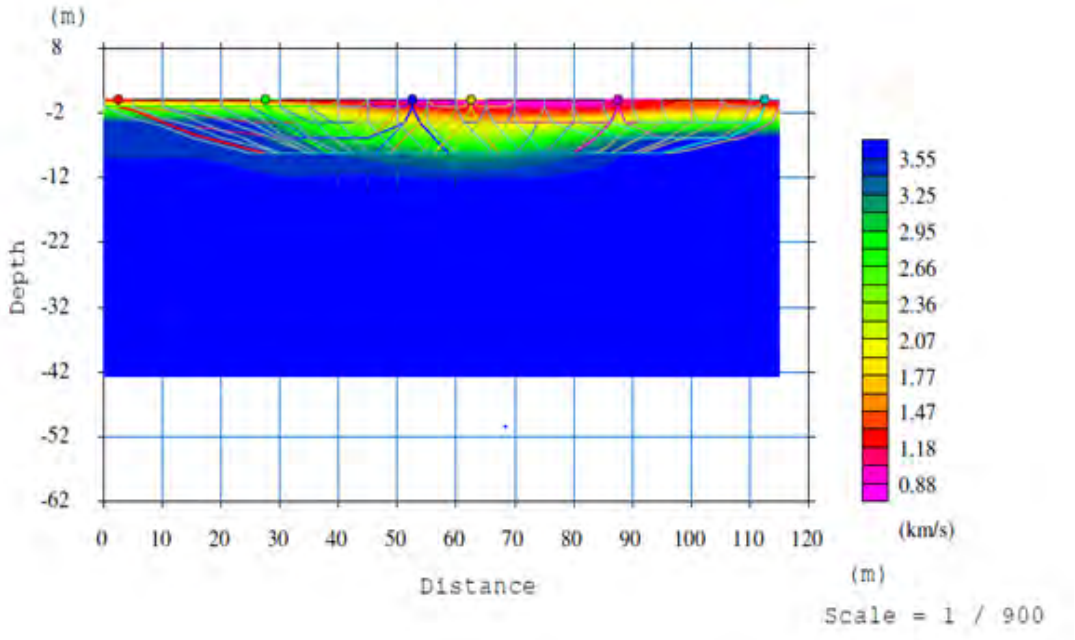

Figure 2.22: P-wave refraction result along profile 2. The P-wave velocity values are shown by the colour Coded legend and the lines are the seismic ray paths the traversed or scanned medium for the CBE New Building Site [1].

The coordinates of the two geophysical survey profiles are 473005E/996598N – 472997E/996723N (Profile-1) and 473000E/996724N –73048E/996646N (Profile-2).The ground surface was well leveled and the altitude is about 2332m above mean sea level. Before the commencement of the geophysical surveys, the construction site was excavated to a depth of 20m.

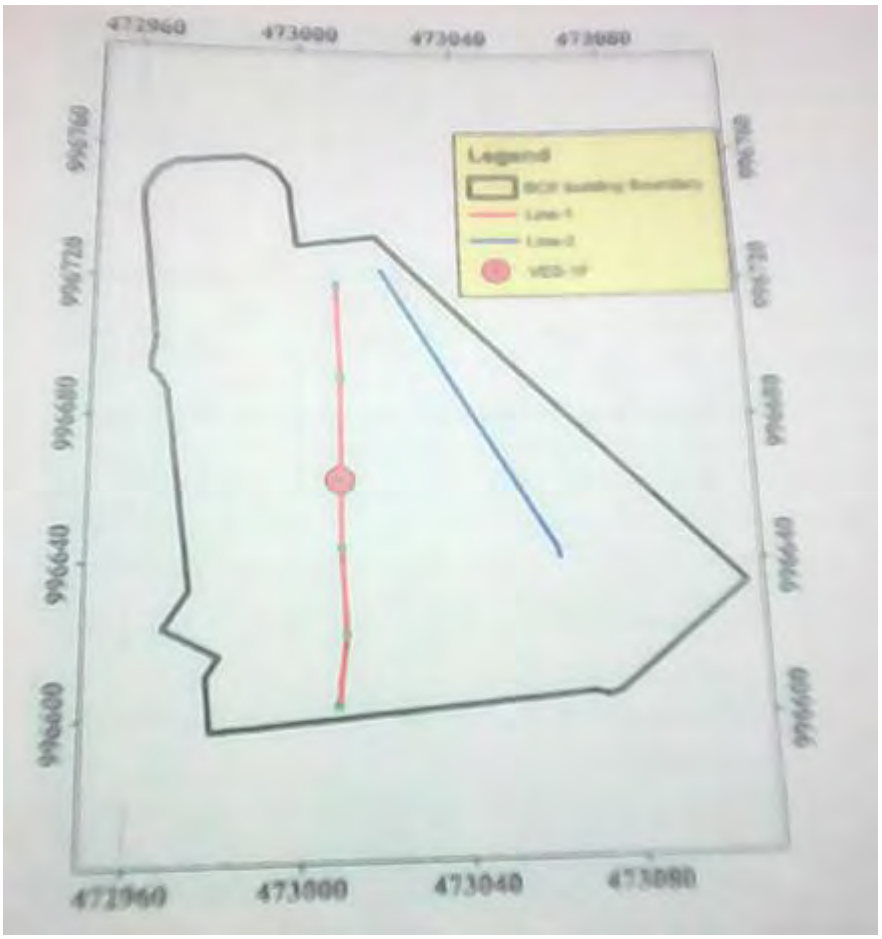

Figure 2.23: Location of the survey site and alignment of the geophysical survey profiles (thin red lines) modified from Google earth map [1].

2.14 Seismic hazards in Ethiopia and its historical record

2.14.1 Historical records of earthquakes in Ethiopia

The magnitude of the earthquake as per the report published in September, 1999 by Addis Ababa RADIUS group is 6.5, which is predicated by the seismologist to happen in areas of close proximity to Addis Ababa. Addis Ababa is very close to Main Ethiopian Rift Valley about 75-100 kilometers away. The Rift Valley is said to be the hotbed of tremor and active volcanoes. Other major cities in Ethiopia like Nazret, Dire Dawa and Awassa are very near the main fault lines such as the Wonji fault, the Nazret fault, the Addis-Ambo-Ghedo fault, and the Fil Woha fault lines along which numerous earthquakes of varying magnitude have occurred over the years. The presence of the Fil Woha hot springs in the middle of Addis Ababa about 365m from the CBE New Building Site is an indicative that Addis Ababa lies on the fault lines. These fault lines have a very low building strain which is accumulated over time and there release could cause the earthquake phenomena.

Pierre Gouin, founder and long-time director of the Geophysical Observatory at the Addis Ababa University has extensively written about earthquake hazards in Ethiopia, particularly from the 1400's to 1977 in his now classic book: Earthquake History of Ethiopia and the Horn of Africa. In his book, Gouin describes the earthquakes of 1906 and 1961 that shook Addis Ababa and caused widespread panic [8]. Gouin writes,

The magnitude of the main shock of 25 August 1906 was 6.75; the estimated epicentral location, 100 km south of Addis Ababa. The August tremors were exceptionally violent. It is also reported that the shock of 28 October was strong enough to cause the bells of the Church in the Finfine district to ring spontaneously." He further adds, "*The population of Addis Ababa was greatly afraid. Damage, however, was slight because: the town, being barely 10-years-old, had not yet fully developed.*

Chapter 3 Modelling

3.1 Introduction

3.2 Project description and site condition

The Commercial Bank of Ethiopia New Headquarter Building project is currently under construction .The building comprises of five basement levels and 46 floors above ground level. The geotechnical investigation was conducted by design and Share Company limited. The ground water was encountered at 5m below the natural ground level (NGL) during testing. The detailed design for the lateral support and foundation was conducted by China State Engineering Corporation and included but not limited to; soldier piles and shotcrete lagging techniques which retained the soil. The solider piles were driven at intervals of 1800mm along the planned excavation perimeter. The lagging consisting of steel mesh was inserted behind the front pile flanges as the excavation proceeded and concrete of grade C-20 was sprayed to the lasgging.The wall was designed to receive additional support from the anchors of different free and bonded length placed in layers. This study is to investigate the shoring of the commercial bank of Ethiopia project using the secant pile wall as an alternative support scheme.

3.3 Secant Pile Model

The alternative model shown in Figure 3.1 represents the layout of the secant piles as per the site drawing used for the construction (Appendix E).

The components of the retaining wall are illustrated in Figure 3.2.The structure consist of wall facing, anchors, tendons and anchor heads that provide the connection of the tendon to the wall facing. The anchor transmits a tensile force from the main structure through the anchor tendons to the surrounding ground. The shear strength of the ground is used to resist the tensile force. The anchors are composed of a fixed length that is bonded to the grout and unbounded free length that transfers the lateral earth force from the wall to the anchorage. The anchor tendons were constructed of prestressed steel in the form of threaded bars.

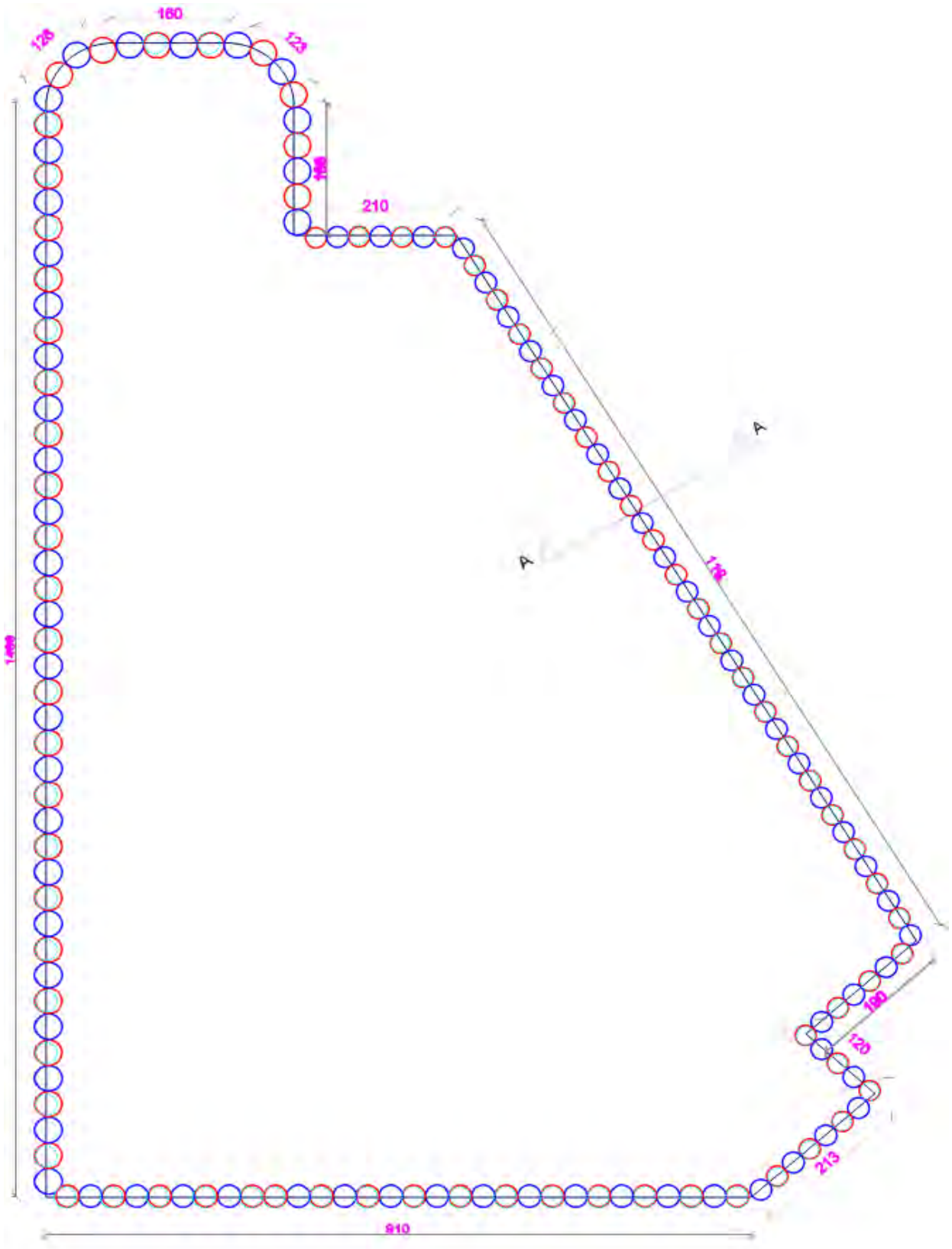

Figure 3.1: Site layout for the alternative wall scheme for using secant pile wall (All dimensions in cm)

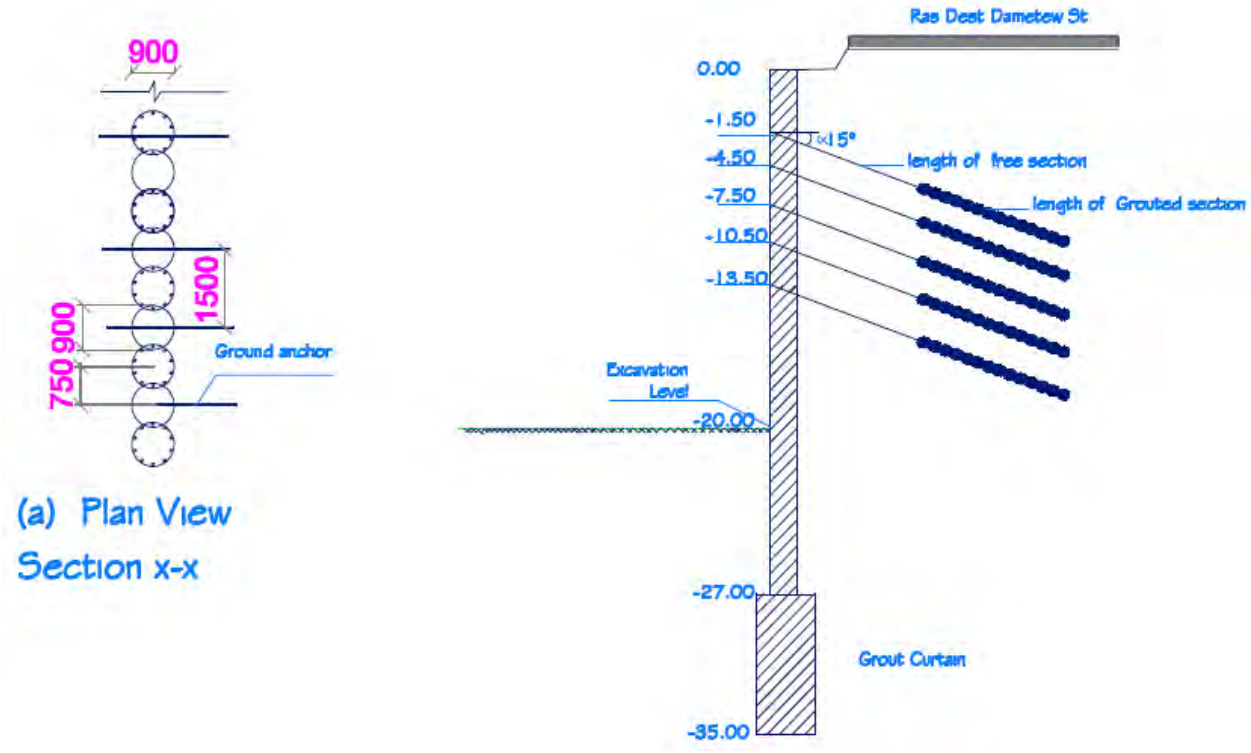

Figure 3.2: Cross section of the secant pile wall as the alternative scheme

3.4 Selection of an appropriate constitutive model and input parameters

3.4.1 Constitutive Model

Basing on the data collected for the CBE site the parameters are not elastic in behavior. Their inelastic behavior under cyclic loading can be described by elastic-plastic constitutive models. According to the constitutive model options available in Plaxis, Hardening soil model with small strain stiffness (HS small) was used for dynamic analysis. However, the model does not include softening behavior under cyclic loading conditions and does not incorporate the liquefaction behavior under loading conditions [3].

3.4.2 Soil and material parameters

The original site information was obtained from the geotechnical report for the Commercial Bank and the P-wave refraction result along the weak profile obtained from the seismic refraction report furnished by seismology department at Arat Kilo Addis Ababa University. The preliminary surface investigation was performed by Design and Share Company Limited under a contract with the China State Engineering Corporation Limited. The totals of 12 sampling borings were taken and the laboratory testing was done.

The Standard Penetration Test (SPT) was useful in profiling, identification and assessing engineering parameters of the soils during boring.

3.4.2.1 Deformability

The technique of seismic refraction was used to determine the compressional waves (p) Figure 2.21 and Figure 2.22, and since the shear wave(s) was not determined correlation of the soils identified from the Standard Penetration Test was done to determine the dynamic Poisson‟s ratio ($\mathcal{V}$).Once the Poisson‟s ratio is known, the elastic modulus was calculated from the equations.

Constrained Modulus, M

$$M_0 = \rho V_P{}^2 \qquad (3.1)$$

The constrained modulus is equal to the reciprocal of the ondometer vertical coefficient, M_v. Referring to the geotechnical investigation report, at borehole No.6 and depth 38.2m the average value the coefficient $M_v = 0.0001343 m^2/kN$. Therefore, the value of the constrained modulus $M = 7446.02 kN/m^2$.

Dynamic (Small strain) shear Modulus

The dynamic shear modulus, G, is of great importance in soil dynamics and earthquake engineering. Most numerical modeling software includes the values of G_0 and $\gamma_{0.7}$ as input parameters to define the stiffness reduction relationship for various geomaterials. The reason given for normalization using the volumetric threshold shear strain $\gamma_{0.7}$ is that the stiffness reduction becomes less prone to error (Benz, 2007).

$$G_0 = \rho V_s{}^2 \qquad (3.2)$$

The compressional wave velocity (p) from the p-waves refraction and the Poisson‟s ratio obtained from correlation can be used to calculate shear wave velocity from the relationship.

$$\upsilon = \frac{V_P{}^2 - 2V_s{}^2}{V_P{}^2 - V_s{}^2} \qquad (3.3)$$

Young's Modulus, E

The soil as identified at each bore hole when conducting the Standard Penetration Test was correlated with values of Appendix B (Tables B.1 and B.2).The values were also checked for accuracy with Young‟s Modulus,E determined based on the dynamic shear modulus, using the relationship.

$$E = 2G(1 + \upsilon) \qquad (3.4)$$

Characterization of the soil to determine the input soil parameters used for modelling by applying the soil parameters and seismic parameters obtained from the geotechnical investigation report and seismic refraction test conducted by Design and Share Company Limited and Seismology Department Addis Ababa University respectively. Tables 3.1 and 3.2. Further, the material properties from the catalog of the manufacturer were used to determine the composite properties of materials by combining the Young‟s modulus, shear modulus and Poisson‟s ratio using Halpin-Tsai Equations. Tables 3.3 to 3.6 summarize the engineering properties of the composite secant pile wall.

Table 3.1: Summary of ground conditions encountered in borehole

STRATA DESCRIPTION	Elv	E_{50}	E_{Oed}	E_{ur}	γ_{uns}	γ_{sat}	c^{ref}	φ	m	R_{int}
	m	MPa			kN/m^3		MPa	deg	–	
Soft, organic silty CLAY	4.00	4.00	4.00	12.00	12.4	14.7	0.015	13	1.00	1.00
Silty CLAY	6.60	4.00	4.00	12.00	13.8	15.3	0.02	17	0.90	0.95
Highly weathered BASALT	8.80	2770	2770	8310	22.6	32.7	7.8	33	0.90	0.95
Medium strong, intensively fract to fragmented slightly to moderately weather BASALT	15.00	20630	20630	61890	24	35	18	34	0.70	0.80
Silty CLAY	18.20	4.00	4.00	12.00	12.4	14.2	0.02	17	0.90	0.95
Stiff, sandy clayey SILT	21.00	4.00	4.00	12.00	14.2	16.7	0	28	0.85	0.90
Highly weathered scoriaceous BASALT, decomp to silty CLAY	25.50	630	630	1890	22.4	32.9	13.6	32	0.90	0.95
Moderately weathered BASALT	39.00	20630	20630	61890	23.9	34.5	26	36	0.70	0.80
Stiff, swelling clayey SILT	45.00	4.00	4.00	12.00	15.3	17.4	0.015	22	0.90	0.95
Moderately weathered BASALT	52.00	2063	2063	6189	24	35	26	35	0.70	0.80
Strong, slightly fractured, fresh to faintly weathered BASALT	61.00	46510	46510	139530	25.7	36.8	29	38	0.50	0.60
Moderately weathered Basalt	75.00	20630	20630	61890	24	35	25	34	0.70	0.80
Strong, slightly fractured, fresh to faintly weathered BASALT	83.00	46510	46510	139530	26	37	29	38	0.50	0.60

Table 3.2 : Summary of Seismic properties encountered in borehole

STRATA DESCRIPTION	Elv	V_p	V_s	E_{ur}	G_{ur}	G_0	E_0	γ_{sat}	μ	G_0/G_{ur}
	m	m/s			GPa			kN/m^3	$-$	$-$
Soft, organic silty CLAY	4.00	1790	731	0.012	0.005	8E-04	0.002	14.7	0.30	0.1735
Silty CLAY	6.60	1950	796	0.012	0.005	1E-03	0.003	15.3	0.30	0.2141
Highly weathered BASALT occassionally, fresh rock present	8.80	2100	1277	8.31	3.272	0.005	0.014	32.7	0.27	0.0017
Moderately weathered BASALT	15.00	2730	1555	61.89	24.56	0.009	0.022	35	0.26	0.0004
Silty CLAY	18.20	2730	1115	0.012	0.005	0.002	0.005	14.2	0.30	0.3896
Stiff, sandy clayey SILT	21.00	2730	1672	0.012	0.005	0.005	0.011	16.7	0.20	0.9518
Highly weathered scoriaceous Basalt, decomp to silty CLAY	25.50	2730	1719	1.89	0.744	0.01	0.025	32.9	0.27	0.0133
Moderately weathered BASALT	39.00	2730	1719	61.89	24.37	0.01	0.026	34.5	0.27	0.0004
Stiff, swelling clayey SILT	45.00	2730	1672	0.012	0.005	0.005	0.012	17.4	0.20	0.9917
Moderately weathered Basalt	52.00	2730	1719	61.89	24.37	0.011	0.027	35	0.27	0.0004
Strong, slightly fractured, fresh to faintly weathered BASALT	61.00	2730	1689	139.5	58.61	0.011	0.025	36.8	0.19	0.0002
Silty CLAY	62.00	2730	1115	0.012	0.005	0.002	0.005	15	0.30	0.4115
Moderately weathered BASALT	75.00	2730	1555	61.89	24.56	0.009	0.022	35	0.26	0.0004
Strong, slightly fractured, fresh to faintly weathered BASALT	83.00	2730	2730	139.5	58.61	0.028	0.067	37	0.19	0.0005

Table 3.3: Material properties of rebar anchor

Manufacturer Trade Name	Steel grade	Yield strength(MPa)	Tensile Strength(MPa)	Poisson's Ratio
TIANJIN STEEL CO.LTD	PSB 500	500	6300	0.2

Table 3.4: Material properties of Concrete

Equation	Concrete grade	Young's Modulus(GPa)	Shear Modulus(GPa)	Poisson's Ratio
$E_C = 4700\sqrt{f'c}$	C 35	27.81	12.09	0.15

Composite parameters for the secant pile wall

Secant pile wall can be represented by composite parameters, generally expressed in terms of the material properties shown in table 3.3 and table 3.4.The parameters required for the composite secant pile wall are: Young"s modulus(E),Poisson"s ratio(v) and Shear modulus(G).

a) Young's modulus

$$E_1 = fE_f + (1-f)E_m \quad (2.6)$$

$$E_1 = 0.65(0.5) + (1-0.65)27.81$$

$$\mathbf{E_1 = 10.06\ GPa}$$

$$E_2 = \frac{E_f E_m}{fE_m + (1-f)E_f} \quad (2.8)$$

$$E_2 = \frac{E_f E_m}{fE_m + (1-f)E_f}$$

$$\mathbf{E_2 = 0.76\ GPa}$$

b) Poisson's ratio

$$v_{12} = fv_f + (1-f)v_m \quad (2.9)$$

$$v_{12} = 0.65 \text{ x } 0.2 + (1-0.65) \text{ x } 0.15$$

$$\mathbf{v_{12} = 0.18}$$

Poisson"s ratio (v_{12}), describes the contraction in the two directions when a stress is applied in the perpendicular direction, composite efficiency factor (f), Poisson"s ratio of steel (v_f) and concrete (v_m) can be used to obtain (v_{12}) from the rule of mixtures.

c) Shear modulus

$$G = G_m\left(\frac{G_f(1+f)+G_m(1-f)}{G_m(1+f)+G_f(1-f)}\right) \quad (2.4)$$

$$= 12.09\left(\frac{0.5(1+0.65)+12.09(1-0.65)}{12.09(1+0.65)+0.5(1-0.65)}\right)$$

G_{12} = 3.038 GPa

The shear modulus G_{12} indicates the ratio of shear stress (acting in one direction on the plane with a normal in the two directions)

The composite body does not rotate, therefore $G_{ij} = G_{ji}$ and since for aligned fibre composites, the 2 and 3 directions are equivalent, there are only two shear moduli as:

$$G_{12} = G_{21} = G_{13} = G_{31} \neq G_{23} = G_{32}$$

$$\mathbf{G_{12} = G_{13} = 3.04\ GPa}$$

$$G_{23} = \frac{E_2}{2(1+v_{23})} \tag{2.10}$$

$$v_{23} = 1 - v_{21} - \frac{E_2}{3k} \tag{2.10.1}$$

$$v_{21} = [fv_f + (1-f)v_m]\frac{E_2}{E_1} \tag{2.10.2}$$

$$= [0.65x0.5(1-0.65)\ x\ 0.15]\ x\frac{0.76}{10.06}$$

$$v_{21} = 0.0187$$

$$k = \left[\frac{f}{k_f} + \frac{1-f}{k_m}\right]^{-1} \tag{2.10.1.1}$$

k- bulk modulus of the composite material for tability of an unconstrained block of material

$$k_f = \frac{E_f}{3(1-2v_f)} \tag{2.10.1.2}$$

$$k_f = \frac{6.3}{3(1-2\ x\ 0.3)}$$

$$k_f = 5.25$$

$$k_m = \frac{E_m}{3(1-2v_m)} \tag{2.10.1.3}$$

$$k_m = \frac{E_m}{3(1-2v_m)}$$

$$k_m = \frac{27.81}{3(1-2\ x\ 0.15)}$$

$$k_m = 13.24$$

$$k = \left[\frac{f}{k_f} + \frac{1-f}{k_m}\right]^{-1}$$

$$k = \left[\frac{0.65}{5.25} + \frac{1 - 0.65}{13.24}\right]^{-1}$$

$$k = 6.656$$

$$v_{23} = 1 - v_{21} - \frac{E_2}{3k}$$

$$v_{23} = 1 - 0.0187 - \frac{0.76}{3 \text{ x } 6.656}$$

$$v_{23} = 0.943$$

$$G_{23} = \frac{E_2}{2(1 + v_{23})}$$

$$G_{23} = \frac{0.76}{2(1 + 0.943)}$$

$$\mathbf{G_{23} = 0.196}$$

Table 3.5: Material properties of composite secant pile wall

Parameter	***Name***	***Secant pile(Composite)***	***Unit***
Thickness	d	0.9	m
Unit Weight	γ	2.2	kN/m^3
Material behaviour	Type	Linear,Non-Isotropic	-
Young's Modulus	E_1	10.06E+3	MPa
	E_2	0.76E+3	MPa
Poisson's ratio	V_{12}	0.25	-
Shear Modulus	G_{12}	3.04E+3	MPa
	G_{13}	3.04E+3	MPa
	G_{23}	1.96E+2	MPa

Table 3.6: Material properties of various composite secant pile wall

Parameter	*Name*	*Pile 1*	*Pile 2*	*Pile 3*	*Pile 4*	*Unit*
Thickness	d	0.9	0.65	1.15	1.4	m
Unit Weight	γ	2.2	1.59	2.81	3.43	kN/m^3
Young's Modulus	E_1	10.06E+3	5.25E+3	16.43E+3	24.34E+3	MPa
	E_2	0.76E+3	0.4E+3	1.24E+3	1.84E+3	MPa
Poisson's ratio	V_{12}	0.25	0.25	0.25	0.25	-
Shear Modulus	G_{12}	3.04E+3	1.59E+3	4.96E+3	7.35E+3	MPa
	G_{13}	3.04E+3	1.59E+3	4.96E+3	7.35E+3	MPa
	G_{23}	1.96E+2	1.02E+3	3.2E+3	4.74E+3	MPa

3.5 Model Geometry

The soil stratum consists of various layers of soil and decomposed basalt with 83.0m depth as determined from the SPT result. The soil stratigraphy, the general water level and the initial conditions of the soil layers were considered in the modelling. A finite element numerical analysis using non-linear time history dynamic analysis was performed by using Plaxis 2D and 3D software. Figure 3.3 shows the finite element model of the soil strata. In the study the soil strata was subjected to real earthquake waves(upland earthquake) which occurred in1989.Figure 3.4 shows the acceleration time histoy for Loma Prieta earthquake.

In a 2D model, plane strain elements with 15 nodes and Hardening Soil model were used to model the soil.Tnsion cut off was used to prevent the tensile stress which are not allowed in the soil element during the analysis.

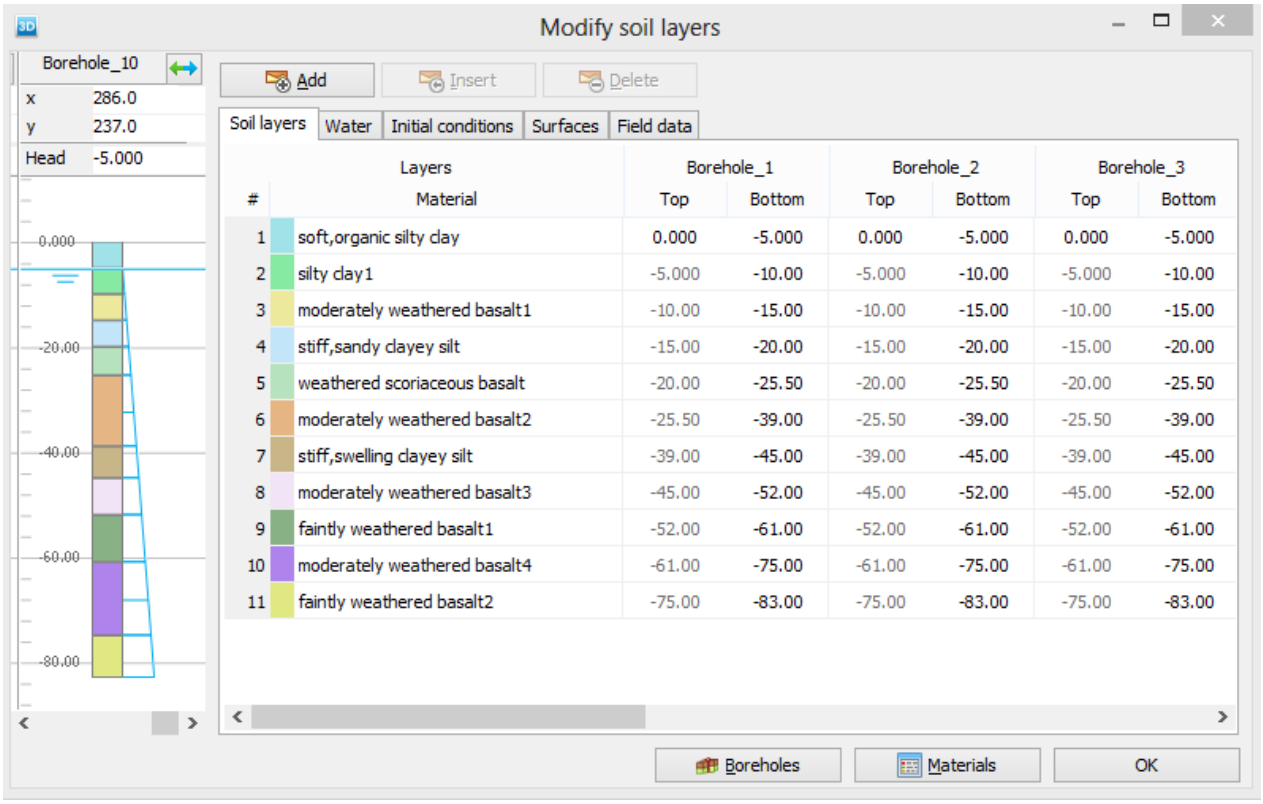

#	Layers: Material	Borehole_1 Top	Borehole_1 Bottom	Borehole_2 Top	Borehole_2 Bottom	Borehole_3 Top	Borehole_3 Bottom
1	soft,organic silty clay	0.000	-5.000	0.000	-5.000	0.000	-5.000
2	silty clay1	-5.000	-10.00	-5.000	-10.00	-5.000	-10.00
3	moderately weathered basalt1	-10.00	-15.00	-10.00	-15.00	-10.00	-15.00
4	stiff,sandy clayey silt	-15.00	-20.00	-15.00	-20.00	-15.00	-20.00
5	weathered scoriaceous basalt	-20.00	-25.50	-20.00	-25.50	-20.00	-25.50
6	moderately weathered basalt2	-25.50	-39.00	-25.50	-39.00	-25.50	-39.00
7	stiff,swelling clayey silt	-39.00	-45.00	-39.00	-45.00	-39.00	-45.00
8	moderately weathered basalt3	-45.00	-52.00	-45.00	-52.00	-45.00	-52.00
9	faintly weathered basalt1	-52.00	-61.00	-52.00	-61.00	-52.00	-61.00
10	moderately weathered basalt4	-61.00	-75.00	-61.00	-75.00	-61.00	-75.00
11	faintly weathered basalt2	-75.00	-83.00	-75.00	-83.00	-75.00	-83.00

Figure 3.3: Soil profile in plaxis3D Model

3.5.1 Static loading

Due to the existence of several buildings around the excavation and the associated traffic, large surcharge load is expected to take care of the adjoining structures and the traffic loading. Since the existing site surcharge could not be estimated accurately, the applied overload of 150kPa was used in the modeling. This load was also used in 3D finite element analysis of a deep excavation for the Odeon project in Monaco [22].

3.5.2 Dynamic loading

In order to stimulate the actual condition, the dynamic load considered in this study is the upland earthquake of 18 Oct, 1989 of real accelerogram which occurred at Del Valle Dam Station. The Finite Element analysis with PLAXIS 3D software was applied. In PLAXIS 3D non option is selected, it is assumed that the base of the model is rigid and the seismic signal is trapped within the soil deposit and cannot escape through the bottom boundary. The real accelerogram of strong motion was assigned as dynamic multiplier and the generated spectrum was adjusted to the acceleration of 0.12g for the case of Addis Ababa area. PLAXIS allows the use of earthquake

records in standard strong motion CD-ROM (SMC) format as input data for earthquake loading. Figure 3.4 shows the real accelerogram of Loma Prieta Earthquake used as input for modelling the dynamic parameters of the secant pile wall and additional parameter for the dynamic response of the soil during the earthquake.

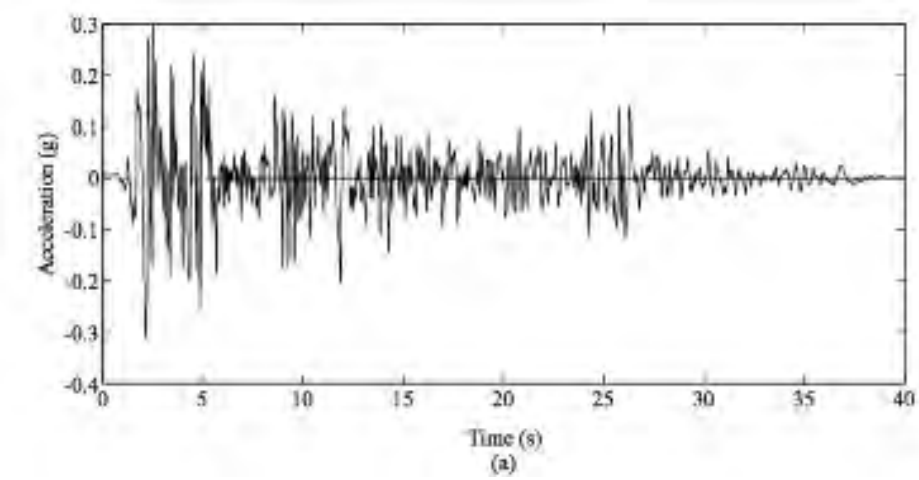

Figure 3.4: Real time accelerogram of Del Valle Dam - Loma Prieta Earthquake

In order to define the secant pile wall and the corresponding interfaces, all the vertical surfaces created as the volume of the soil was decomposed were selected and create plate option was used as the boundary condition. Figures 3.5.The create data set for the secant pile wall (plates) according to table 3.5 and 3.6 was assigned to all vertical walls.

The surface load was defined by creating a surface load around the periphery of the excavated area and uniformly distributed load was applied all round the excavation. Figure 3.5 shows the surface load applied at the top view of the model geometry.Non-isotropic (different stiffnesses in the two directions) secant pile walls are defined. As the vertical direction is generally the stiffest direction, the local axis shall point in the z-direction.

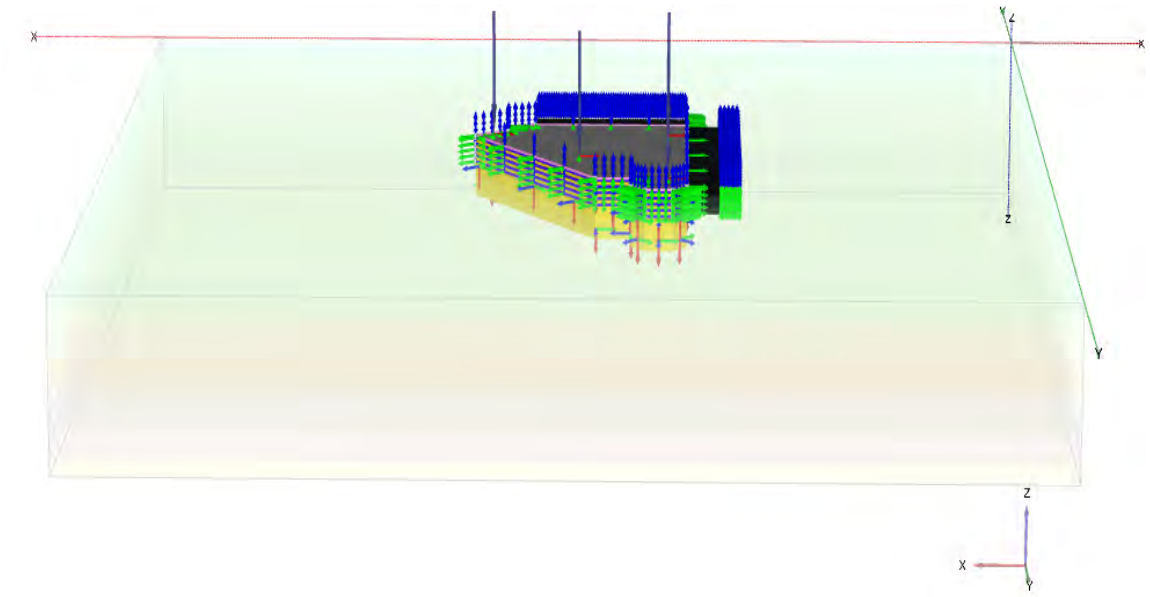

Figure 3.5: Static loading

3.5.3 Base case model and mesh set up

The project data from the project drawings were initially used to develop 3D geometric model to represent the construction process by reconciling field report and simulating the actual construction process of the project.

The refinement of the mesh affects the calculation results in the FE Analysis. The refinement of the mesh is also related to the calculation time. The large mesh elements generated require large calculation time due to the large stiffness matrices. The balance between accuracy and efficiency is key to the mesh setup. In PLAXIS 3D, the mesh is generated automatically with the global refinement as set in Figure 3.6.

The model is based on the site dimensions and the actual conditions. Figure 3.7 shows the resulting finite element model represents a close approximation to the original geometric model with PLAXIS 3D.

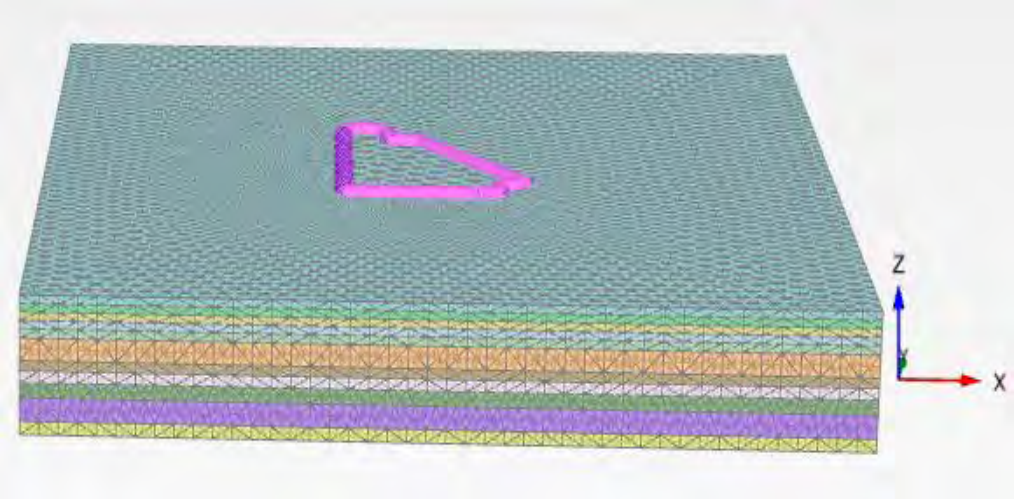

Figure 3.6: Overview of mesh set up for model in Plaxis 3D model

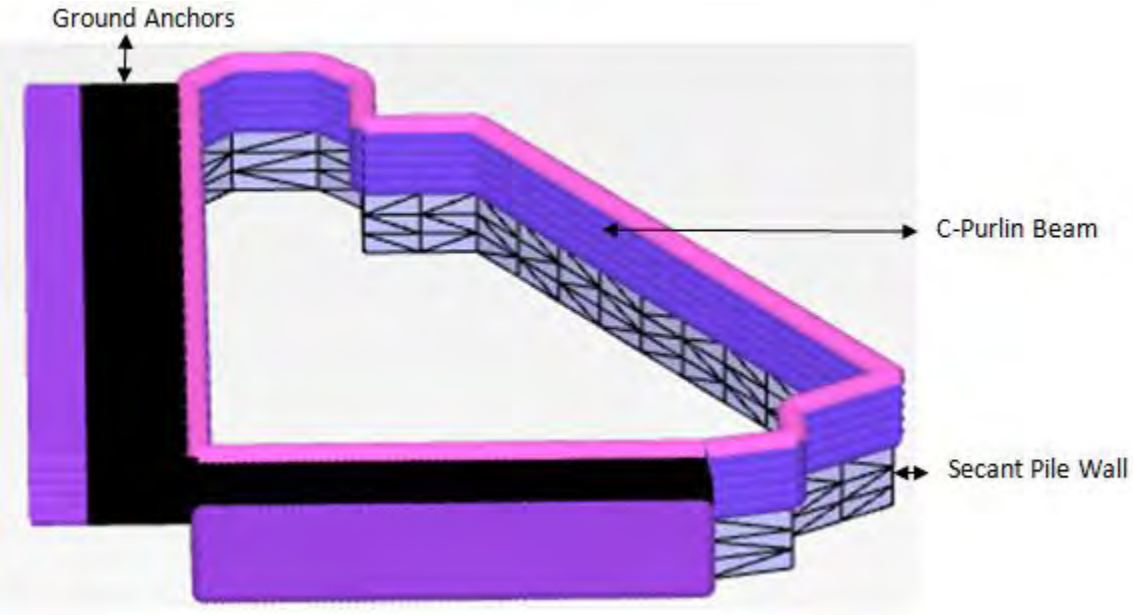

Figure 3.7: Overview of model and ground Anchors in Plaxis 3D model

3.6 Plaxis 2D Model

The excavation was modeled as plain strain condition. The general procedure when modeling is; to define the geometry with elements and corresponding materials,

to define loads and boundary conditions,

to create FEM-mesh,

to define the initial condition and perform the FEM-calculations.

Plate elements are composed of beams elements. The beam element has three degrees of freedom per node and has three respective 5nodes when used with 6nodes volume elements and 15nodes volume elements.

The 15nodes and 6nodes triangular elements are used to model volume clusters. Materials properties are assigned to each volume cluster. In order to perform calculations on the created model, the geometry was divided in to finite elements.

Geogrid element has tensile strength i.e no compressive strength or bending moment strength. Interface elements are used for modelling of interaction between two materials. In FEM calculations just one displacement is allowed in a specific node.

When creating geometry, first define points, geometry lines and cluster (areas) and assign different properties. The clusters are given a soil element and soil materials, geometry line is given either a structural element or a boundary condition. There different elements available in plaxis 2D:

There are two different elements implemented for soil modelling in Plaxis 2D.These are both triangular elements and have 6nodes respective 15nodes and have 3 respective 12 stress points (Gaussian integration points). Figure 3.8.

Plaxis has the ability to create the mesh automatically. However; the automatically created mesh may not be accurate enough to perform an acceptable numerical analysis. To prevent this, the mesh can be manually refined, both as whole and in areas where large stress and strain concentration or gradient occur.

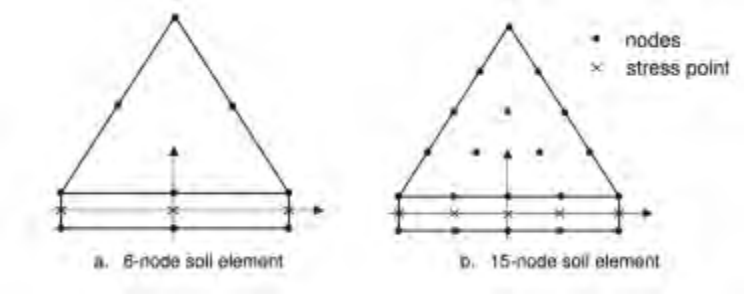

Figure: 3.8: Distribution of nodes and stress points in interface elements and their connection to soil Elements [19]

3.7 Comparision of results according to Plaxis 2D and 3D

The sectional forces obtained from the design of the excavation and those arising from the seismic action are compared for both 2D modelling.

The dynamic analysis yields for the peak axial force 4520 kN/m, which is 2.6% less than the design excavation force.

The dynamic analysis yields peak bending moment of 6860 kN/m which is 1.6% higher than the design bending moment.

The dynamic analysis yields peak shear force of 2700 kN/m which is 1.5% higher than the design shear force.

The total displacement before the earthquake event for 2D and 3D are 0.94378E-3m and 0.1104E-3m respectively.The 3D yields 88.3% less the 2D displacement under static load condition.

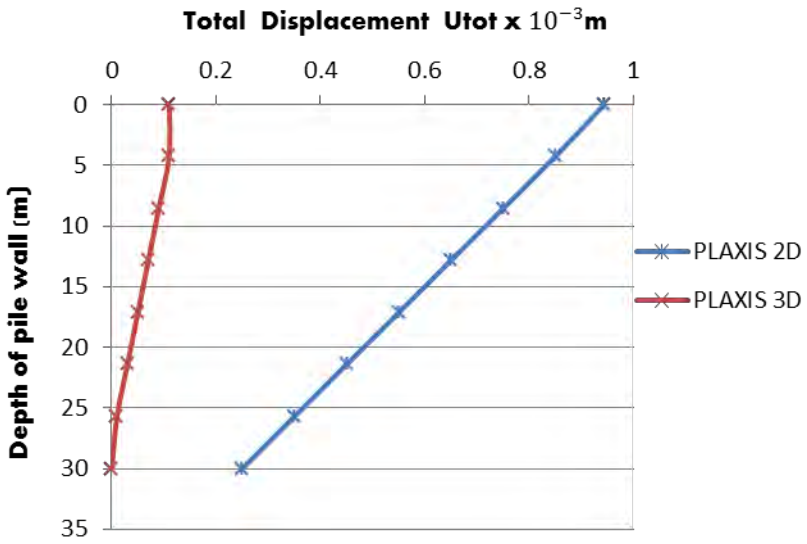

Figure 3.9: Static load condition

After the earthquake,the total displacement recorded for 2D and 3D are 38.05E-6m and 0.3375E-3m respectively. The 3D yields 88.7% more than 2D displacement under dynamic load condition.The bigger difference could be due to the non realistic modelling of the 2D.

2D plain strain modelling assumes the out-of-plane geometry is large and or constrained and that the loading does not vary in the out-of-plane direction(z) such that the z- displacements are neglected ,whereas 3D modelling takes width effect in to account and therefore provides insight in to better modelling results than 2D finite element model.Inaddition modelling errors may have occurred in the model.

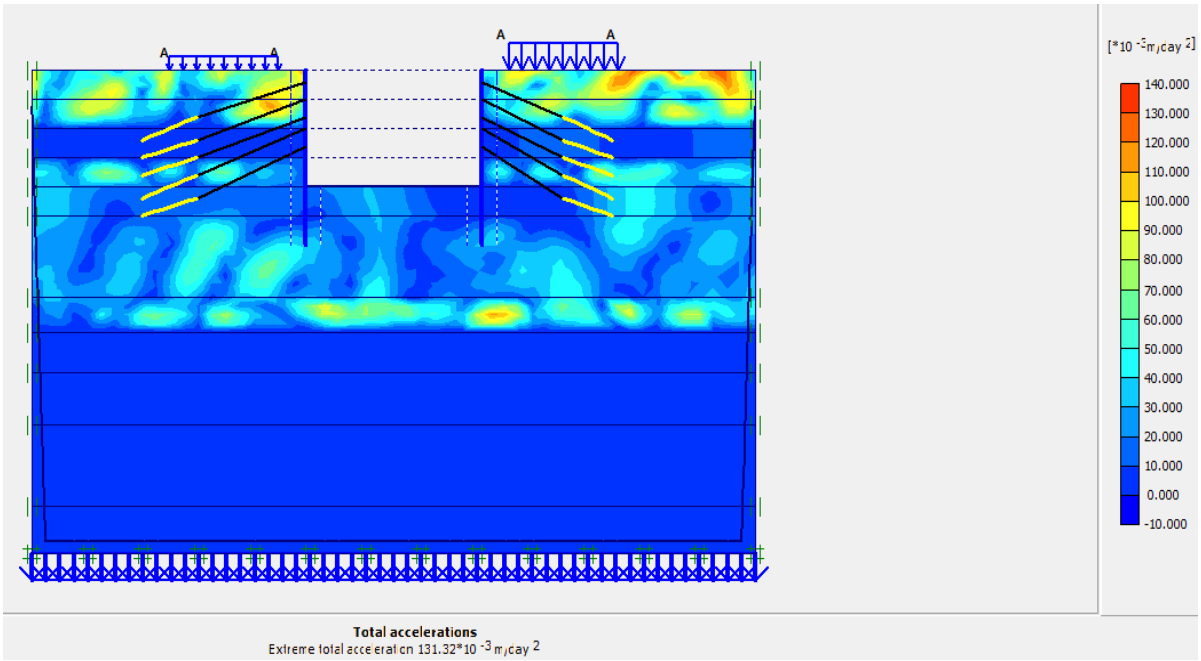

Figure 3.10: Total Acceleration

The results from the modelling indicate that there is great difference in values between the 2D and 3D analysis. The reason for this discrepancy may be found in the different geometry of the structure and the plain strain condition on which the 2D analysis is based.

Plaxis 2D modelling in plain strain is used in geometries which are more or less uniform cross sections and correspoinding stress state and loading scheme over certain length perpendicular to the cross section (Z-direction).Practically ,this means that 2D plain strain model considers one dimension to be relatively long(imagine the 2D cross-section being extruded infinitely in out of plane direction).

3D model alternative secant pile support system is clearly not a plane strain situation because some 3D effects are not captured in a 2D plane strain model.Thus,the excavation geometry and loading conditions can only be fully modelled using plaxis 3D analysis.

The load condition was changed to be applied uniformly all around the perimeter of the excavation.This would stumulate the construction condition and also the acting surcharge from the adjacent structures.

The geometry model, which is seen in figure 3.1 is based on construction drawings for the CBE headquarter site and the soil parameter evaluations.The plaxis 2D is used to carry out analysis of deformations and stability problems for different geotechnical situations in two dimensions.However,when the 3D problems to be investigated are simplified in to 2D there is possibility of obtaining matching results. Figure 3.11 shows multiple cross sections representing different types of geotechnical situations in 2D.

In order to make clear comparision for the alternative secant pile according to 2D and 3D modelling, the model geometry should be simplified to 2D as seen in the first figure (from left to right) Figure 3.11.

The research conducted at Graz University of Technology using diaphragm wall model for comprision of 2D and 3D model showed matching results Figure 3.12.

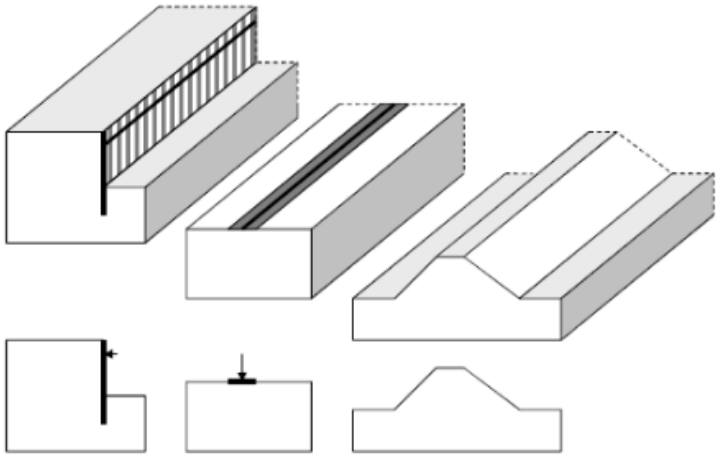

Figure: 3.11: Examples of plane strain situation

The research conducted at Graz University of Technology was an attempt to demonstrate the application of the ground anchor in 3D foundation; the diaphragm wall was modelled as a continuum element. The results from the 3D calculation with HS-Model compared well to the 2D solution.

The deviation of forces in the node-to-node anchor between both calculations is less than 4%.Furthermore; the vertical displacements behind the diaphragm wall from the 3D calculation are very similar to those obtained from 2D solution [7].

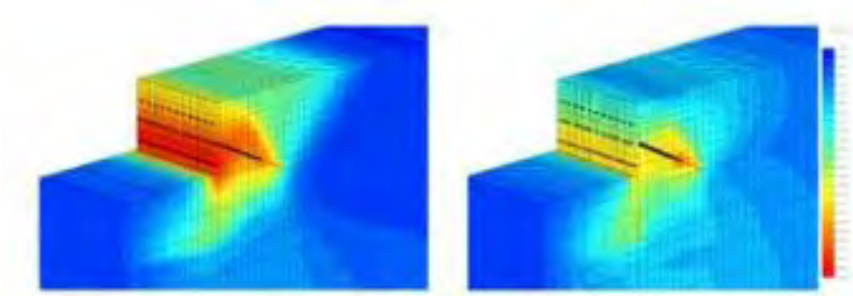

Figure 3.12: comparision of 3D results with 2D reference solution [7].

Chapter 4 Parametric studies

4.1 Introduction

One of the purposes for this study was to study the parameters due to the anchored secant pile wall by varying; length of the piles, anchor spacing and pile diameter under static and dynamic load condition. The analysis was performed on the model with the same characteristics (except pile length, anchor spacing and pile diameter).The plastic analysis using plaxis 3D Anniversary Edition was performed because the excavation process takes short period of time. Stage construction was also considered in the analysis and consolidation analysis which would be important to determine the future behavior of the structure was not performed since the excavation process takes short period of time.

4.2 Parameter analysis

In order to evaluate the impact of some parameters due to anchored pile wall on the deformation analysis, a parameter analysis is performed. In this analysis some important parameters; pile length, anchored spacing and pile diameter was analyzed by changing the values of each of them according to the specific parameter. Stage excavation, was also included in the analyses.

4.2.1 Effect of stage excavation

The excavation steps used in modeling the effect of stage construction are in intervals of 5m depth. This is the conservative design, which leads to more calculation steps and more calculation time. The excavation steps considered are: 5m, 10m, 15m, and 20m from surfaces are added to stimulate each single excavation step and number of calculation steps. The excavation steps in 3D model were added by deactivating the soil layers in the respective step.

Due to the different excavation steps the distribution of the lateral displacements of the secant pile wall changes dramatically. Figure 4.1 and 4.2.shows the displacements of the secant pile at 20m deep for static and dynamic loading respectively.

The small excavation step 5m requires more calculation steps and more time and yields less deformations. While the large excavation step takes short time and results to high lateral displacement.

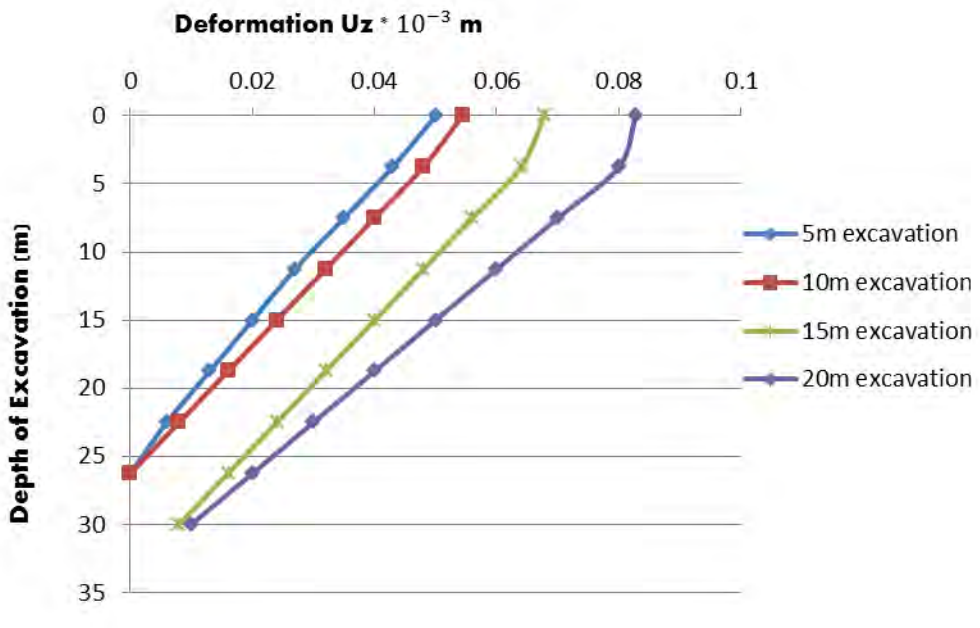

Figure 4.1: Effect of stage excavation on deformation under static loading

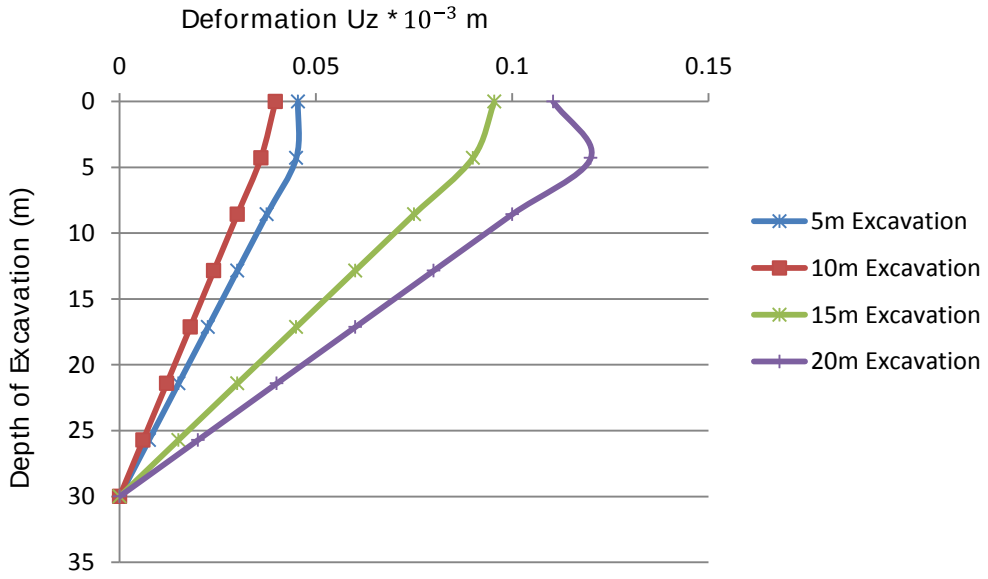

Figure 4.2: Effect of stage excavation on deformation under dynamic loading

4.2.2 Diameter of Pile wall

The diameter of pile wall was increased from 650mm to 1400mm.There was a change in structural stiffness. In Plaxis 3D the pile wall was modelled with diameter of pile 650mm, 900mm, 1150mm and 1400mm.Increase in diameter of the pile increases displacement near the surface of the wall in x and y directions Figure 4.3.

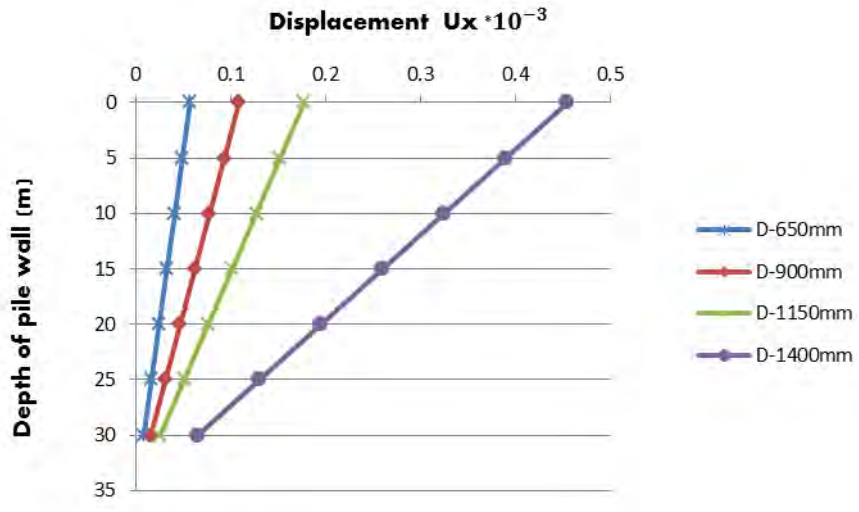

Figure 4.3: Maximum displacement U_x versus pile wall diameter under static and dynamic loading

4.2.3 Height of the pile wall

The parametric study in varying the height of the wall and the deformation obtain from plaxis output. The height of the wall used is 30m. This parameter was varied for different wall length of 24, 27, 30, 33 and 36m in the study. Figure 4.4 shows the results obtained from plaxis analysis. The pile wall lateral deflection and pile wall depth below the ground are normalized. The maximum excavation depth H_e for the project is 20m commencing from the natural ground level. The wall length H_w is 24m, 27m, 30m, and 36m and the maximum excavation H_e is 20m.It was observed that the height of the wall increased with increase in displacement. The high unusual displacement at wall height 27m would be the basalt failure produced due to weak, highly weathered scoriaceous basalt material and modelling error may have occurred in the model due to the constraints to temporarily working nodes thus, rapid increase in displacement.

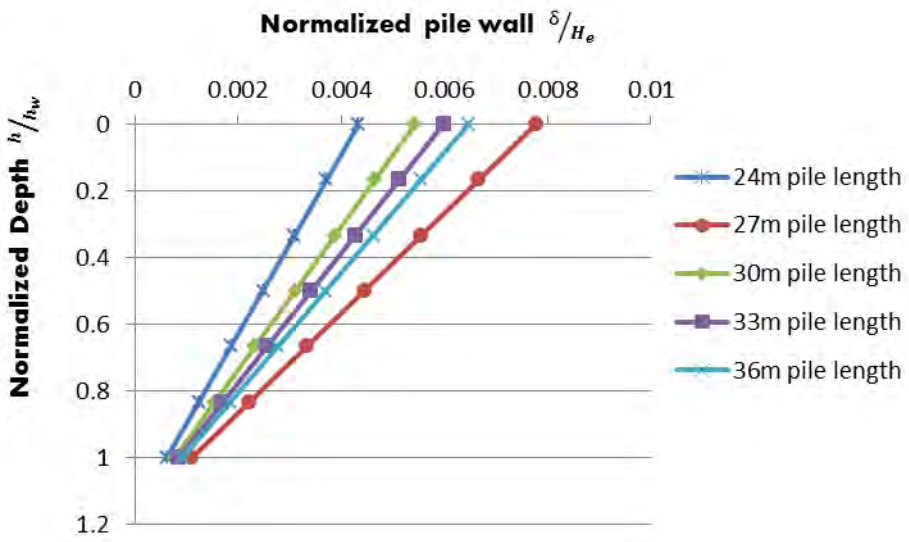

Figure 4.4: Effect of length of pile on lateral deformation of pile wall under static and dynamic loading

4.2.4 Anchor spacing

Horizontal and vertical spacing of anchors. The analysis was conducted with horizontal spacing of 2m, 3m, 4m, and 5m and vertical spacing was also varied; 3m, 4m and 5m.

One level of ground anchors was spaced at 2m in the horizontal direction and installed at an inclination of angle of 15° below the horizontal direction (left to right).The anchors were also spaced at 3m in the vertical direction(top to bottom).

Decreasing the horizontal spacing can increase the stiffness of the anchor per unit width. With high anchor stiffness, the compression of the anchor will be quite small, and the maximum deformation occurs near the excavation surface. Figure 4.5 shows the results obtained from plaxis analysis.

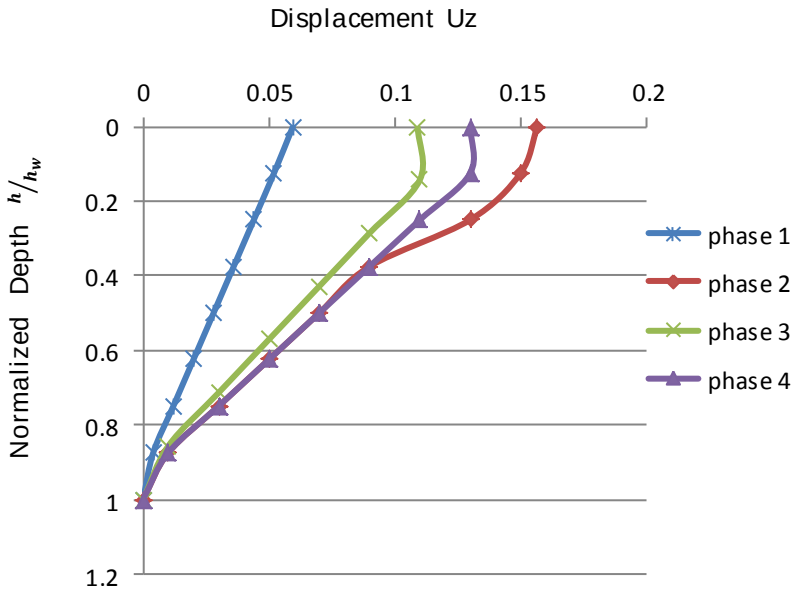

Figure 4.5: Anchor spacing 4m for static and dynamic loading

4.3 Seismic Site Response

The influence of local geologic and soil conditions on the intensity of ground shaking and earthquake damage has been recognized for many years. Local site conditions can profoundly influence all of the important characteristics of strong ground motion: amplitude, frequency content and duration. The effect of their influence depends on the geometry and material properties of the subsurface materials on the site topography, and on the characteristics of the input motion. Based on the seismic damage data for the 1906 San Francisco California, earthquake, Wood argued that the local site conditions emerge a dominant factor controlling the amplification of damage during the earthquakes (Woods, 1916).The Northridge (1994), and Loma Prieta (1989) earthquake have predicted the role of local site conditions in modifying the characteristics of strong motions.

Damage patterns in Mexico City after the 1985 Michoacán earthquake demonstrates conclusively the significant effect of the local site conditions on the seismic ground response. Thus understanding of local site effects of the strong ground motion is of particular importance for the mitigation of earthquake disasters as well as well as aiding the earthquake resistant design. In order to estimate the behavior of the ground during an earthquake, this study considers

site condition as one of the most important ground motion parameters for engineering design and it is often characterized by a set of simplified parameters such as site predominant period, ground amplification. The purpose for this is to avoid the situation where the fundamental periods of the structure is close to the predominant period of the site, thus the induced resonance like phenomenon led to serious damage of the structure.

Surface geotechnical and geophysical data for the New Commercial Bank site was obtained and used to estimate the local site condition on the earthquake ground motion. The ground response analysis was conducted considering the nonlinear behavior of the soil using plaxis 3D.The nonlinear site response analysis was used to estimate the site response and study the soil behavior during the earthquake wave propagation. The nonlinear site response was estimated by elastro-plastic constitutive model. The results for seismic site response obtained from plaxis output are discussed below.

4.3.1 Accelerations

The seismic body and surface waves create inertia forces with in the secant pile wall. When the wall starts shaking it is subjected to inertia forces. Thus, responding to Newton‟s second law of motion.

Acceleration or the rate of change of velocity of the waves setting the structure mass or weight in motion. The acceleration is measured in terms of the acceleration due to gravity or „g‟ which is the change of velocity of the freely falling body in space. Figure 4.6 shows the magnitude of acceleration of different earthquakes.

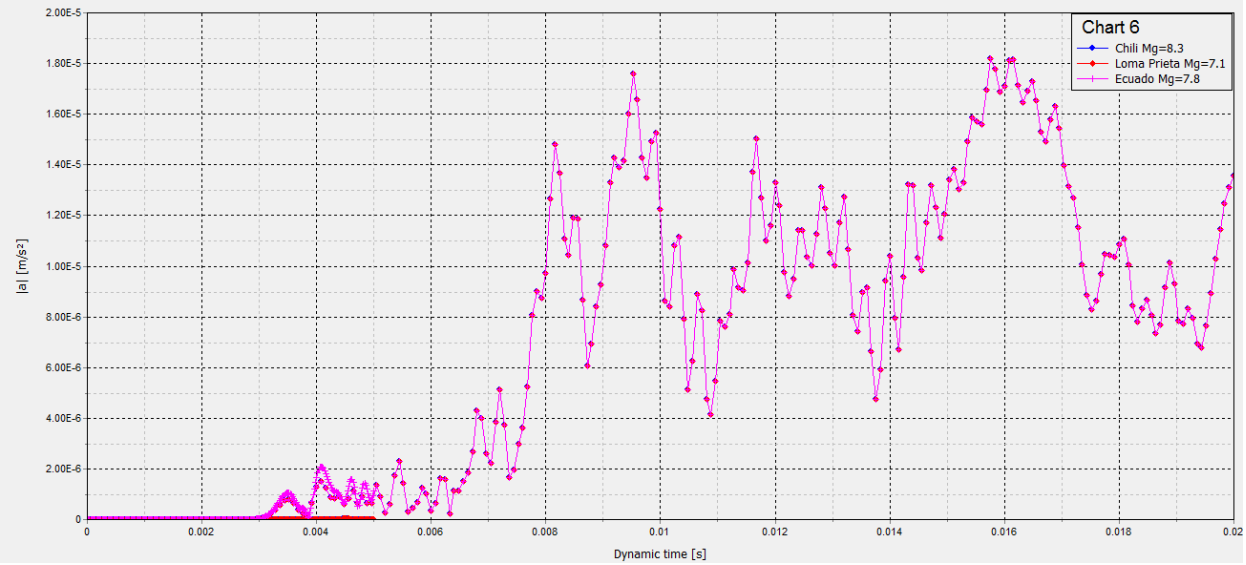

Figure 4.6: Magnitude of acceleration

4.3.2 Site Response Spectrum

A site respose spectrum is a graph that plots the maximum respose values acceleration velocity,and displacement against the period and frequency.The spectrum shows on vertical ordinate the acceleration,velocities and displacements that may be expected at varying periods on the horizontal ordinate. Figure 4.7 show the site response spectrum.

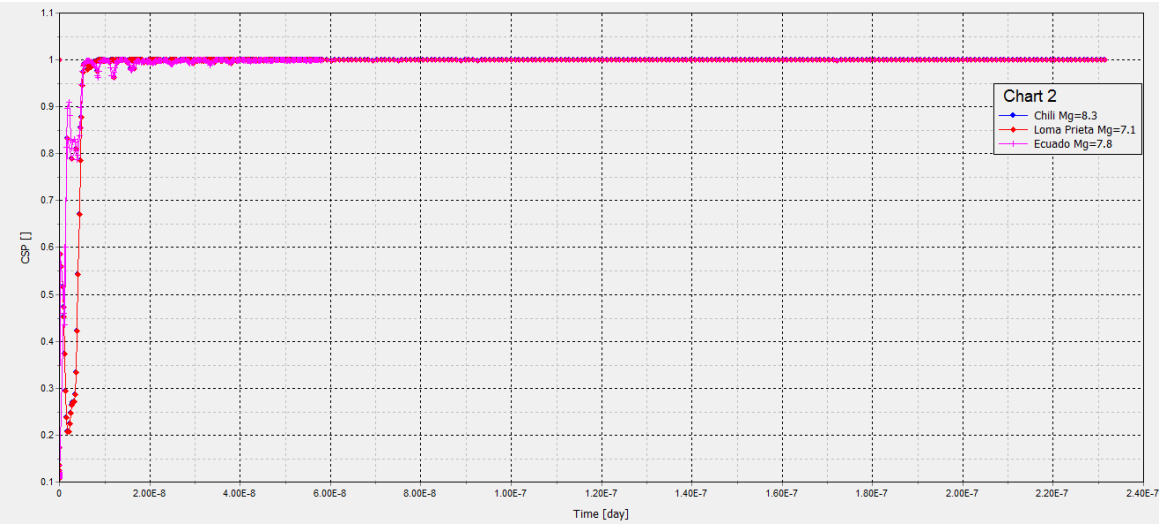

Figure 4.7: Site Response Spectrum

4.3.3 Velocities

The velocity of motion on the ground caused by seismic wave is quite slow.This is because large quantities of earth and the rock are moved Figure 4.8 and Figure 4.9.As result the motion of the structure is slow and the displacements are very low.

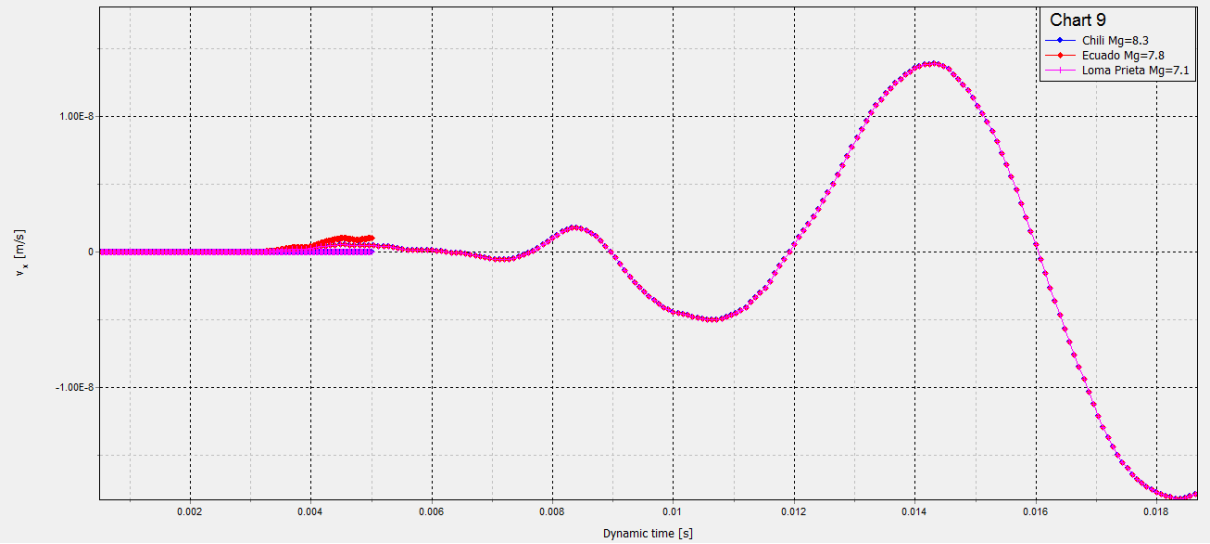

Figure 4.8: Velocity in horizontal direction

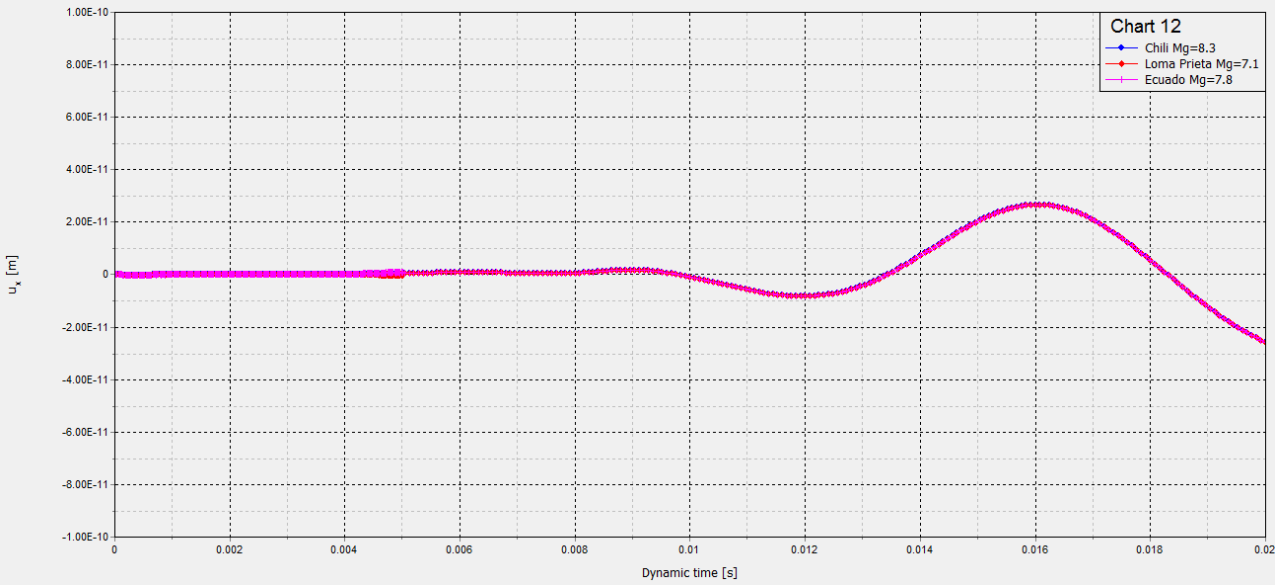

Figure 4.9: Velocity in vertical direction

4.3.4 Ground Amplification

Earthquake shaking is initiated by a fault slippage in the underlying rock. As the shaking propagates to the surface, it may be amplified depending on the intensity of shaking, the surface soil and depth of the layers and the nature of the rock.

Weaker layers of soft soil may results in to higher amplification factor over the rock shaking. The amplification factor 1.0 indicates the soils are firm. The amplification also tends to decrease as the level of shaking is increased. The earthquake damage tends to be more severe in areas of soft soils. Figure 4.10 shows the site amplification factor.

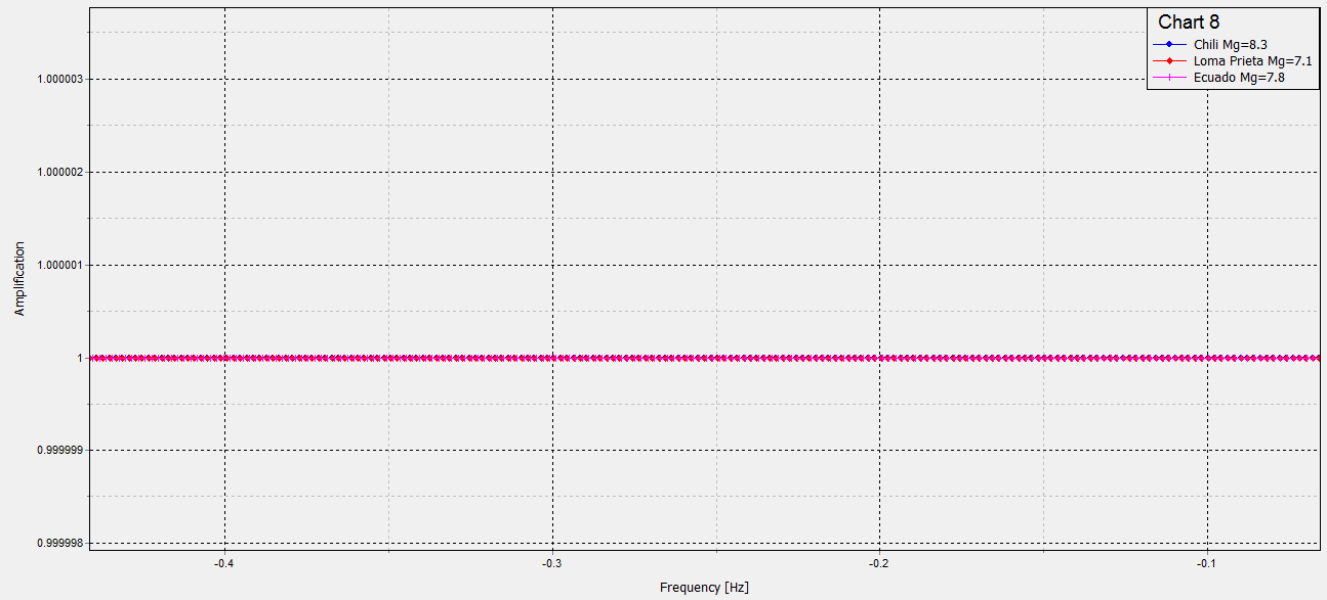

Figure 4.10: Ground Amplification

Chapter 5 – Results and Discussion

The analyses for stage excavation indicate that the maximum displacement (U_z) for 20m stage excavation was 0.1104E-3m and 5m stage excavation was 0.02785E-3 for static condition. The dynamic analysis also resulted to displacements (U_z) for 20m and 5m excavation depths as respectively 0.1104E-3 and 0.04542E-3. This analysis reveals that the deeper the foundation excavation was, the larger the deformation. Since the excavation width is very wide, it also follows that the wider the excavation, the larger the deformation. As a matter of fact, for a typical excavation the wider the excavation, the larger are the unbalanced forces, the larger the unbalanced forces, the greater is the wall deformation. The magnitude of wall movement is determined by the excavation-induced unbalanced forces. The unbalanced forces are as results of factors such as excavation width, excavation depth and the preload. The stresses and deformation caused by excavation arise from their unbalanced forces.

Also the dynamic analysis for stage excavation indicates that for the same materials property the deformation increases with increase in excavation depth in the z-direction. The displacement at 5m and 10m stage excavation was respectively 0.04542E-3m and 0.03969E-3m.This further reveals that soft soil material is displaced more than the firm material during the earthquake event.

The effect of wall height. The modelling and analysis was performed to investigate the effect of wall height (H) with increasing wall penetration depth (D) on the secant pile wall. The maximum excavation depth (H_e) was 20m and the modelling was as per the site conditions. This parametric study was conducted for 24, 27, 30, 33 and 36 m high wall. The soil parameters as in the investigation presented the effect of this parametric study on the wall behavior. The analysis results in terms of wall displacements for soil parameter studied in the modelling were obtained. It was observed that as the height of the wall increased from 24m to 27m the displacement Uz of the wall increased. Further increase in height from 27m to 30m observed was the decrease in displacement Uz of the wall and 33m to 36m resulted to significant increase in displacement. The high unusual displacement at wall height 27m would be the basalt failure produced due to weak, highly weathered scoriaceous basalt material and modelling error may have occurred in the model due to the constraints to temporarily working nodes thus, rapid increase in displacement.

Effect of pile diameter. The diameter of secant pile wall was increased from 650mm to 1400mm in the study. The deformation of the secant pile in horizontal and vertical directions (U_x and U_y) increased as the diameter of the pile increased. During pile driving the increase in pile diameter resulted to increase in deformation near the surface of the pile in horizontal and vertical direction. The same observation was made during the dynamic analysis.

Horizontal and vertical spacing of anchors. The analysis was conducted with horizontal spacing of 2m, 3m, 4m, and 5m and vertical spacing was also varied; 3m, 4m and 5m.The deformations arising from anchor spacing can be distinguished in to that of horizontal spacing and vertical spacing.

One level of ground anchors was spaced at 2m in the horizontal direction and installed at an inclination of angle of 15° below the horizontal direction (left to right).The anchors were also spaced at 3m in the vertical direction(top to bottom).

Decreasing the horizontal spacing can increase the stiffness of the anchor per unit width. With high anchor stiffness, the compression of the anchor will be quite small, and the maximum deformation occurs near the excavation surface.

The material of the interface element was defined by creating a new material, specific for the interface element. The interface element could also be used to smoothen the mesh around the areas with high stress and strain gradients (eg. sharp edges, stiff material). Standard volume elements have difficulties to produce physical stress oscillation in such areas. Smoothening is created by applying interfaces around the area and activating them during mesh generation and deactivating during calculation.

With the start of the first stage of excavation, wall movement will be produced. The second stage of excavation starts after the installation of the first level anchors. Since the stiffness of the anchor is high, the compression of the anchor will be small so that the anchored retaining wall will rotate about the contact point between the anchor connection bolt and the wall, and the wall deformation is generated. The maximum wall deformation will occur near the excavation surface. With the completion of the second level of the anchors, the third level of excavation starts.

As the spacing between the anchors is increased, implying the stiffness of the anchors has been reduced, the compression of the anchor increases. There will be large wall displacement around the contact point during the second phase of excavation.

The final deformation pattern of the retaining wall will be close to linear type and the maximum deformation will be produced at the top of the retaining wall.

The uniformly distributed load (UDL) is applied across the site, and this gives the better estimate on the change of horizontal soil stresses due to surcharge application. The application of the UDL modifies both active and passive limits of the underlying soil. Initial stresses are built up in the calculation step and in the initial step in the calculations, by setting values of K_0 and over consolidation ratio. The ground water level was set to 5m below the ground surface. Plastic analysis is selected as calculation type due to that no time effect is considered on deformation analysis.

.

Chapter 6 – Conclusions and Recommendations

6.1 Introduction

The finite element program Plaxis 3D was used in the modelling. Two different constitutive models in plaxis i.e Hardening soil model and Hardening soil model with small strain, were used to stimulate the secant pile wall and soil behavior.

The 3D models presented in this thesis allow the parametric studies for the pile length, pile diameter and anchor spacing to be tested. The test results show that varying the pile length, pile diameter and anchor spacing can have a great influence over the response of the secant pile wall.

With continued excavation, there was increase in deformation as the excavation depth was increased. The excavation in 3D is attained by deactivating the soil layers. The parametric study was conducted for static and dynamic loading case. The dynamic load used was one earthquake and in order to determine the behavior of the ground during and after the earthquake, there was need to use different earthquakes with different magnitudes, frequencies and epicentral distances etc. All earthquakes were real accelerograms obtained from center for strong ground motion site (USGS data).

6.2 Conclusions of Modeling

According to the parametric analysis; changing the stiffness modulus and varying the pile diameter, pile length and anchor spacing, affects the deformation analysis. Special care was taken when choosing the value and condition of these parameters most especially, the stiffness modulus of the soil. The following conclusions have been drawn from the analysis.

Effect of stage excavation. The analyses for stage excavation showed that the deformations increased as the excavation depth increased. This was due to increase in the magnitude of the unbalanced forces as result of increase in depth of excavation, thus increasing stresses and deformations.

Effect of wall height. The analysis was performed to investigate the effect of wall height with increasing wall penetration depth on the secant pile wall. It was observed that as the height of the wall increased from 24m to 27m, the deformation U_z of the wall increased rapidly. Further increase in the height from 27m to 30m showed decrease in deformation of the wall and 33m to

36m resulted to significant increase in deformation. The erratic increase in deformation at wall height 27m would be the basalt failure produced as result of highly weathered scoriaceous basalt at that depth and modelling error may have occurred in the model due to the constraints to temporarily working nodes thus, rapid increase in displacement.

Diameter of the pile wall was increased from 650mm to 1400mm.The decrease in displacement of the retaining wall was observed as the diameter of the retaining wall increased. Increase in diameter of pile wall reduces displacement of the pile due to increase in structural stiffness.

Decreasing the horizontal and vertical spacing of the anchors increased stiffness of the anchor per unit width. With high anchor stiffness, displacement occurs near the excavation surface.

The modulus of deformability of the soil has great importance in the settlement of the soil. It is visible that when the thickness of the wall increases, the horizontal and vertical displacement near the wall increases.

The displacement at the base of the wall was very small; this is because the wall has the tendency to insert in the soil.

6.3 Recommendations

There is need to consider the anticipated responses of the adjacent buildings during construction. This will require the design professional to survey the condition of the adjacent properties to understand their present condition and fragility, establish acceptable limits, conduct soil-structure analyses of various support systems and develop limits on their respective movements, and develop a monitoring strategy.

Monitoring information is compared with anticipated behavior predicted by analysis to evaluate performance and provide information that can be used to understand adjacent building responses.

In addition measurement of vibrations to evaluate the likelihood of the damage and capture the source vibrations at the foundation level and understand how those source vibrations attenuate or amplify through the structure.

Further investigations on parameters and other conditions that affect seismic analysis like density and shear modulus thus, compressional (p) waves and shear (s) waves can calculated from those soil parameters for each layer and result can be compared with those from seismic refraction test.

Increasing the accuracy of the investigation of the modulus of deformability in different stratification layers and other conditions would increase the accuracy of the simulated results.

3D model presents more realistic results than 2D model. The 3D effects are not captured in a 2D model, which assumes plain strain condition. Thus, excavation geometry and the loading conditions can only be fully modelled using Plaxis 3D analysis.

Reference

[1] Atalay, A. (2016).Unpublished Seismic Investigation report for the CBE, new building site.

[2] Bowles, J.E. (1977). Foundation Analysis and Design. MC Graw- Hill, Inc. New York.

[3] Brinkgreve, R.B.J., Swolfs, W.M., Engine, E. (2011).Plaxis User‟s manual, Plaxis Bv, the Netherlands.

[4] Bryson.L.,Calvello,Finno.J.,Richard.(2002).Analysis and Performance of the excavation for the Chicago State subway Renovation project and its effect on Adjacent Structures. Northwest University.

[5] Clough, G.W., O‟Rourke, T.D. (1990).Construction Induced movement of in situ walls.Proc. Design and performance of earth retaining structure, ASCE special conference, Ithaca, Newyork, pp.439-470.

[6] Erin H.Y.Leung., Charles W.W.Ng. (1992).Wall and Ground Movements Associated with Deep Excavations Supported by cast insitu wall in Mixed Ground Conditions. Journal of Geotechnical and Geotechnical Engineering-Vol.118.

[7] Franz.T., Helmut.S. (2012).Application of the ground anchor facility in plaxis 3D Foundation. Graz University of Technology.

[8] Gouin, Pierre. (1979). Earthquake History of Ethiopia and the Horn of Africa. International Development Research Center. Ottawa, Canada, IDRC-118e, 259p.

[9] Halpin, J.C., Tsai, S.W. (1996).Effects of Environmental Factors on Composite Materials, AFML-TR-67-423.

[10] Hashash, Y.M.A., Whittle, A.J. (1996). Ground movement prediction for deep excavations In Soft clays.JGeotech Eng, ASCE, 122(6):474-486.

[11] Hau, K.W. (2003).Application of a three surface kinematic hardening model to the repeated loading of thinly surface pavements. PhD Thesis. Department of Civil Engineering, University of Nottingham, UK.

[12] Institution of Civil Engineers (ICE), 2007.Specification for pilling and Embedded Retaining Walls. Thomas Telford Ltd, second edition, 264p.

[13] Jen, L.C. (1998). The design and performance of deep excavation in clay. PhD Thesis MIT.

[14] Jones, R.M, 2nd ed. (1999).Mechanics of Composite Materials. Taylor and Francis, USA. 253pp.

[15] Mana, A.I., Clough (1981).Prediction of movements for braced cuts in clay.JGeotech Eng.ASCE, 106(6):759-777.

[16] Moormann, C. (2004).Analysis of wall and ground movement due to deep excavation in soft Soils based on a new worldwide data base. Soils and Foundations, voil.44, No.1, 87.

[17] Ng, C.W.W. (1998). Observed performance of multi-propped excavation in stiff Clay.JGeotech Geoenviron Eng, ASCE124 (9):889-905.

[18] Obrzud, R., Truty, A. (2012).The Hardening Soil Model. A practical Guidebook Z soil.Pc 100701 Report.

[19] Plaxis 2D reference manual, (2011).Plaxis Finite Element software. Delft University of Technology and Plaxis Bv. The Netherlands.

[20] Perk, R.B. (1969). Deep excavation and tunneling in soft ground. In: proceeding of the 7th International conference on soil mechanics and Foundation engineering, Mexico City, State-of-the-Art Volume, pp225-290.

[21] Sabatini, P.J., Pass, D.G., and Bachus, R.C. (1999). Ground anchors and anchored systems. Geotechnical Circular No.4, FHWA-IF-99-015, Federal Highway Administration, Department of Transportation, Washington, D.C.

[22] Spring (2011).Plaxis Bulletin/www.plaxis.nl

[23] Suroor, Hadi. (2007).Performance Evaluation of Instrumented LNG Retention Dikes on Louisiana Soft clays. 7th International Symposium on Field Measurements in Geomechanics, Boston, USA.

[24] Truty A. Hardening soil model with small strain stiffness. Technical Report 080901.

[25] Wharmby, N., Leach, B., Storer, K., Murray. (2007).Construction of deep emergency access And ventilation shaft at Waihi gold mine, in proceedings Tenth Australia New Zealand conference on Geomechanics, 2:448-53p.

[26] Wood, D., Muir. (1990).Soil behavior and critical state soil mechanics. Cambridge University press.ISBN0-521-3249-4.

Appendices

Appendix A- Hardening Soil Model

Hardening Mechanism in Finite Element simulation

In the Hardening soil model, accounting for stress path is possible. Isotropic and deviatoric. In isotropic, the volumetric plastic mechanism in the form of cap surface is introduced to account for a threshold point (preconsolidation pressure) beyond which important plastic straining occurs characterizing a normally-consolidated state of soil. The shear mechanism generates no volumetric plastic strain; the model without volumetric mechanism could significantly overestimate soil stiffness in the virgin compression conditions, particularly for normally and lightly over consolidated cohesive soils. The isotropic mechanism is thus important when modeling consolidation problems related to ground lowering.

Hardening-soil model

It is an advanced hyperbolic soil model formulated in the framework of hardening plasticity. The main difference with the Mohr-Coulomb model is the stiffness approach. Here, the soil is described much more accurately by using three different input stiffness: triaxial loading stiffness E_{50}, triaxial unloading stiffness E_{ur}, and the oedometer loading stiffness E_{Oed}. Apart from that, it accounts for stress-dependency of the stiffness moduli, all stiffnesses increase with pressure (all three inputs relate to reference stress, 100 kPa).

The Hardening Soil model has been presented before as a hyperbolic model. Often hyperbolic soil models have been used to describe the nonlinear behavior; this is also a suitable application in this research as sand usually behaves as a linear elastic material with shear modulus for shear strains up to $\approx 10{-}5$, and afterward the stress-strain relationship is strongly non-linear .The background of this kind of models is the hyperbolic relationship between vertical strain and deviatoric stress in primary triaxial loading. However, the Hardening-soil model is far better than the original hyperbolic model as it uses theory of plasticity instead of theory of elasticity and because it includes soil dilatancy and a yield cap. In contrast to an elastic perfectly plastic model like Mohr-Coulomb, now the yield surface is not fixed but can expand due to plastic straining [24].

The main characteristics of the model:

Stress dependent stiffness according to power law (defined by parameter m)

Plastic straining due to primary deviatoric stress (defined by parameter E_{50}^{ref})

Plastic straining due to primary compression (defined by parameter E_{Oed}^{ref})

Elastic unloading/reloading (defined by parameter E_{ur}^{ref},v_{ur})

In the Hardening Soil model, the associated flow rule is defined as a relationship between rates of plastic shear strain γ^p and plastic volumetric strain ϵ_v^p ; it has the linear form:

$$\epsilon_v^p = sin\ \psi_m \gamma^p$$

Where ψ_m is the mobilized dilatancy angle, defined as:

$$sin\ \psi_m = \frac{sin\ \varphi_m - sin\ \varphi_{cv}}{1 - sin\ \varphi_m sin\ \varphi_{cv}}$$

With φ_{cv} the critical state friction angle, constant for a certain material, independent of the density, and φ_m the mobilized friction angle that can be calculated:

$$sin\ \varphi_m = \frac{\sigma'_1 - \sigma'_3}{\sigma'_1 + \sigma'_3 - 2c\ cos\varphi}$$

According to Rowe"s stress-dilatancy theory (1962), material contracts for small stress ratios ($\varphi_m < \varphi_{cv}$) and dilates for high stress-ratios ($\varphi_m > \varphi_{cv}$). At failure, the mobilized friction angle equals the failure one and:

$$sin\ \psi_m = \frac{sin\ \varphi - sin\ \varphi_{cv}}{1 - sin\ \varphi sin\ \varphi_{cv}}$$

$$sin\ \varphi_{cv} = \frac{sin\ \varphi - sin\ \psi}{1 - sin\varphi\ sin\psi}$$

Secant stiffness in standard drained triaxial test: E_{50}^{ref}, and then:

$$E_{50}(\sigma) = E_{50}^{ref}\left(\frac{c\ cos\ \varphi - \sigma'_3}{c\ cos\ \varphi + p^{ref} sin\varphi}\right)$$

Tangent stiffness for primary oedometer loading: E_{Oed}^{ref}

Power for stress-level dependency of stiffness: m

Unloading/reloading stiffness: E_{ur}^{ref}(default: $E_{ur}^{ref} = 3\ E_{50}^{ref}$), and then:

$$E_{ur}(\sigma) = E_{ur}^{ref}\left(\frac{c\cos\varphi - \sigma'_3}{c\cos\varphi + p^{ref}\sin\varphi}\right)$$

Poisson"s ratio for unloading/reloading: v_{ur}(default: v_{ur}= 0.2)

Reference stress for stiffness: p^{ref}(default: p^{ref} = 100 stress units)

K_O value for normal consolidation: K_0^{nc}(default: K_0^{nc}= 1− $\sin\varphi$)

Failure ratio: $R_f = \frac{q_f}{q_a}$ (default: R_f = 0.9)

Tensile strength: $\sigma_{tension}$(default: $\sigma_{tension}$ = 0)

Also it defines the oedometer stiffness:

$$E_{Oed} = E_{Oed}^{ref}\left(\frac{c\cos\varphi - \sigma'_1\sin\varphi}{c\cos\varphi + p^{ref}\sin\varphi}\right)^m$$

Note that the oedometer stiffness relates to oedometer testing, therefore to the compaction hardening part. On the other hand, E_{50} and E_{ur} relate to triaxial testing and so to the friction hardening part. To explain the plastic volumetric strain in isotropic compression, a second yield surface closes the elastic region in the direction of the p-axis. While the shear yield surface is mainly controlled by the triaxial modulus, the oedometer modulus controls the cap yield surface.

Appendix B - Geotechnical properties of soil

Typical values of soil Young's modulus for different soils according to USCS.

In general, the soil stiffness and elastic modulus depends on the consistency and the parking (density) of the soil. Typical values of soil Young"s modulus are given below as guideline.

USCS	Description	Loose	Medium	Dense
GW,SW	Gravel/sand well-graded	30-80	80-160	160-320
SP	Sand ,uniform	10-30	30-50	50-80
GM,SM	Sand/Gravel silty	7-12	12-20	20-30

Table B.1: Typical values of Young"s modulus for granular material (MPa) [18].

USCS	Description	Very soft to soft	Medium	Stiff to very stiff	Hard
ML	Silts with slight plasticity	2.5-8	10-15	15-40	40-80
ML,CL	Silts with low plasticity	1.5-6	6-10	10-30	30-60
CL	Clays with low-medium plasticity	0.5-5	5-8	8-30	30-70
CH	Clay with high plasticity	0.35-4	4-7	7-20	20-32
OL	Organic silts	-	0.5-5	-	-
OH	Organic clays	-	0.5-4	-	-

Table B.2: Typical values of Young"s modulus for cohesive material (MPa) [18].

Type of soil	μ
Clay (saturate)	0.4-0.5
Clay(unsaturated)	0.1-0.3
Sandy clay	0.2-0.3
Silt	0.3-0.35
Sand – dense	0.2-0.4
Sand –coarse (void ratio =0.4-0.7)	0.15
Sand – fine grained (void ratio =0.4-0.7)	0.25
Rock	0.1-0.4(depends on type of rock)
Loess	0.1-0.3
Ice	0.36
Concrete	0.15

Table B.3: Typical values of Poisson"s ratio for soils and other material [2].

Appendix C – Modelling Outputs for 2D Analyses

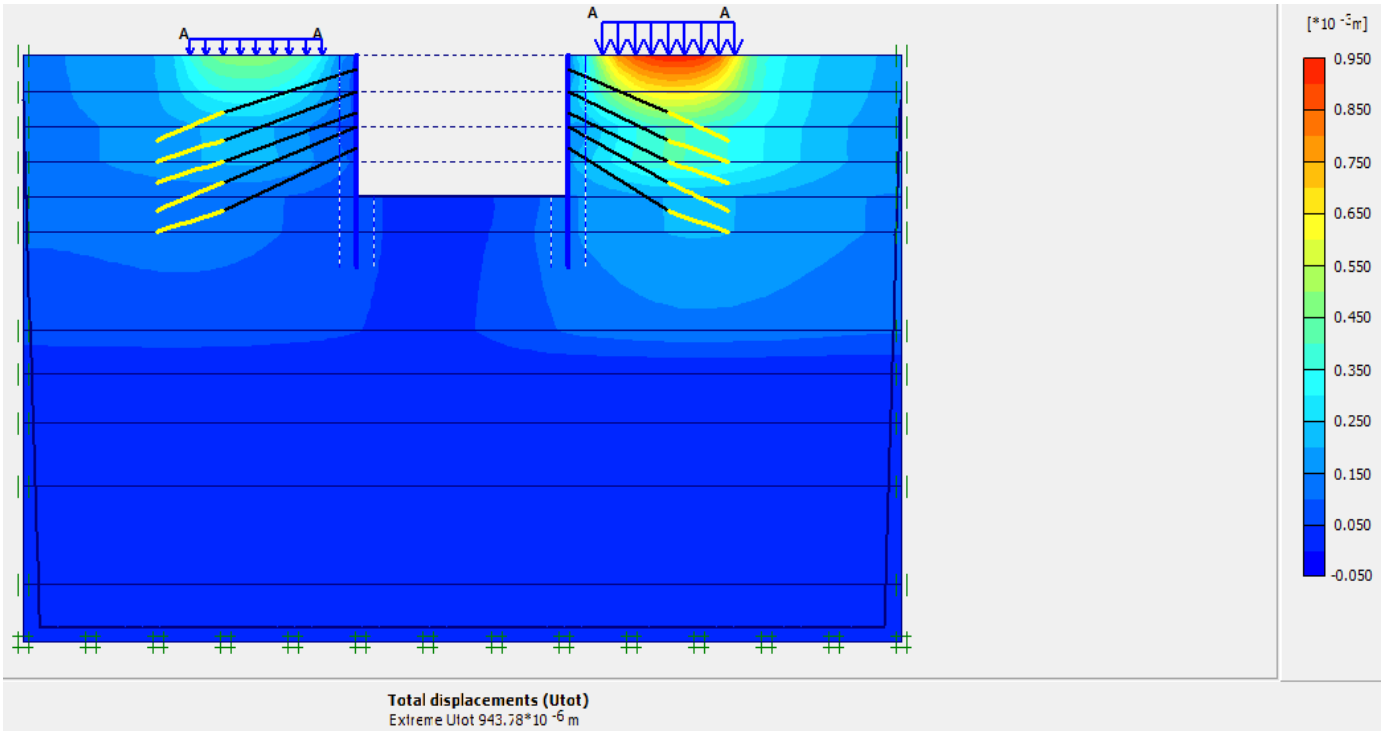

Figure C.1 :Total displacement under static load condition

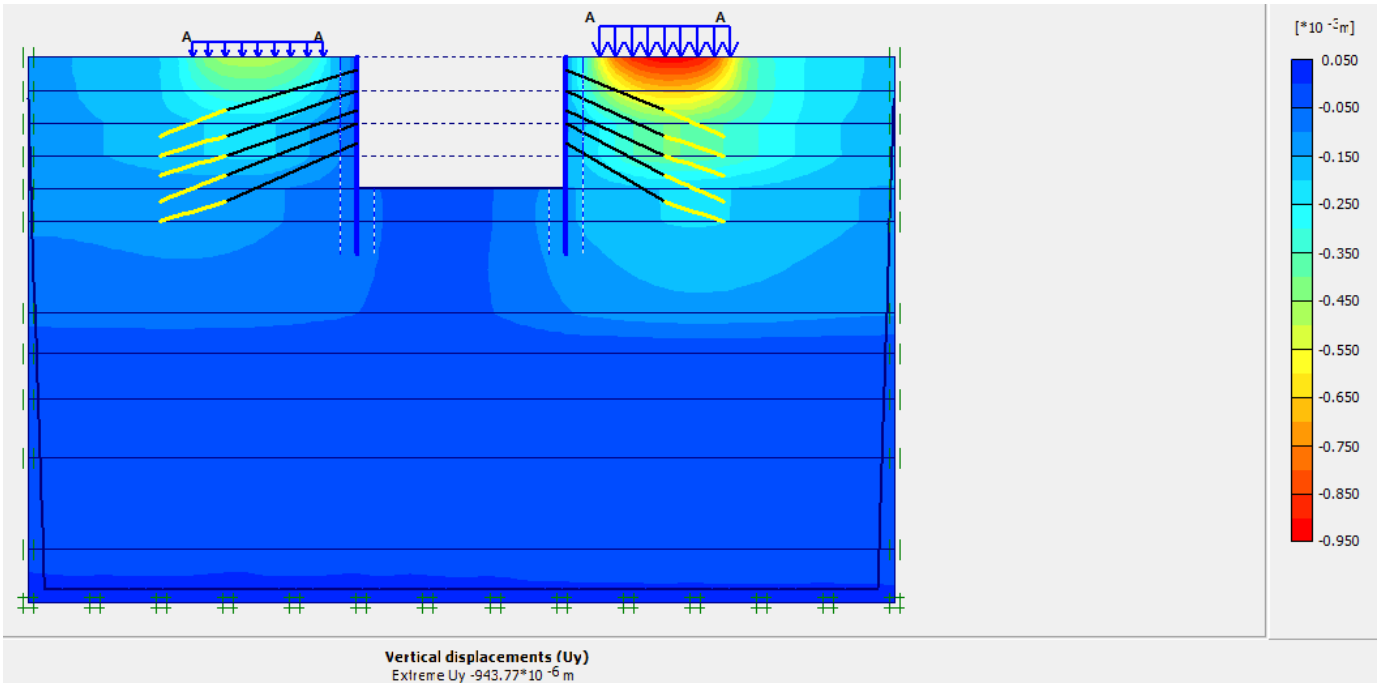

Figure C.2 :Vertical displacement under static load condition

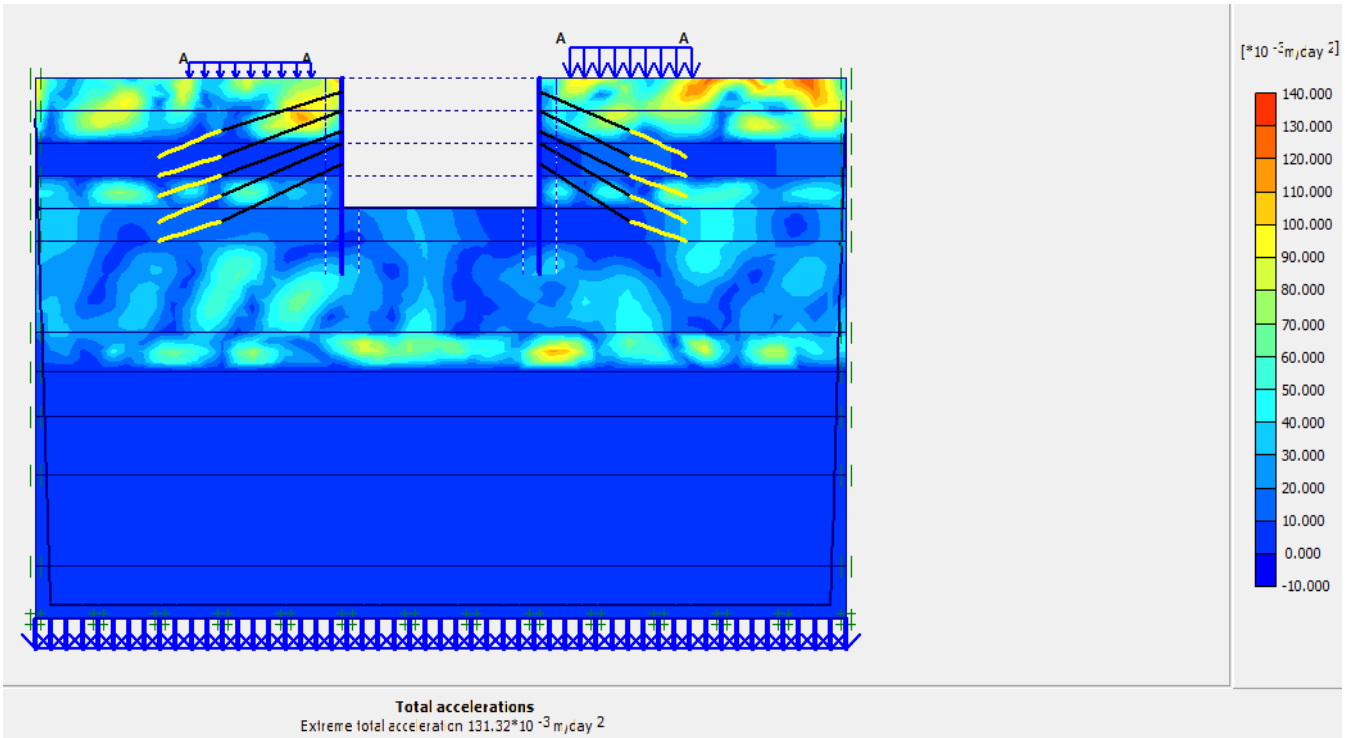

Figure C.3 :Total Acceleration

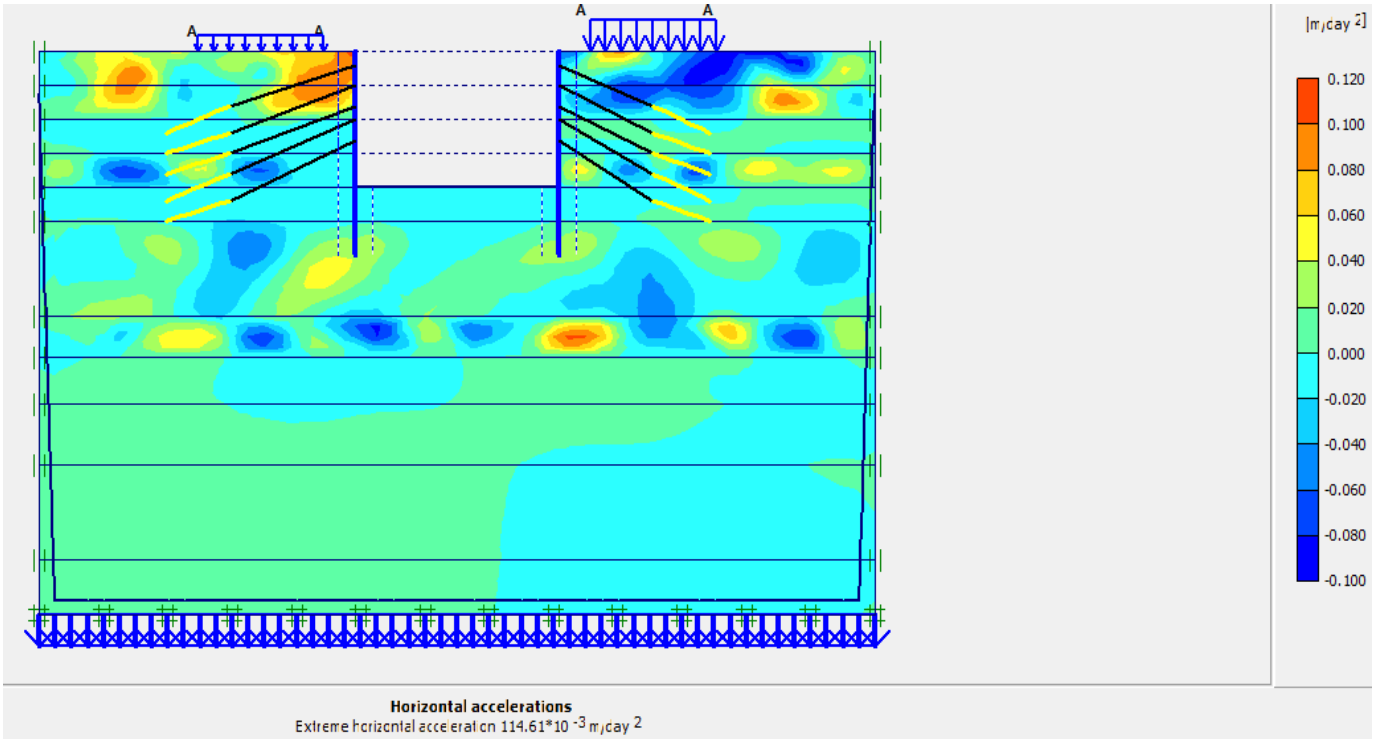

Fig C.4 : Horrizontal Acceleration

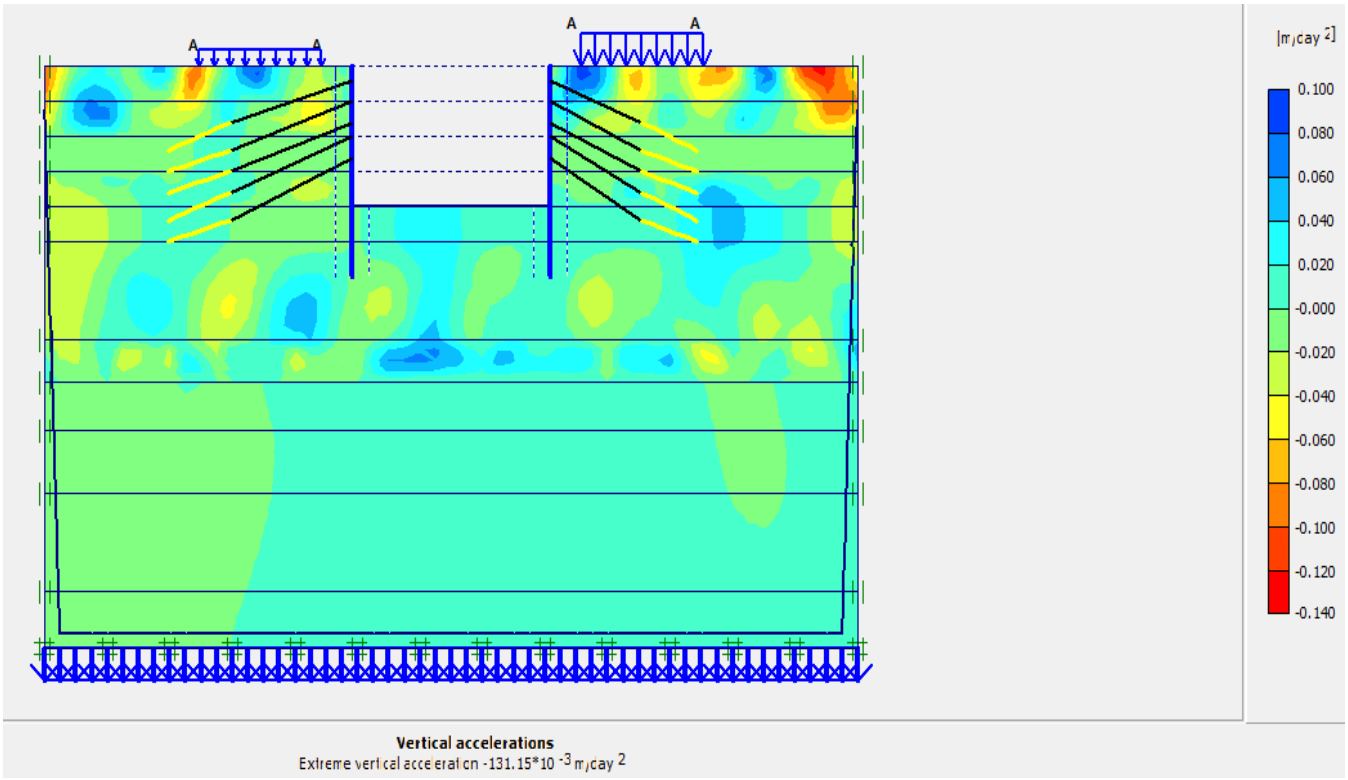

Figure C.5 : Vertical Acceleration

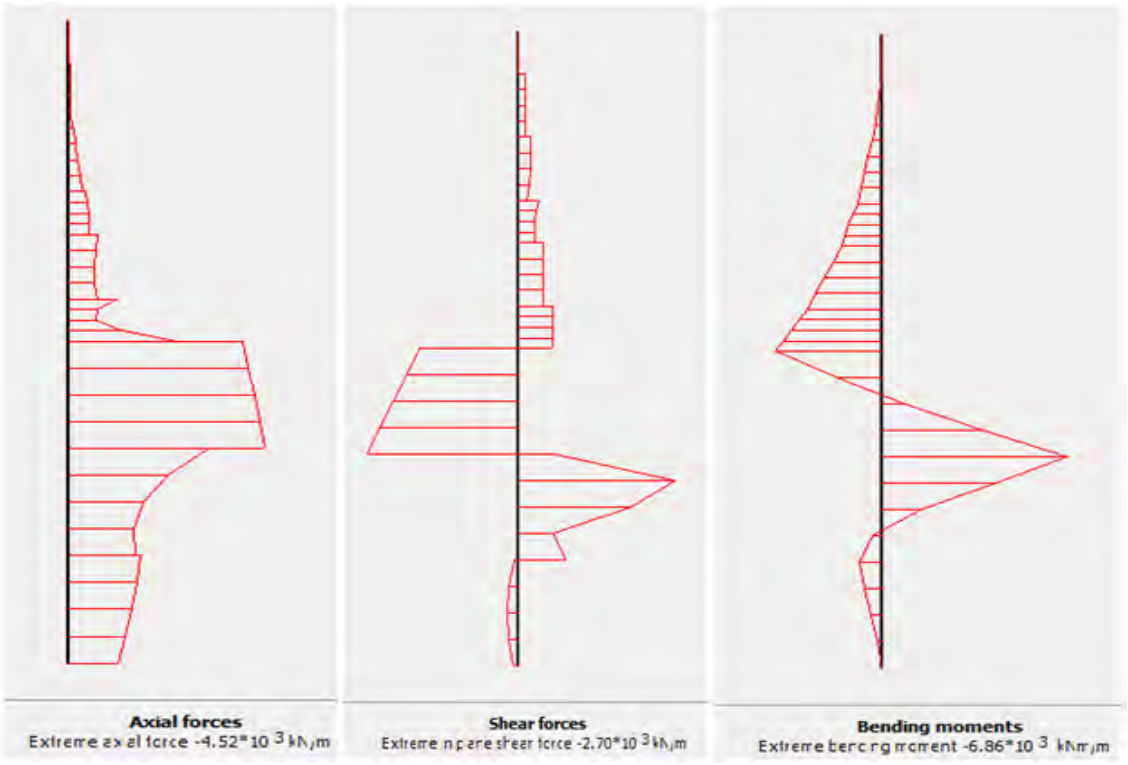

Figure C.6: Peak Axial, Bending and Shear forces under dynamic load condition

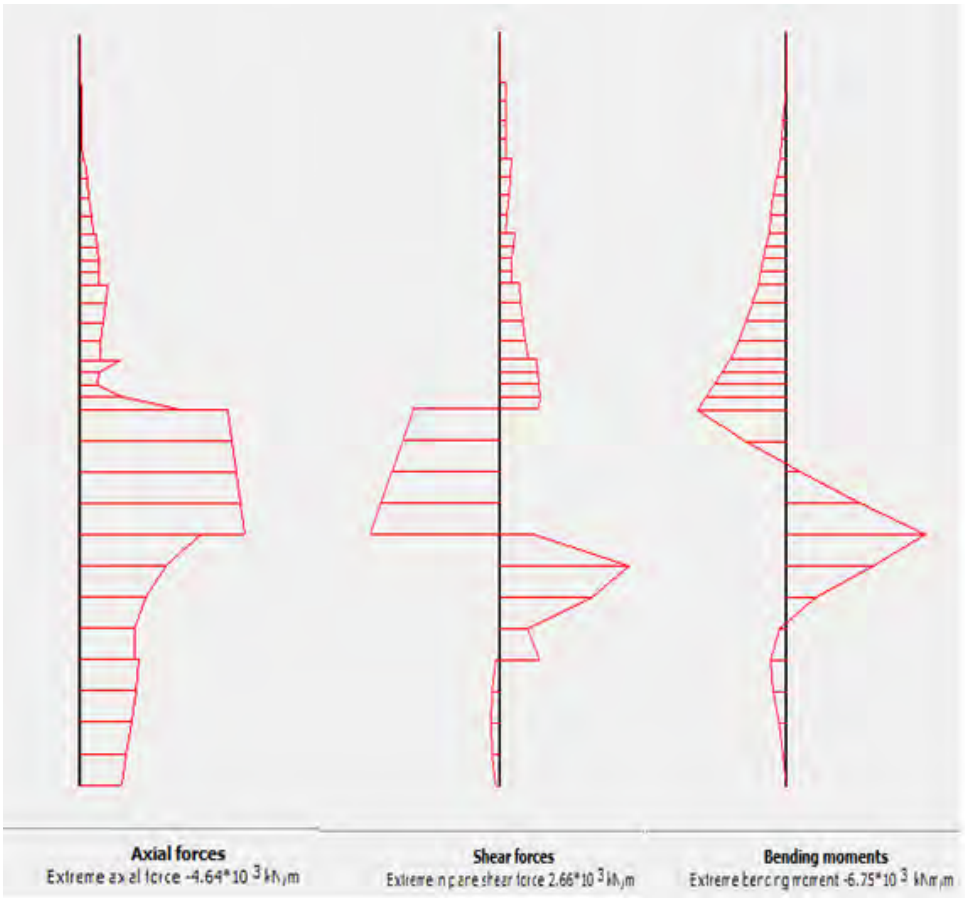

Figure C.7: Peak Axial, Bending and Shear forces under static load condition

Appendix D – Modelling Outputs for 3D Analyses

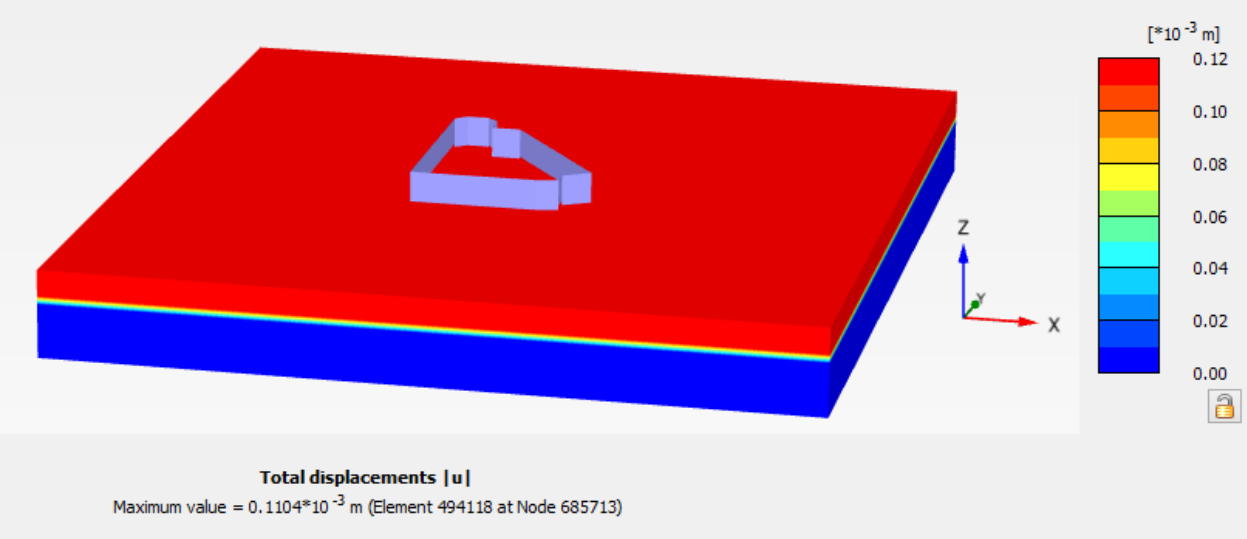

Figure D.1 Total displacement under static load condition

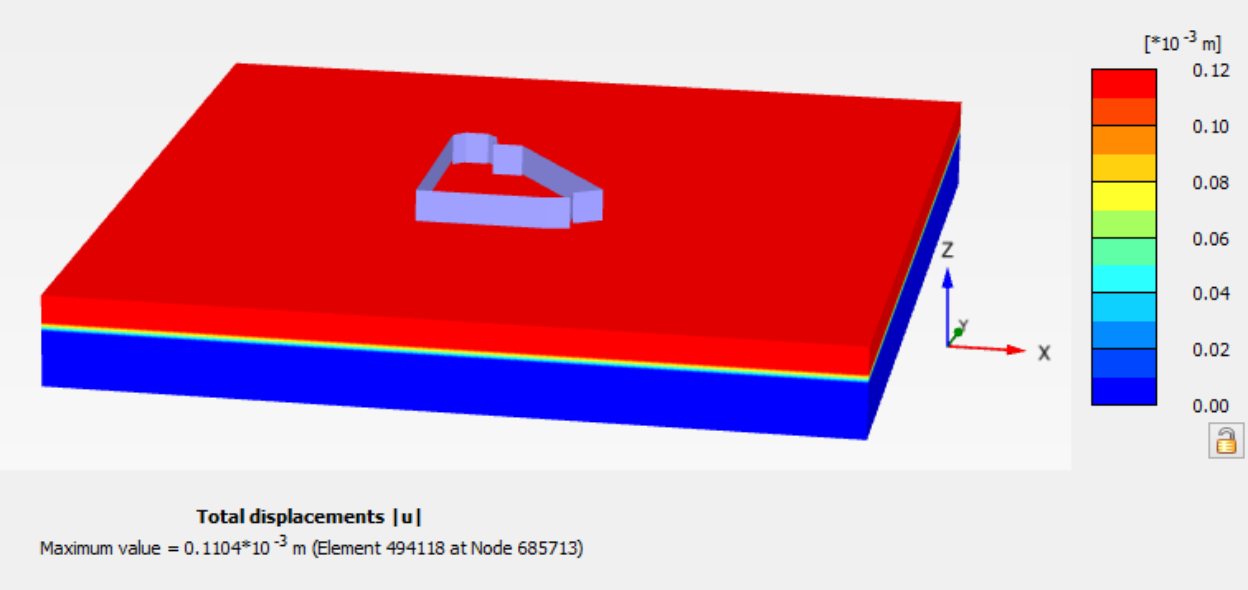

Figure D.2: Total displacement for stage excavation under dynamic load condition

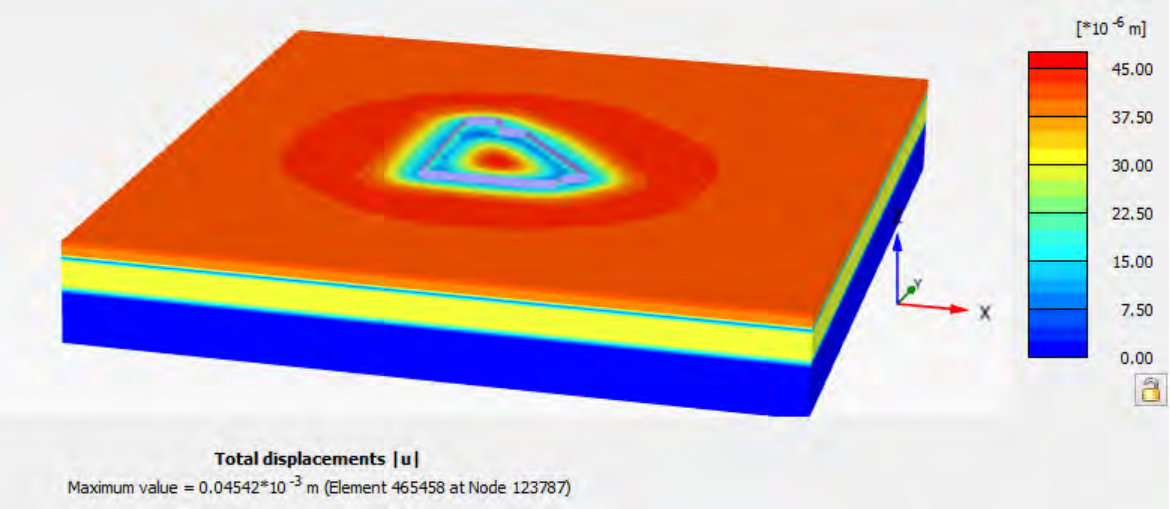

Figure D.3: Stage excavation 5m – Total displacement

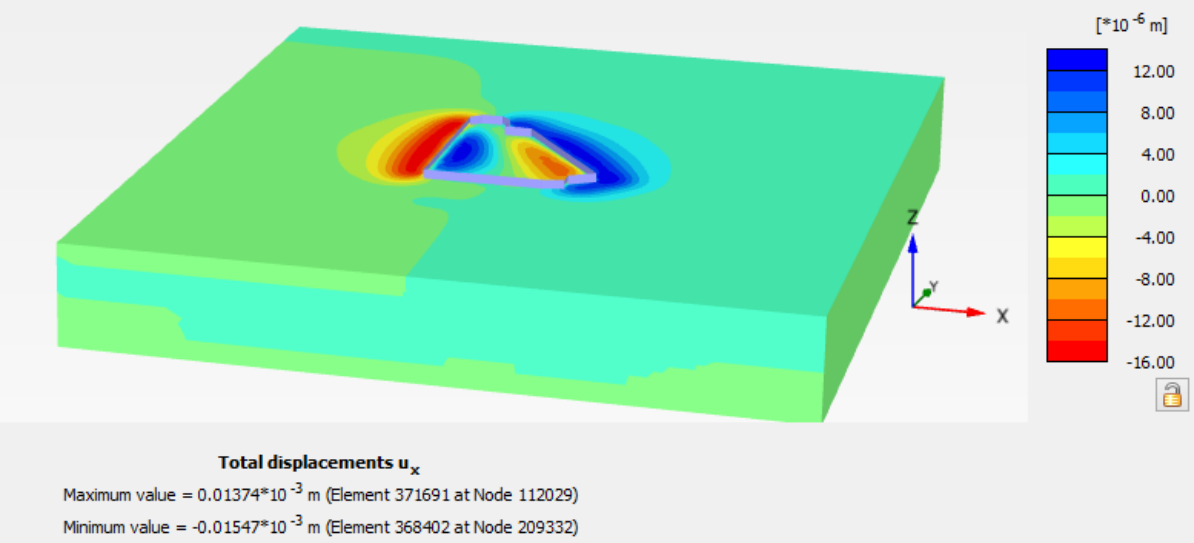

Figure D.4: Stage excavation 5m – horizontal displacement

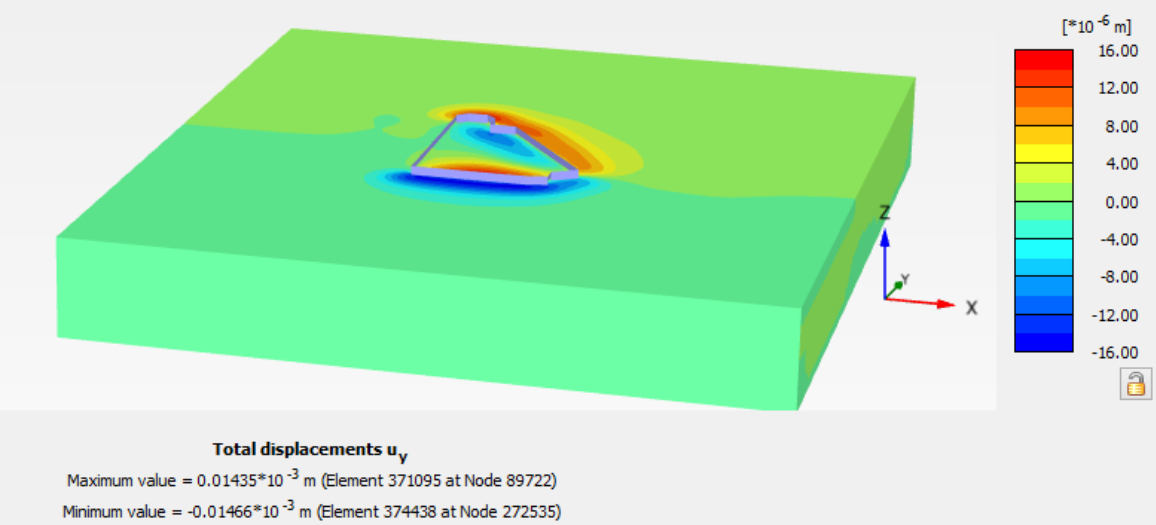

Figure D.5: Stage excavation 5m –vertical displacement

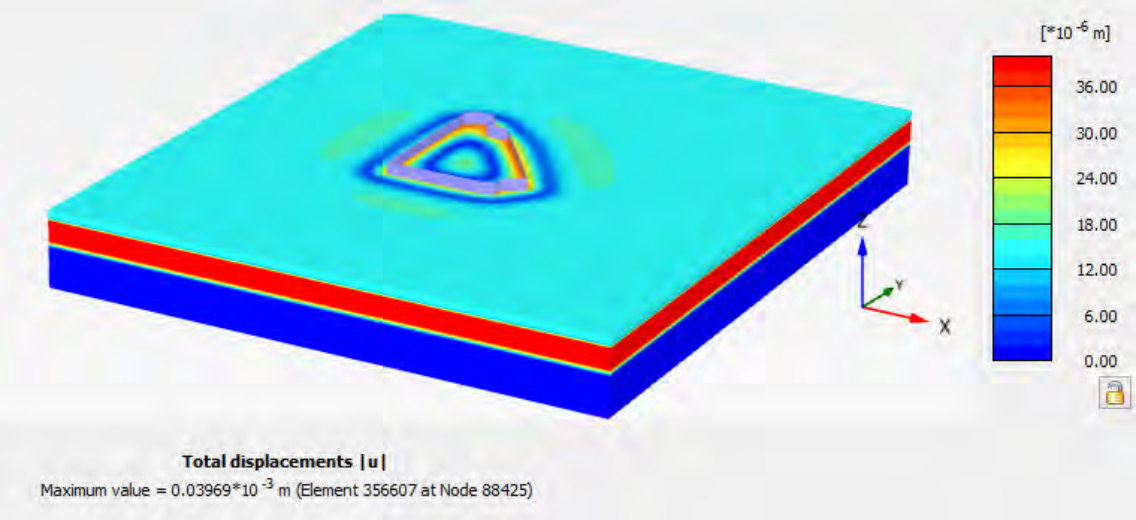

Figure D.6: Stage excavation 10m – Total displacement

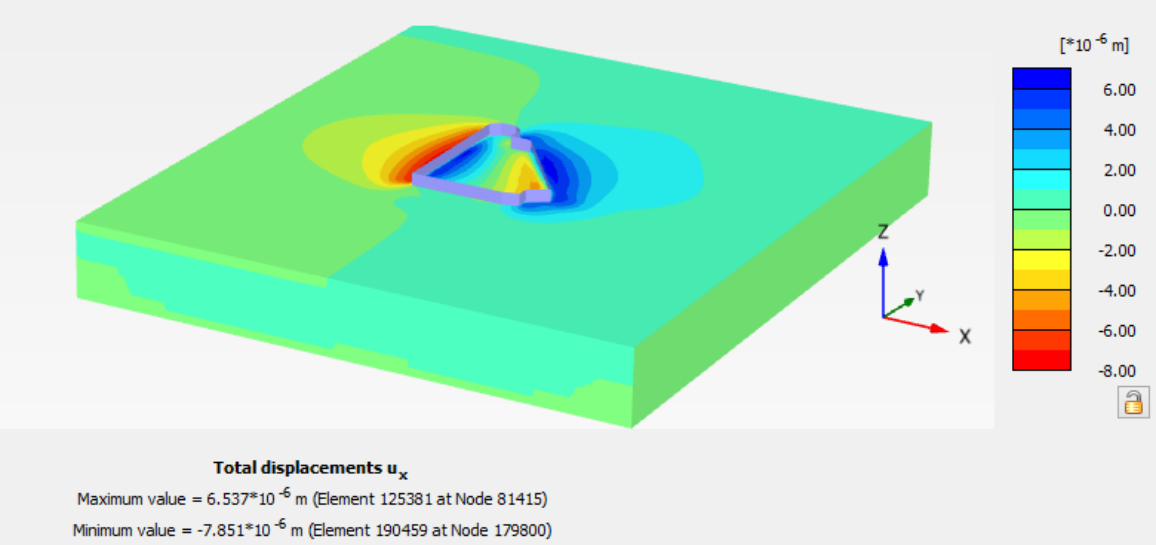

Figure D.7: Stage excavation 10m – horizontal displacement

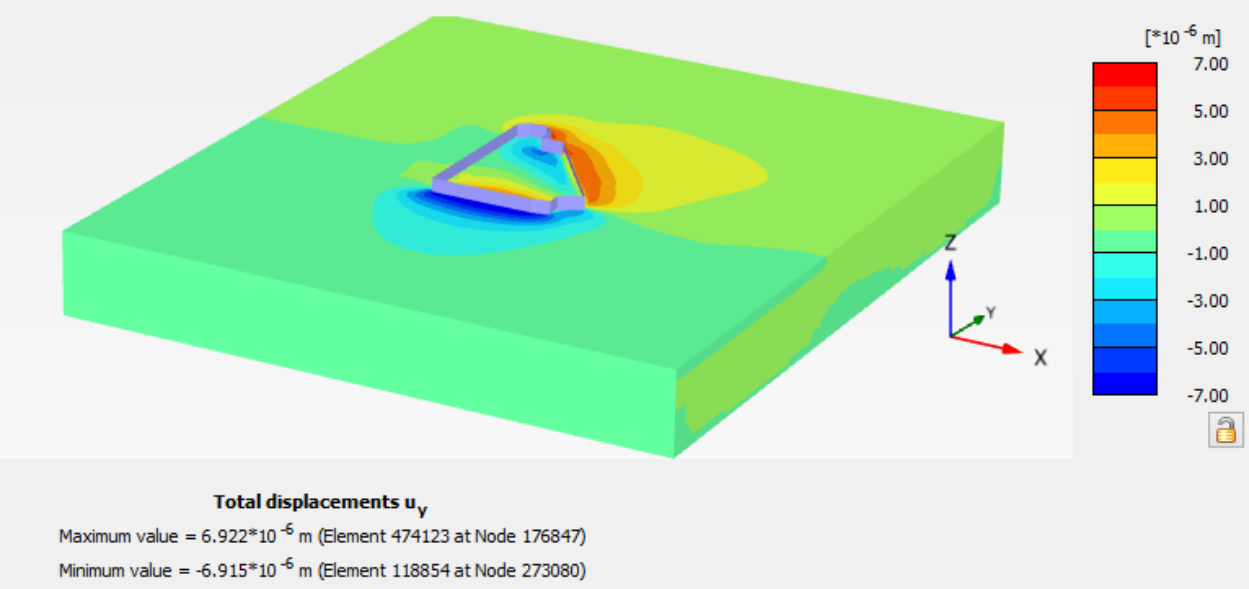

Figure D.8: Stage excavation 10m –vertical displacement

Appendix E – Site layout plan

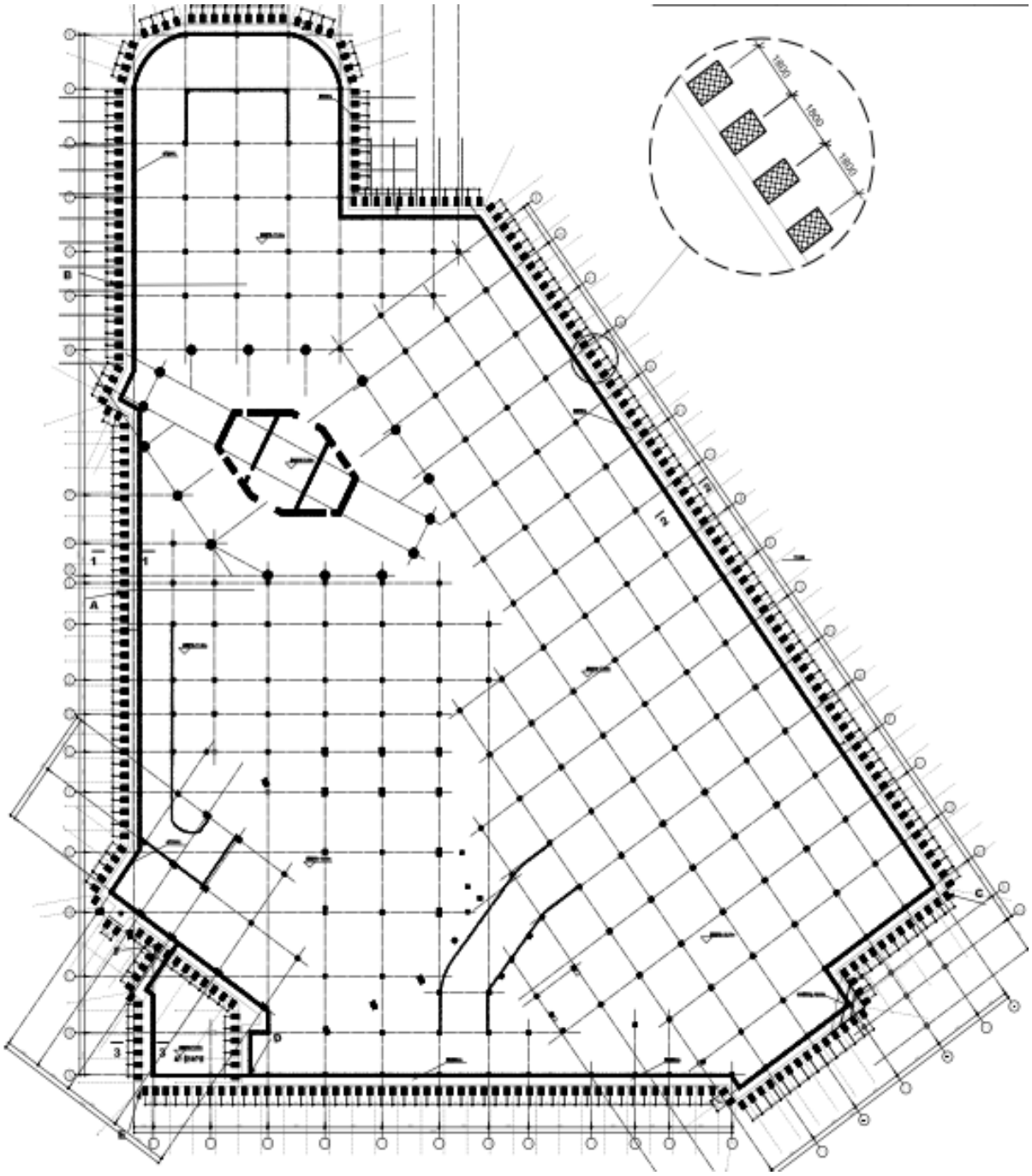

Figure E.1: Site layout for the Commercial Bank of Ethiopia New Headquarter Building